Department of Food and Environmental Sciences
Faculty of Agriculture and Forestry
University of Helsinki

Doctoral Programme in Microbiology and Biotechnology

Structural studies of *O*-acetylglucuronoxylans and their modifications in plant cell walls

Sun-Li Chong

ACADEMIC DISSERTATION

To be presented, with the permission of the Faculty of Agriculture and Forestry, University of Helsinki, for public examination in lecture room B3, Viikki B-building, on 19th December 2014, at 12 noon.

Supervisors: Docent Päivi Tuomainen
Department of Food and Environmental Sciences
University of Helsinki

Professor Maija Tenkanen
Department of Food and Environmental Sciences
University of Helsinki

Members of the thesis follow-up group:
Professor Kurt Fagerstedt
Department of Biosciences
University of Helsinki

Docent Anna Kärkönen
Department of Agricultural Sciences
University of Helsinki

Reviewers: Associate Professor Emma R. Master
Department of Chemical Engineering and Applied Chemistry
University of Toronto, Canada

Docent Tarja Tamminen
VTT Technical Research Center
Helsinki

Opponent: Professor Paul Dupree
Department of Biochemistry
Cambridge University, United Kingdom

Custos: Professor Teemu Teeri
Department of Agricultural Sciences
University of Helsinki

ISBN 978-951-51-0517-2 (paperback)
ISBN 978-951-51-0518-9 (PDF)

ISSN 2342-5423 (print)
ISSN 2342-5431 (online)

Cover: Finnish forest in summer (water color), drawn by Kean-Jin Lim

Hansaprint
Helsinki 2014

Dedicated to all my teachers

ABSTRACT

O-acetylglucuronoxylans (AcGX) are the major hemicelluloses found in the secondary cell wall of dicotyledon species. The backbone is formed by β(1→4)-linked xylopyranosyl (Xyl*p*) residues, which are substituted by α(1→2)-linked (4-*O*-methyl)glucopyranosyluronic acid ((Me)Glc*p*A). The AcGX are also highly acetylated on the 2-*O* or 3-*O*; or both positions of Xyl*p* units. Notably, acetylation patterns in AcGX are not well understood since they are typically destroyed during the alkaline isolation. Accurate quantitation of MeGlc*p*A is also challenged by the lack of commercially available MeGlc*p*A sources, thus the accuracy of MeGlc*p*A content determined with the Glc*p*A standard is unknown.

The current thesis established new procedures of detailed characterization of AcGX. The xylan OLIgosaccharide Mass Profiling (OLIMP) method encompassed endoxylanase hydrolysis and mass spectrometry detection. The endoxylanase cleaves the xylan backbone into acetylated xylooligosaccharides (AcXOS). As the action is hindered by the side groups, endoxylanase can be a selective tool to liberate AcXOS from plant tissues for fingerprinting the acetylation pattern in AcGX. Additionally, mass fragmentation analyses were performed to elucidate the spatial distribution of acetyl residues. The accuracy of MeGlc*p*A quantitation using the Glc*p*A standard was examined by comparing it to the in-house purified MeGlc*p*A in acid methanolysis and gas chromatography (GC) analysis.

Several of the genes responsible for the biosynthesis of AcGX were previously identified using *Arabidopsis thaliana* as the model plant. Herein, the structures of AcGX in Arabidopsis wild-type and biosynthetic mutant plants that are defective in reducing end tetrasaccharide sequence or backbone synthesis, *irx7*, *irx9*, *irx10* and *irx14*; and (Me)Glc*p*A addition, *gux1gux2* were analyzed using methods established for structural characterization of AcGX. Mono-acetylations (2-*O* or 3-*O* position) were reduced in *irx7*, *irx9* and *irx14*, whereas 2-*O* acetylation was elevated in the (Me)Glc*p*A deficient mutant, *gux1gux2*, indicating that the addition of (Me)Glc*p*A residues is taking place before acetylation of xylans. Structural elucidation on the major AcXOS liberated from wild-type plant suggests that the acetyl residues are added in every other Xyl*p* residue in AcGX. Interestingly, a novel pentose substitution on the Glc*p*A side group in AcGX was identified.

In acid methanolysis, the Glc*p*A standard was partially lactonized, thus yielding six derivatives in GC chromatogram. When all six Glc*p*A derivatives were used in the calibration

curve, the MeGlc*p*A content was underestimated by nearly 30%. The MeGlc*p*A content can be closely estimated by choosing the appropriate Glc*p*A derivatives in the calibration curve. The method was used to investigate the impact of *Schizophyllum commune* glycoside hydrolase family 115 α-glucuronidase (AGU) transgene expressed in Arabidopsis. The (Me)Glc*p*A content in the *Sc*AGU115 expressing plants was surprisingly unchanged despite the active recombinant enzyme present within the cell walls.

In this work, the acetylation pattern in the AcGX of Arabidopsis wild-type and mutant plants was studied in detail. The methods developed herein revealed that the acetylation of AcGX was reduced in Arabidopsis lines that encode a defective biosynthetic gene related to backbone or reducing end sequence synthesis, suggesting pleiotropic effect of a single gene mutation in xylan biosynthesis. The (Me)Glc*p*A substituents in AcGX can be effectively reduced by disruption of the glucoronyltrasnferases; however, the substitution in the AcGX of *gux1gux2* was compensated by acetylation. On the other hand, constitutive transgenic expression of *Sc*AGU115 α-glucuronidase did not remove the (Me)Glc*p*A substituents *in planta*. The reason may be ascribed to the shielding by neighbouring acetyl substituents, or limited accessibility of the recombinant enzyme to cell wall substrates. Therefore, a viable approach for the effective tailoring of AcGX substituents *in planta* could be co-expression with an acetyl xylan esterase to obtain synergism between these side-group removing enzymes.

ACKNOWLEDGEMENT

This study was carried out at the Department of Food and Environmental Sciences, University of Helsinki. The financial support from the Academy of Finland, the Nordic Forest Research, the Glycoscience Graduate School, and the Finnish Cultural Foundation are gratefully acknowledged. Part of the work was carried out at the Department of microbiology, University of Utrecht, The Netherlands, and the Department of Forest Genetic and Plant Physiology, Swedish University of Agricultural Sciences. I thank the COST 928, the COST FP0602, and the Nordforsk Researcher Network for funding these research visits.

I express my deepest gratitude to my supervisors, Professor Maija Tenkanen and Docent Päivi Tuomainen for their continuous support of my PhD study and research. I thank Maija for bringing me into the field of plant cell walls, for her motivation, persistence, patience, and enthusiasm in science. I thank Päivi for the guidance in chromatography and mass spectrometry. Besides, I want to thank Professor Ewa Mellerowicz and Dr. Sanna Koutaniemi for introducing plant biology to me, and for their support throughout my study. In addition, Professor Teemu Teeri, Professor Kurt Fagerstedt and Docent Anna Kärkönen are acknowledged for participating in my thesis follow-up group.

I sincerely thank the thesis pre-examiners, Docent Tarja Tamminen and Associate Professor Emma R. Master for giving their constructive comments and suggestions to the thesis. I am also indebted to all the co-authors, collaborators, group leaders, postdocs, and others: Docent Raimo Ketola, Dr. Teemu Nissilä, Docent Liisa Virkki, Docent Hannu Maaheimo, Dr. Marta Derba-Maceluch, Prashant Mohan Pawar, Professor Björn Sundberg, Dr. Melissa Roach, Professor Simon McQueen-Mason, Dr. Leonardo D. Gómez, Professor Ronald de Vries, Dr. Evy Battaglia, Professor Bernard Henrissat, Professor Pedro M. Coutinho, Professor Annele Hatakka, Dr. Miia R. Mäkelä, Docent Kristiina Mäkinen, Dr. ChunLin Xu, Minna Juvonen, Henna Pynnönen, Tanja Paasela, and Jonne Hakanpää. Thank you for providing me with the facilities, and your expertise in the experimental work and manuscript revision. In addition, the lab technicians, Taru Rautavesi, Maija Ylinen, Mikka Olin, and Pirjo Kukkonen are warmly thanked for their helps at the laboratory.

My gratitudes are extended to my former and current colleagues in the Viikki D-building: Helena Pastell, Kirsti Parikka, Kirsi Mikkonen, Leena Pitkänen, Ndegwa Henry Maina, Susanna Heikkinen, Qiao Shi, YaXi Hou, Laura Huikko, Abdul Ghafar, Jaana Valo, Paula Hirsilä, and Suvi Alakalhunmaa. Though we may not involve in the same project, I treasure

the moments that we have spent together. I also wish to thank Ling Zou, YiJing Zhang, and many others who have spent wonderful time together at the Finnish summer cottage. This is one the Finnish experience that I will not forget.

My heartfelt thanks go to my parents and siblings in Malaysia; you all make up part of my life. I also wish to thank all my friends outside academia for their long lasting friendship. Lastly, I am deeply thankful to my husband, Kean-Jin Lim, for always believing in me, standing by my side, and offering his comfort and help whenever they are needed.

LIST OF ORIGINAL PUBLICATIONS

This thesis is based on the following publications:

I **Chong S-L**, Koutaniemi S, Virkki L, Pynnönen H, Tuomainen P, Tenkanen M (2013) Quantitation of 4-*O*-methylglucuronic acid from plant cell walls. *Carbohydrate Polymers* 91:626-630

II **Chong S-L**, Nissilä T, Ketola RA, Koutaniemi S, Maceluch MD, Mellerowicz EJ, Tenkanen M, Tuomainen P (2011) Feasibility of using atmospheric pressure matrix-assisted laser desorption/ionization with ion trap mass spectrometry in the analysis of acetylated xylooligosaccharides derived from hardwoods and *Arabidopsis thaliana*. *Analytical & Bioanalytical Chemistry* 401:2995-3009

III **Chong S-L**, Koutaniemi S, Juvonen M, Maceluch MD, Mellerowicz EJ, Tenkanen M. Glucuronic acid in *Arabidopsis thaliana* xylans carries a novel pentose substituent. *Submitted*

IV **Chong S-L**, Virkki L, Maaheimo H, Juvonen M, Maceluch MD, Koutaniemi S, Roach M, Sundberg B, Tuomainen P, Mellerowicz EJ, Tenkanen M (2014) *O*-acetylation of glucuronoxylans in *Arabidopsis thaliana* wild type and its change in xylan biosynthesis mutants. *Glycobiology* 24: 494-506

V **Chong S-L**, Battaglia E, Coutinho PM, Henrissat B, Tenkanen M, de Vries R (2011) The α-glucuronidase Agu1 from *Schizophyllum commune* is a member of a novel Glycoside Hydrolase family (GH115). *Applied Microbiology and Biotechnology* 90:1323-1332

VI **Chong S-L**, Maceluch MD, Koutaniemi S, Gómez LD, McQueen-Mason SJ, Tenkanen M, Mellerowicz EJ. An active fungal GH115 α-glucuronidase produced in *Arabidopsis thaliana* does not change the decoration pattern of glucuronoxylans. *Submitted*

ABBREVIATIONS

AcGX	(*O*-acetyl)glucuronoxylans
ACN	acetonitrile
AE	Acetyl Esterase
AXE	Acetyl Xylan Esterase
AGX	arabinoglucuronoxylans
AIR	Alcohol Insoluble Residues
AP-MALDI	Atmospheric Pressured-Matrix-Assisted Laser Desorption Ionization
Ara(*f*)	arabinose (arabinofuranosyl)
AXE	Acetyl Xylan Esterase
CAZy	Carbohydrate-Active enZymes
CE	Capillary Electrophoresis
CWI	Cell Wall Integrity
D_2O	deuterium oxide
DA	Degree of Acetylation
DASH	DNA sequencer-Assisted Saccharide analysis in High throughput
DHB	dihydroxybenzoic acid
DP	Degree of Polymerization
DUF	Domain of Unknown Function
ESI	ElectroSpray Ionization
Gal(*p*)	galactose (galactopyranosyl)
Gal(*p*)A	galacturonic acid (galactopyranosyl uronic acid)
GAX	(glucurono)arabinoxylans
GC	Gas Chromatography
GH	Glycoside Hydrolase
Glc(*p*)	glucose (glucopyranosyl)
Glc(*p*)A	glucuronic acid (glucopyranosyl uronic acid)
Glc*f*A	glucofuranosyl uronic acid
GlcAT	glucoronosyltransferase
GT	Glycosyl Transferase
GX	glucuronoxylans
GXMT1	GX Methyl Transferase 1
GUX	GlucUronic acid substitution of Xylan
H	Hexose

HPAEC-PAD	High Performance Anion Exchange Chromatography-Pulsed Amperometric Detection
HSQC	Heteronuclear Single Quantum Coherence
IRX	IRregular Xylem
IT	Ion Trap
Man(*p*)	mannose (mannopyranosyl)
MeGlc(*p*)A	4-*O*-methylglucuronic acid (4-*O*-methylglucopyranosyluronic acid)
MFA	MicroFibril Angle
MS	Mass Spectrometry
MS^n	multistage mass spectrometry
MWCO	Molecular Weight Cut-Off
NMR	Nuclear Magnetic Resonance
OLIMP	OLIgosaccharide Mass Profiling
P	Pentose
PACE	carbohydrate gel electrophoresis
PCA	Principal Components Analysis
PCR	Polymerase Chain Reaction
PGC	Porous Graphitized Carbon
Rha(*p*)	rhamnose (rhamnopyranosyl)
RS	tetrasaccharide Reducing end Sequence
RT	Retention Time
RWA	Reduced Wall Acetylation
SDS-PAGE	sodium dodecyl sulfate-polyacrylamide gel electrophoresis
SPE	Solid Phase Extraction
TLC	Thin Layer Chromatography
TFA	triflouroacetic acid
TBL	Trichome Birefringency Like
XAX	Xylosyl Arabinosyl of Xylan
XOS	xylooligosaccharide
XG	xyloglucan
Xyl_{red}	reducing end Xyl
Xyl(*p*)	xylose (xylopyranosyl)
Xyl_t	nonreducing end Xyl
WT	Wild Type

TABLE OF CONTENT

1. INTRODUCTION

The occurrence of secondary plant cell walls is believed to have co-evolved with the emergence of vascular plants. Once the land plants adapted and colonized the land area, the competitive environment imparted a pressure to grow tall in order to battle for sun light and space, as well as for protection. The plants growing upright, accompanied by the development of branches and leaves, had driven secondary wall deposition on the weakening primary cell wall in order to strengthen the vascular stems that transport water and nutrients from roots to stem tips and branches against the force of gravity. Additionally, the stratified cell walls in plants have acted as a barrier against biotic and abiotic stresses.

A plant cell wall is primarily constituted of cellulose that is embedded in a matrix of hemicellulose, pectin, phenolics and proteins. Hemicelluloses, the second most abundant component in the cell wall, interact with cellulose via hydrogen bonding, locking the cellulose bundles in place for load-bearing support. Their structures are heterogenic, and the compositions are both tissue and species dependent. Further, they are also susceptible to modification, thereby cross-linking within themselves or with other wall components, such as pectin or lignin, to control cell growth and reinforce wall supports.

Cell wall polysaccharides represent a plentiful source of carbon on Earth that can be exploited as a renewable raw material for producing fuels, chemicals and materials. However, harnessing the greatest benefits from the structurally complex plant cell walls remains challenging. For example, cellulase hydrolysis can be inhibited by xylans that remain on cellulose fibers after pretreatment, thus more complex enzyme mixtures and higer doses can be necessary, leading to higher costs to liberate fermentable sugars (Öhgren et al., 2007). For reducing the cost of biofuel or biomaterial production, one of the viable strategies is to develop an efficient plant that is structurally tailored for an easy breakdown of cellulose or a high extractability of polysaccharides.

For the improvement of plants amenable to better cell wall digestibility or polymer extractability, the knowledge about genetic information involved in cell wall biosynthesis, as well as their effects on plant development and cell wall structure, are needed (Hao and Mohnen, 2014). Besides manipulating the endogenous genes for *in planta* modification of cell wall polysaccharides, the expression of a microbial carbohydrate active enzyme targeting specific linkages in cell wall is another approachable method (Taylor et al., 2008).

O-acetylglucuronoxylans (AcGX) are the major hemicelluloses found in the secondary cell wall of dicotyledon species. The abundant genetic resources available in the dicot model plant *Arabidopsis thaliana* have promoted a rapid growth in AcGX biosynthetic studies. Analytical techniques, such as nuclear magnetic resonance spectroscopy (Peña et al., 2007), mass spectrometry (Bauer, 2012), high performance liquid chromatography (Ordaz-Ortiz et al., 2005), and electrophoresis (Mortimer et al., 2010) used for xylan structural studies have shown to be useful for identifying differences in the structure of xylans. Moreover, in-situ labeling of xylans or their side chain epitodes using specific antibodies (Pattathil et al., 2010) has allowed the localization of the tissue specific xylans. However, considering the heterogenic structure in xylans, more selective tools are needed for detailed structural studies, especially to characterize the changes in substituents that imply possible altered interactions with other wall components. In addition, quantitation of the monomeric sugars in a cell wall polysaccharide, typically carried out with chromatographic methods, is important to measure the changes in cell wall chemistry.

This thesis reviews the structural variations, biosynthesis, and modification of AcGX in plant cell walls, as well as the analytical methods employed for xylan compositional and structural studies. The experimental part summarizes the production of an authentic 4-*O*-methylglucuronic acid (MeGlcA) standard for comparing the accuracy of MeGlcA quantitation using GlcA as a standard (paper **I**); the development of the xylan OLIgosaccharide Mass Profiling method for structural studies of AcGX, and the comparison of altered xylan structures in the biosynthetic mutants (paper **II, III** & **IV**); as well as the *in planta* modification of (Me)GlcA in AcGX using a microbial glycoside hydrolase family 115 α-glucuronidase (paper **V** & **VI**). The results are discussed and concluded.

2. REVIEW OF THE LITERATURE

2.1. Xylan structures

2.1.1. Plant cell walls

Following the division from vascular cambium, the progenitor cells continue differentiating to attain their final functional forms. The growing cells are cemented by middle lamella and casted by a thin layer of primary wall that is strong but dynamic, as it confers support to withstand mechanical stress and is capable of controlled modification to allow cell expansion (Somerville et al., 2004). Additionally, the primary wall is hydrolyzable by endogenous enzymes, liberating fragment oligosaccharides that function as the regulatory elements provoking defense against pathogenic attack (McNeil et al., 1984). When cell growth ceases, cell wall synthesis continues in some cell types by depositing a thicker layer, the secondary wall, at the interior part of primary wall to strengthen wall support. In the course of secondary wall deposition, onset of programed cell death is necessary to create the vacant cell hollow that is needed for water transport and wall support (Kenrick and Crane, 1997).

The primary wall entities are highly complex and dynamic, thus their detailed structures are probably spatial and temporal depending on the plant developmental stage. For the average structure, the main constituent is cellulose, followed by hemicelluloses, pectins and structural proteins (**Table 1)** (McNeil et al., 1984). The composition of hemicelluloses is species-dependent, wherein the type I primary wall commonly found in dicots, non-commelinid monocots and gymnosperms (also known as conifers), is constituted of xyloglucan (XG) (McNeil et al., 1984; Vogel, 2008). The type II primary wall is found in commelinid monocots, harbors (glucurono)arabinoxylans (GAX). In addition, within the commelinid monocots, the primary wall in the family of poaceae (also known as grasses) contains a significant amount of mixed linkage β-glucan (**Table 1**) (Vogel, 2008).

The primary wall organization has been postulated for many years, yet the theory is still evolving (Carpita and Gibeaut, 1993; Cosgrove, 2005; Park and Cosgrove, 2012). The cellulose is formed by (1→4)-linked β-glucan chains that are bundled into microfibrils via hydrogen bonding (Cosgrove, 2005). The cellulose microfibrils are the load-bearing substances, and also interact with hemicellulose via hydrogen bonding, forming a tethered network that is embedded in a matrix of hydrophilic gel like pectic polysaccharides (**Figure**

1) (Carpita and Gibeaut, 1993; Cosgrove, 2005). In dicots, the xyloglucan-cellulose structural network resists the turgor driven tensile stress and also regulates wall expansion (Cosgrove, 2005). Wall loosening is required prior to enlargement and that can be aided by endoglucanase hydrolysis within the non-crystalline region of the microfibril cellulose (Mellerowicz, 2006), or by non-covalent disruption with an acidic protein, such as expansin, which is capable of inducing cell wall stress relaxation by disrupting the hydrogen bonding between the glucan chains (Cosgrove, 1999). Additionally, the wall might also be extendable by cutting an XG chain and re-integrating the new end to another existing, or nascent, XG chain by the enzymatic activity of the xyloglucan endotransglucosylase/hydrolase (XTH) present in the primary wall (McNeil et al., 1984).

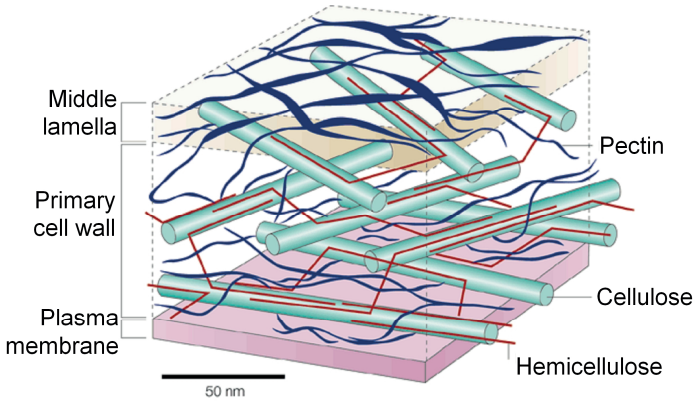

Figure 1. The primary cell wall model (reproduced from Smith, (2000) with permission).

The secondary wall synthesis may initiate before cell expansion ceases (Fromm, 2013). It contains three interlayers (S1, S2 and S3) (**Figure 2**) that are rich in cellulose, xylan and lignin, and to a lesser extent, pectin (**Table 1**). Unlike the primary wall that is rich in gel-like pectic polysaccharides, the secondary wall is dehydrated, and filled with the hydrophobic lignins. Thus, the secondary wall is waterproofing to facilitate water conduction (Donaldson, 2001). The secondary wall architecture is highly compact since it is enriched in cellulose microfibrils (50%) that are organized at an angle correlating to the longitudinal cell axis,

which defines the stiffness and mechanical property of the wall (Barnett and Bonham, 2004). The microfibril angle (MFA) varies between three interlayers, of which the thickest layer, S2, possesses the smallest MFA and the highest stiffness (Fromm, 2013). Xylans are hypothetically entrapped in the cellulose microfibrils via hydrogen bonding, whereas lignins that are polymerized in the presence of peroxidases and laccases (Donaldson, 2001) may interact either covalently or non-covalently with xylans, reinforcing wall support. The detail association between the secondary wall components remains elusive and will be subject to many more years of investigation. Nonetheless, many details related to secondary wall synthesis have been revealed, aided by advancements in molecular genetics and analytical tools developed for cell wall structural studies. The remaining sections of the literature review will focus on the current understanding towards xylan structures, biosynthesis and modifications, as well as the compositional and structural studies of xylans using various analytical tools.

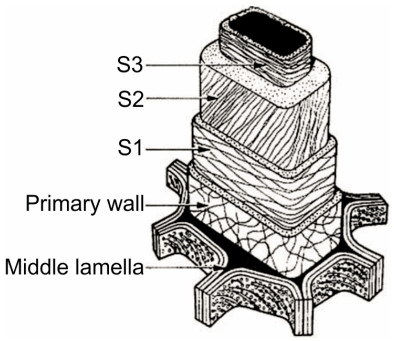

Figure 2. Wood fiber, or tracheid, showing a three-layered secondary wall (S1, S2, S3). (reproduced from Barnett and Bonham, (2004) with permission.)

Table 1. Typical biopolymers present in the primary and secondary cell walls of conifer, dicot and grass. The composition may vary according to tissue types.

	Primary wall			Secondary wall		
	Conifer	**Dicot**	**Grass**	**Conifer**	**Dicot**	**Grass**
Cellulose	20-30[f]	33[c]	20-40[c]	40[g]	45-50[a]	35-45[a]
Hemicellulose						
Glucuronoxylan	-	-	-	-	20-30[d]	-
Glucuronoarabinoxylan	2[d]	5[a,d]	20-40[a,d]	5-15[d]	-	40-50[a,d]
Xyloglucan	10[d]	20-25[a,d]	1-5[a,d]	-	±[a,d]	±[a,d]
β-Glucan	-	-	10-30[a]	-	-	±[a,d]
Glucomannan	5-10[f]	3-5[d]	2[a]	10-30[d]	2-5[a,d]	0-5[a]
Pectin	+	20 - 35[a,b]	2 - 10[b]	±[h]	±[a]	±[a]
Structural protein	+	10[a]	±[a]	+	±[a]	±[a]
Lignin	+	±[a]	±[a]	27[g]	20[e]	7-10[e]

a, Vogel, 2008; b, Mohnen, 2008; c, Caffall and Mohnen, 2009; d, Scheller and Ulvskov, 2010; e, Ishii, 1997; f, O'Neill and York, 2003; g, Sjöström, 1993; h, Timell, 1967; +, present but quantitative amount unknown; ±, minor amount; -, not detected.

2.1.2. Xylan structural variation in dicots and grasses

The architecture of plant cell walls is evolving in the course of adaptation for survival and reproduction (Sarkar et al., 2009). Cellulose microfibrils in the cell wall are indispensable for land plants and their presence has been traced back to multicellular green algae, charophytes, which might be the closest ancestor to land plants (Niklas, 2004). Xylans are found in the algae polysaccharides as well, among which, most of the backbone is either constituted by (1→4)-, (1→3)- or (1→3; 1→4)-linked β-xylopyranosyl (Xyl*p*) residues (Deniaud et al., 2003; Ebringerová and Heinze, 2000; Popper and Tuohy, 2010). However, the xylans present in the vascular plants appear to be restricted to β-(1→4)-linked xylans that are substituted by (1→2)-linked 4-*O*-methyl-α-D-glucopyranosyl uronic acid (MeGlc*p*A) and/or α-D-

glucopyranosyl uronic acid (Glc*p*A), which are also known as glucuronoxylans (GX) (Ebringerová and Heinze, 2000).

The structures of xylans (**Table 2**) have been studied in detail in the seed bearing plants gymnosperm and angiosperm, probably due to their economic importance and plentiful availability. In gymnosperms, GX are the second most abundant hemicellulose after galactoglucomannan, in which the backbone is decorated by (1→3)-linked α-arabinofuranosyl (Ara*f*) residues. Therefore, they are referred to as arabinoglucuronoxylans (AGX) (Ebringerová and Heinze, 2000). GX mainly found in the secondary wall of dicots are highly acetylated at the 3-*O* and/or 2-*O* positions of Xyl*p* residues (Evtuguin et al., 2003; Teleman et al., 2000). In addition, the reducing end of the GX backbone of several dicot and gymnosperm species is linked with a tetrasaccharide sequence (β-D-Xyl*p*-(1→3)-α-L-Rha*p*-(1→2)-α-D-Gal*p*A-(1→4)-β-D-Xyl) (Andersson et al., 1983; Johansson and Samuelson, 1977; Peña et al., 2007).

The xylans in grasses have diverged so that the xylan backbone is substituted by (1→3)-linked α-Ara*f* and have less acetyl side groups (Ebringerová and Heinze, 2000). The xylan backbone may not carry a tetrasaccharide sequence at the reducing end since the evidence is still lacking (Kulkarni et al., 2013). Nonetheless, the nonsystematic addition of Ara*f* and/or Glc*p*A residues at the reducing end and penultimate Xyl*p* residues has been observed in the arabinoxylan isolated from wheat endospermic tissue (Ratnayake et al., 2014). The endospermic cell walls in grains of grasses contain different types of xylans as the backbone is substituted by (1→3)- and/or (1→2)-linked α-Ara*f* and a minor amount of (Me)Glc*p*A (Ratnayake et al., 2014), thus they are otherwise known as arabinoxylans.

2.1.3. Further branching in xylans of dicots and grasses

Further branching at the side groups of xylans may indicate the interactions with other wall components. Though the examples of such were scarcely found in dicots, the GX in eucalyptus carry an α-galactopyranosyl (Gal*p*) or β-glucopyranosyl (Glc*p*) residue at the MeGlc*p*A side branch (**Table 2**) (Shatalov et al., 1999). The α-Gal*p* and β-Glc*p* substitutions are speculated to form cross-links between GX and rhamnogalaturonan or glucan, but this is yet to be confirmed. Additionally, the covalent linkage between GX and lignins has been

implicated by the detection of lignin carbohydrate complex (LCC) in the lignin isolate (Balakshin et al., 2007; Takahashi and Koshijima, 1988).

Esterification of the hydroxycinnamic acid derivatives ferulic and *p*-coumaric acid at 5-*O* position of the α-(1→3)-linked Ara*f* residue is commonly found in (glucurono)arabinoxylan (GAX) of grasses (Ishii, 1997). Furthermore, further branching at the feruloylated Ara*f* (FA-Ara) have been identified, and these include FA-Ara carrying a Xyl*p* residue at 2-*O* position of α-Ara*f* (Wende and Fry, 1997), with the Xyl*p* side group being further substituted by a Gal*p* residue (Appeldoorn et al., 2013). The ferulate substituents are dimerized by an oxidative reaction to cross-link two adjacent xylan chains, thereby rigidifying the cell wall to attain higher recalcitrance and controlled cell growth (de O. Buanafina, 2009). Apart from the feruloylation of GAX, a disaccharide side branch also found in some grass species consisting β-(1→2)-linked Xyl*p* substituted at the α-(1→3)-linked Ara*f* side group (Chiniquy et al. 2012; Hoije et al., 2006; Pastell et al., 2009).

Table 2. Xylan compositions in gymnosperm, dicotyledon and commelinid monocotyledon species

	Backbone	**Substituents**			**Further branching**	**Reference**
	Xyl*p* β(1→4)	(Me)Glc*p*A α(1→2)	Ara*f* α(1→3)	Ac esterified 3-*O* and/or 2-*O*		
Gymnosperm	+	+	+	-	-	Ebringerová and Heinze, 2000; Jacobs and Dahlman, 2001
Angiosperm						
Dicotyledon	+	+	±	+	α-Gal*p*-(1→2)-α-MeGlc*p*A	Evtuguin et al., 2003; Naran et al., 2009; Shatalov et al., 1999; Teleman et al., 2000
Commelinid monocotyledon (grass)	+	+	+*	+	β-Xyl*p*-(1→2)-α-Ara*f* β-Xyl*p*-(1→2)(5-*O*-feruloyl)-α-L-Ara*f* α-Gal*p*-(1→2)-β-Xyl*p*-(1→2)(5-*O*-feruloyl)-α-L-Ara*f*	Appeldoorn et al., 2013; Chiniquy et al., 2012; Obel et al., 2002; Pastell et al., 2009; Wende and Fry, 1997

Xyl*p*, xylopyranosyl; (Me)Glc*p*A, (4-*O*-methyl)glucopyranosyl uronic acid; Ara*f*, arabinofuranoyl; Ac, acetyl; Gal*p*, galactopyranosyl; +, present; -, not detected; *, α-(1→3)- and/or (1→2)-linked Ara*f* in grains of grass; ±, minor amount

2.2. CAZymes hydrolyzing xylans

2.2.1. Xylan backbone acting enzymes

The Carbohydrate-Active enZymes (CAZymes) are found in all forms of life, including archaea, bacteria and eukaryotes. In plants, they are important for the biosynthesis and remodeling of cell wall polysaccharides in response to different developmental stages (Aspeborg et al. 2006; Chin et al., 1999; Geisler-Lee et al., 2006). On the other hand, microbes are capable of secreting a cocktail of CAZymes to decompose biomass for food, and also to facilitate invasion (Choi et al., 2013). The enzyme entries in the CAZy database (http://www.cazy.org/) are classified into different families based on their amino acid sequence similarities and protein hydrophobic clustering (Henrissat, 1991).

The complete breakdown of the structurally heterogenic *O*-acetylglucuronoxylans (AcGX) requires the concerted action of various xylanolytic enzymes (**Figure 3**). The dominant enzymes are β-1,4-xylanase (EC 3.2.1.8) cleaving the backbone of β-(1→4)-linked xylan, which primarily belong to glycoside hydrolase (GH) families GH10 and GH11. In GH10 endoxylanases, the catalytic active site +1 tolerates a substituted Xyl*p* residue, while the -1 subsite requires a non-substituted Xyl*p* residue. As a result, α-MeGlc*p*A-(1→2)-β-Xyl*p*-(1→4)-β-Xyl*p*-(1→4)-β-Xyl (UXX; Fauré et al., 2009) was the shortest acidic xylooligosaccharide (XOS) released by GH10 endoxylanase from deacetylated GX (Biely et al., 1997). Apart from that, the subsites -2 and -1 in GH10 endoxylanase require productive substrate binding for an active hydrolytic action (Biely et al., 1997; Collins et al., 2005; Kolenová et al., 2006). The catalytic action of GH11 endoxylanase is more restrictive since the +1 catalytic site can only accommodate a non-substituted Xyl*p* residue, thus β-Xyl*p*-(1→4)-[α-MeGlc*p*A-(1→2)]-β-Xyl*p*-(1→4)-β-Xyl*p*-(1→4)-β-Xyl (XUXX) was the shortest XOS produced from the hydrolysis of GX (Biely et al., 1997).

The microbial GH30 endoxylanases exhibit a totally different mode of action as the enzymes strictly require a (Me)Glc*p*A substituted Xyl*p* residue to catalyze the reaction. The final products released are a mixture of acidic XOS carrying MeGlc*p*A at the penultimate Xyl*p* residue from the reducing end (St. John et al., 2006; Vršanská et al., 2007). However, the minor xylanase, XYN IV produced by *Trichoderma reesei* Rut C30 is not a (Me)Glc*p*A dependent enzyme as it shows exo-hydrolytic activity by releasing Xyl*p* residue from the reducing end of linear or branched XOS (Tenkanen et al., 2013).

The β-1,4-xylosidases (EC 3.2.1.37) involved in the final breakdown of GX. This is an exo-hydrolytic enzyme liberating a Xyl*p* residue from the nonreducing end of XOS. The GH3 β-xylosidases form the largest family. This enzyme produced by *T. reesei* Rut C30 was able to hydrolyze xylobiose, as well as xylan polymers albeit more slowly (Margolles-Clark et al., 1996). The enzymatic action of β-xylosidases was impeded by the substituted XOS e.g. MeGlc*p*A-XOS, thus produced XOS carrying a MeGlc*p*A at the nonreducing end (Tenkanen et al., 1996). In addition, the Ara*f* substituents were more restrictive as the final product released was the XOS harboring an Ara*f* substituent at the penultimate Xyl*p* from the nonreducing end (Tenkanen et al., 1996).

2.2.2. Accessory enzymes

Accessory enzymes are involved in side group removal and modification. The synergistic actions between accessory enzymes and xylanases, as well as β-xylosidases, are necessary to hydrolyze the heteroxylans effectively. α-Glucuronidases (EC 3.2.1.131) cleave the α-(1→2) linkage between (Me)Glc*p*A and Xyl*p* residues in XOS or GX. The α-glucuronidases belonging to GH67 act only on (Me)Glc*p*A α-(1→2)-linked to the nonreducing end Xyl*p* residues in short XOS. Thus, they require cooperation from endoxylanase and β-xylosidase to liberate (Me)Glc*p*A effectively from GX polymers (Siika-aho et al., 1994; de Vries et al., 1998; Choi et al., 2000; Lee et al., 2012b). The α-glucuronidases of the other family GH115 are acting on the internal (Me)Glc*p*A and are active towards GX polymers (Kolenova et al., 2010; Ryabova et al., 2009; Tenkanen and Siika-aho, 2000).

Two types of esterases, acetyl esterase (AE; EC3.1.1.6) and acetyl xylan esterase (AXE; EC 3.1.1.72), are classified into carbohydrate esterase (CE) families (Biely, 2012). They remove the acetyl groups esterified on xylans and are differing in their substrate and positional specificities. AEs act on XOS, whereas AXEs are active on AcGX polymers in addition to XOS. The CE1, 5 and 6 AXEs were capable of deacetylating 2-*O* and 3-*O* position in the mono- or di-acetylated Xyl*p* residues (Koutaniemi et al., 2013; Uhliariková et al., 2013) with a high preference to the 2-*O* position (Biely et al., 2011). In contrast, the CE4 AXEs were only active on 2-*O* or 3-*O* acetylated Xyl*p* residue (Uhliariková et al., 2013). None of these enzymes were able to deacetylate the 3-*O* acetylated Xyl*p*, which also carried a MeGlc*p*A residue. The CE16 exo-AEs acted on this structural compound only when both MeGlc*p*A and

acetyl residues were placed on the nonreducing end of XOS aided by the cooperative enzymatic actions of endoxylanase and β-xylosidase (Biely et al., 2014; Koutaniemi et al., 2013). Therefore, MeGlc*p*A and acetyl side groups in the GX could be (almost) completely removed with the synergistic actions of a multitude of xylanolytic enzymes i.e. CE1 or 5 AXE, CE16 AE, GH10/GH11 endoxylanase, β-xylosidase, and GH115 α-glucuronidase (Biely et al., 2014; Koutaniemi et al., 2013).

The GAX in grasses require more tools for debranching compared to the AcGX in dicots. The α-arabinofuranosidases (EC3.2.1.55) remove the terminal α-Ara*f* (1→2) and/or (1→3) linked to the backbone of GAX (Saha, 2000). Some of the α-arabinofuranosidases act only on the (1→2)- and (1→3)-linked mono-substituted Ara*f*, whereas, others are able to release an Ara*f* residue from the C3 position of doubly substituted Xyl*p* in the xylan backbone (Pastell et al., 2008). The ester linkage between ferulic acid or *p*-coumaric acid and xylans is cleaved by the feruloyl esterases (EC 3.1.1.73) (Fazary and Ju, 2007).

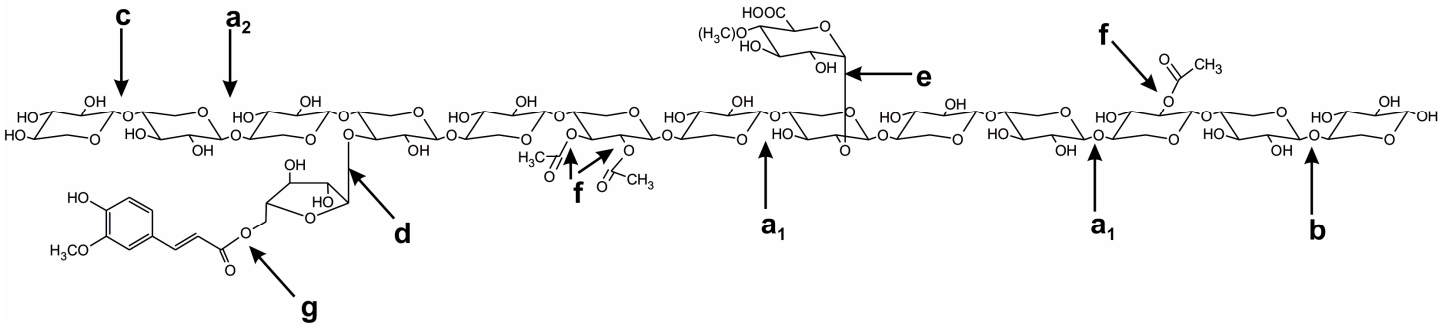

a$_1$, GH10 endo-β-1,4-xylanase (EC3.2.1.8)
a$_2$, GH11 endo-β-1,4-xylanase (EC3.2.1.8)
b, exo-β-1,4-xylanase (EC 3.2.1.156)
c, β-xylosidase (EC 3.2.1.37)
d, α-arabinofuranosidase (EC 3.2.1.55)
e, α-glucuronidase (EC 3.2.1.131)
f, acetyl xylan esterase (EC 3.1.1.72)
g, feruloyl esterase (EC 3.1.1.73)

Figure 3. Hypothetical strucutre of (glucurono)arabinoxylan (GAX), and the Carbohydrate Active enZymes (CAZymes) responsible for the hydrolysis of backbone (a-c) and substituents (d-g) of GAX.

2.3. Xylan biosynthesis

2.3.1. Synthesis of reducing end sequence and xylan backbone in Arabidopsis

The genes involved in secondary wall formation were previously discovered by identification of collapsed or deformed xylems in the Arabidopsis mutant plants (Turner and Somerville, 1997). The IRregular Xylem (IRX) phenotype resulted from negative pressure generated during water transport through cells with altered secondary walls. Specifically, *irx1*, *irx3* and *irx5* mutants lacked in cellulose content, and the defected genes were responsible for the cellulose biosynthesis in the secondary wall (Turner and Somerville, 1997). Using the IRX1, IRX3 and IRX5 encoding genes as the indicators, global gene expression analyses identified potential glycosyltransferases (GT) (Coutinho et al., 2003) involved in AcGX biosynthesis based on their co-expression patterns during secondary wall formation (Brown et al., 2005; Persson et al., 2005). The co-expression data, coupled with reverse genetic analyses, have contributed to an understanding of AcGX biosynthesis in the secondary wall (**Table 3**).

IRX7/F8H (member of GT47); and IRX8 and PARVUS (members of GT8) were hypothesized to be responsible for synthesizing different linkages in the reducing end sequence (RS) (Lee et al., 2007; Peña et al., 2007; Scheller and Ulvskov, 2010). The knock-out mutants lack the RS in GX and have decreased xylan content (Brown et al., 2007; Lee et al., 2007; Peña et al., 2007; Zhong et al., 2005). Heterologous production of the recombinant proteins was mostly inactive. However, the recombinant IRX7 showed xylosyltransferase activity when tested against a broad set of sugar acceptors (Scheller and Ulvskov, 2010), thus the IRX7 enzyme is likely involved in transferring UDP-α-Xyl to the terminal rhamnose in RS. Two hypotheses have been proposed for the function of RS: 1) it might work as a primer for initiating the synthesis of xylans, and 2) the xylan backbone synthesis is terminated by the RS to thereby control the degree of polymerization (DP) (Hao and Mohnen, 2014; Peña et al., 2007; Scheller and Ulvskov, 2010).

IRX9, I9H/IRX9L, IRX14, and I14H/IRX14L (members of GT43); and IRX10 and IRX10L (members of GT47) were implicated in the elongation of the GX backbone (Brown et al., 2007; Brown et al., 2009; Lee et al., 2010; Peña et al., 2007; Wu et al., 2009; Wu et al., 2010). The *irx9*, *irx14*, and *irx10* x *irx10-l* double mutants exhibited low xylosyltransferase activity; thus, a shorter GX backbone and impaired xylan content were detected in these mutants

(Brown et al., 2007; Brown et al., 2009; Lee et al., 2010). The function of IRX9 and IRX14 were non-redundant since the expression of IRX9 in the *irx14* mutant, or vice versa, did not help to rescue the phenotype (Lee et al., 2010; Wu et al., 2010). In addition, the expression of rice OsIRX9 and OsIRX9L, and OsIRX14 homologs in *irx9* and *irx14*, respectively, were able to complement the xylose content, molecular mass and stem strength comparable to that of the wild type plant (Chiniquy et al., 2013), showing that these genes, essential for backbone elongation, were conserved in the commelinid monocot lineage.

Methylation of the Glc*p*A side group was increased in the mutants of backbone formation and reducing end sequence biosynthesis, which showed that the methylation activity was not compromised by reduced xylosyltransferase activity or missing reducing end sequence (Peña et al., 2007; Brown et al. 2007; Brown et al. 2009; Wu et al. 2009; Wu et al. 2010).

2.3.2. Addition of side groups in xylans of Arabidopsis and grasses

Several members of GT8 were implied for the addition of Glc*p*A onto the backbone of AcGX. The knockout of GUX1 and GUX2 in Arabidopsis had led to a remarkable reduction of (Me)Glc*p*A substituents in AcGX (Mortimer et al., 2010). The GUX1 and GUX2 enzymes were responsible for different patterns of GlcA decorations on the xylan backbone (Bromley et al., 2013). The major domain was formed by GUX1 adding Glc*p*A substituents on evenly spaced Xyl*p* residues, preferably at the intervals of 6, 8 and 10 non-substituted Xyl*p* residues. On the other hand, the GUX2 decorated the GX with no preference toward even or odd spacing. Biochemical analysis of GUX1 *in vitro* showed that this enzyme has a high preference toward longer XOS, and preferably added Glc*p*A onto a second Xyl*p* residue from the reducing end of xylohexaose (Rennie et al., 2012). Other members of GT8, GUX3 and GUX4, were also implied for their glucuronyltransferase activities via *in vitro* analysis of the overexpressing plants (Lee et al., 2012a; Rennie et al., 2012). No significant phenotypic change was observed in the *gux1gux2* mutant despite the Glc*p*A moieties missing in xylans (Mortimer et al., 2010). However, the simultaneous knockout of GUX1 and GUX2, together with GUX3, led to detrimental growth effects (Lee et al., 2012a).

Methylation of GlcA is carried out by the transferase activity of a DUF579 family protein: GX Methyl Transferase 1 (GXMT1) in the Golgi (Urbanowicz et al., 2012). The GXMT1 was

shown to preferably methylate Glc*p*A linked to xylan compared to Glc*p*A or UDP-Glc*p*A, suggesting that the methylation of Glc*p*A occurs after the Glc*p*A is added on to the xylan backbone.

The acetylation of xylans involved at least two different types of proteins in Arabidopsis: 1) Reduced Wall Acetylation (RWA) family members (1/2/3/4) (Manabe et al., 2011; Lee et al., 2011), which are thought to act as transporters for the acetyl-CoA to the Golgi, and 2) TBL29, a member of the large Trichome Birefringency-Like family, which is an acetyltransferase with high specificity for xylans (Gille and Pauly, 2012; Xiong et al., 2013; Yuan et al., 2013; Urbanowicz et al., 2014). The RWA proteins have wider and redundant specificities, in which the RWA3 and RWA4 proteins have a preference for xylan acetylation (Manabe et al., 2013). Recently, *in vitro* analysis showed that the recombinant TBL29/ESK1 protein catalyzed the transfer of acetyl residues from acetyl-CoA on to either 2-*O* or 3-*O* position of Xyl*p* residues, indicating that this enzyme is only specific to mono-acetylation (Urbanowicz et al., 2014). The knockout of RWA1/2/3/4 and TBL29/ESK1 had led to a 42% (Lee et al., 2011) and 60% reduction of acetyl content in GX, respectively (Xiong et al., 2013; Yuan et al., 2013).

The members of GT61 are involved in the addition of Ara*f* or Xyl*p* substitutent in the xylans of grasses. Two members of GT61 in wheats, *Ta*XAT1 and *Ta*XAT2, are implicated as the arabinotransferases specific to the 3-*O* position of Xyl*p* residue (Anders et al., 2012). In addition, a member in rice: Xylosyl Arabinosyl of Xylan 1 (XAX1) is the xylosyltransferase adding a xylosyl unit on to the (1→3)-linked Ara*f* substituent, forming the β-Xyl*p*-(1→2)-α-Ara*f* disaccharide side branch in xylans (Chiniquy et al., 2012).

Table 3. Enzymes responsible for xylan biosynthesis in Arabidopsis

Activity	Enzyme name	Gene identifier	CAZy/ Protein family	Reference
RS	PARVUS/GLZ1	At1g19300	GT8	Lao et al., 2003; Lee et al., 2007
RS	IRX8	At5g54690	GT8	Brown et al., 2007; Peña et al., 2007
RS	IRX7/FRA8	At2g28110	GT47	Brown et al., 2007; Zhong et al., 2005
RS	F8H	At5g22940	GT47	Lee et al., 2009; Wu et al., 2010
DP	IRX9	At2g37090	GT43	Brown et al., 2007; Peña et al., 2007
DP	IRX9L/I9H	At1g27600	GT43	Lee et al., 2010; Wu et al., 2010
DP	IRX14	At4g36890	GT43	Brown et al., 2007; Peña et al., 2007
DP	IRX14-L/I14H	At5g67230	GT43	Lee et al., 2010; Wu et al., 2010
DP	IRX10	At1g27440	GT47	Brown et al., 2009; Wu et al., 2009
DP	IRX10-L	At5g61840	GT47	Brown et al., 2009; Wu et al., 2009
Glc*p*A addition	GUX1	At3g18660	GT8	Mortimer et al., 2010
Glc*p*A addition	GUX2	At4g33330	GT8	Mortimer et al., 2010
Glc*p*A addition	GUX3	At1g77130	GT8	Lee et al., 2012a
Glc*p*A addition	GUX4	At1g54940	GT8	Rennie et al., 2012
Methylation of Glc*p*A	GXMT1	At1g33800	DUF579	Urbanowicz et al., 2012
Acetylation	TBL29/ESK1	At3g55990	TBL29	Xiong et al., 2013; Yuan et al., 2013
Acetylation	RWA1	At5g46340		Manabe et al., 2011; Lee et al., 2011
Acetylation	RWA2	At3g06550		Manabe et al., 2011; Lee et al., 2011
Acetylation	RWA3	At2g34410		Manabe et al., 2011; Lee et al., 2011
Acetylation	RWA4	At1g29890		Manabe et al., 2011; Lee et al., 2011

DP, Degree of Polymerization; DUF, Domain of Unknown Function; RS, tetrasaccharide Reducing end Sequence; TBL, Trichome Birefringency Like

2.4. *In planta* xylan modification with a microbial enzyme

In planta production of an exogenous enzyme offers the advantage of targeting specific linkages in cell wall polysaccharides for affecting polymer compositions and properties. For the expression of microbial xylanolytic enzymes *in planta* (**Table 4**), endoxylanase can be a tool for degrading the xylan backbone to thereby increase the accessibility of other lignocellulolytic enzymes in plant cell walls. Likewise, *in vitro* analysis shows that the endoxylanase works synergistically with cellulases to improve the liberation of fermentable sugars from pretreated lignocellulosic materials (Hu et al, 2013). The recombinant endoxylanases produced in plants have been either targeted to the apoplast (Borkhardt et al., 2010; Buanafina et al., 2012; Herbers et al., 1995; Weng et al., 2013; Yang et al., 2007) or intracellularly produced (Bae et al., 2008; Buanafina et al., 2012; Kimura et al. 2003; Patel et al., 2000). Generally, the phenotype of corresponding transgenic plants is similar to their wild type counterparts. Exceptions include defected growth phenotypes when the endoxylanase accumulates in the cyotosol (Bae et al., 2008), wheat grain (Harholt et al., 2010), or golgi and apoplast (Buanafina et al., 2012). Xylans were solubilized better in the *Dictyoglomus thermophium* XynA and Xyn B expressing plants after heat treatment of the stem tissues, and thus rendered the cell wall to improved saccharification efficiency (Borkhardt et al., 2010).

Expression of the side group modifying enzymes can be attempted to disrupt the covalent or non-covalent interaction between xylans and other cell wall components. The expression of *Aspergillus nidulans* acetyl xylan esterase (AnAXE), feruloyl esterase (AnFAE), α-arabinofuranosidase/β-xylosidase (AnXA) and the *Xanthomonas oryzae* α-arabinofuranosidase (XoAF) has succeeded in Arabidopsis, and no phenotypic changes were observed (Pogorelko et al., 2011; Pogorelko et al., 2013). On the other hand, the expression of a CE15 glucuronyl esterase (EC3.1.1-), an esterase hydrolyzing the ester linkage between (Me)GlcA and lignin, induced an early senescence of leaves, reduced plant height and delayed flowering in Arabidopsis (Tsai et al., 2012). Xylan extraction was improved in the CE15 glucuronyl esterase expressing plant, and this is likely due to the disruption of intermolecular linkages in corresponding transgenic lines (Tsai et al., 2012). Cell wall digestibility was mildly improved in the AnFAE-, AnXA- and XoAF-expressing plants, but not in the AnAXE-expressing plant, although acetyl content was moderately reduced. This suggests that deacetylation may result in tighter interactions of the xylan chains and cellulose in the cell wall, as acetylation restricts association between xylan chains as well as adsorption to cellulose fibrils.

Table 4. Production of microbial xylanolytic enzymes in plants

Enzymes	Source	Host	Site	Reference
β-1,4-Endoxylanase				
XynZ (GH10)	*Clostridium thermocellum*	Tobacco	apoplast	Herbers et al., 1995
XynA (GH11)	*Neocallimastrix patriciarum*	Barley	grain	Patel et al., 2000
XynA (GH11)	*Clostridium thermocellum*	Rice	grain, cytoplasm	Kimura et al., 2003
XylII (GH11)	*Trichoderma reesei*	Arabidopsis	chloroplast, peroxisome	Hyunjong et al., 2006
XynB (GH11)	*Streptomyces olivaceoviridis*	Potato	apoplast	Yang et al., 2007
XynII (GH11)	*Trichoderma reesei*	Arabidopsis	chloroplast, cytosol	Bae et al., 2008
XynA (GH10), XynB (GH11)	*Dictyoglomus thermophilium*	Arabidopsis	apoplast	Borkhardt et al., 2010
XynA (GH11)	*Bacillus subtilis*	Wheat	grain	Harholt et al., 2010
XynII (GH11)	*Trichoderma reesei*	Tall fescue	apoplast, golgi, vacuole	Buanafina et al., 2012
Acetyl xylan esterase	*Aspergillus nidulans*	Arabidopsis, *Brachypodium distachyon*	apoplast	Pogorelko et al., 2011; Pogorelko et al., 2013
α-Arabinofuranosidase / β-Xylosidase	*Aspergillus nidulans*	Arabidopsis	apoplast	Pogorelko et al., 2011
α-Arabinofuranosidase	*Xanthomonas oryzae*	Arabidopsis	apoplast	Pogorelko et al., 2011
Feruloyl esterase	*Aspergillus nidulans*	Arabidopsis	apoplast	Pogorelko et al., 2011
Glucuronyl esterase	*Phanerochaete carnosa*	Arabidopsis	apoplast	Tsai et al., 2012

2.5. Compositional and structural studies of *O*-acetylglucuronoxylans

The complete structural information e.g. sugar composition, substitution pattern, ring format, sugar sequence, linkage and position of branching in a carbohydrate is obtained via a combination of various analytical tools (**Figure 4**). This section summarizes the analytical methods that have been employed for the compositional and structural analysis of AcGX.

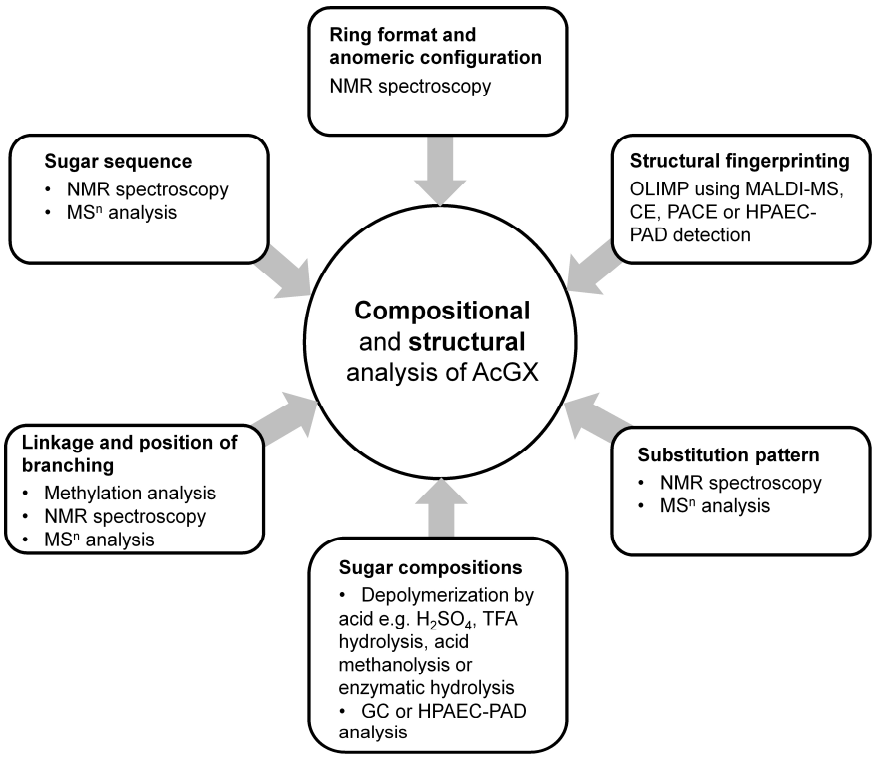

Figure 4. Analytical methods used for compositional and structural analysis of AcGX

2.5.1. Compositional analysis of non-cellulosic sugars in plant cell walls

Gas chromatography (GC) and high performance anion exchange chromatography with pulsed amperometric detection (HPAEC-PAD) are commonly used for the compositional analysis of non-cellulosic sugars in plant cell walls. Prior to the chromatographic analysis, plant polysaccharides are degraded by sulfuric acid or trifluoroacetic acid hydrolysis (De Ruiter et al., 1992), acid methanolysis (Sundberg et al., 1996) or hydrolytic enzymes (Virkki et al., 2008) to liberate individual sugars, which are then separated on a column and quantified using calibration standards.

For the compositional analysis of AcGX, the α-(1→2) linkage between (Me)Glc*p*A and Xyl*p* residue is unexceptionally stable against acid hydrolysis (De Ruiter et al., 1992; Tenkanen et al., 1995). Thus, different hydrolyzing methods might affect the liberation of MeGlc*p*A from the plant biomass. Enzymatic hydrolysis can effectively liberate (Me)Glc*p*A from xylan; however, this method is more suitable for isolated polysaccharides or severely pretreated materials than for whole plant materials (Buchert et al., 1993; Tenkanen et al., 1999). On the other hand, extensive hydrolysis may result in decarboxylation of uronic acids (Testova et al., 2011). In comparison, acid methanolysis, which depolymerizes mainly non-cellulosic polysaccharides, is effective in liberating (Me)Glc*p*A present in plant materials without prior delignification (De Ruiter et al., 1992).

2.5.2. Methylation analysis

The per-*O*-methylation of carbohydrates is carried out by substituting the proton of free hydroxyl group with a methyl group. The reaction needs to be performed in basic and anhydrous condition to achieve a high yield (Ciucanu, 2006). After methylation, carbohydrates are hydrolyzed by acid to release the partially methylated sugars that are then reduced and acetylated for analysis in a gas chromatography-MS (GC-MS) (Ciucanu and Kerek, 1984). Using this method, information regarding monosaccharide compositions and linkage of the depolymerized sugars are determined, but it is not possible to deduce the sequence of these residues in the polymer (Pettolino et al., 2012). One of the problems encountered in methylation analysis is undermethylation of the free –OH causing overestimation of branching points in the depolymerized sugars.

2.5.3. Nuclear Magnetic Resonance (NMR) spectroscopy

NMR spectroscopy is playing a major role in the structural studies of cell wall polysaccharides. The structural parameters that are measurable with NMR spectroscopy include the substitution pattern, ring format, anomeric configuration, sugar sequence, linkage and position of branching in a carbohydrate (Duus et al., 2000). Purified samples are needed for an accurate structural elucidation using NMR analysis. Therefore, the cell wall polysaccharides are generally extracted from biomass prior to the NMR measurement. For the isolation of xylan for NMR studies, GX devoid of acetyl residues are isolated in an alkaline solution that destroys any esterified components including acetyl residues (Peña et al., 2007). On the other hand, AcGX are obtained with dimethyl sulfoxide, but the recovered yield is relatively low (Evtuguin et al., 2003; Gonçalves et al., 2008; Naran et al., 2009). Of the two xylan isolation methods described above, delignification is required prior to xylan extraction. Additionally, partially degraded AcGX are obtainable via a harsher condition such as hydrothermal treatment, and delignification can be omitted in this isolation method (Teleman et al., 2000; Kabel et al., 2003; Garrote et al., 2001).

The anomeric region (5.5 - 4.4 ppm) in the ^{1}H NMR spectrum acquired from deacetylated GX is cleaner and simpler than that of AcGX (**Figure 5**). Therefore, minor peaks corresponding to the anomers of the reducing end tetrasacharides sequence can be clearly detected (**Figure 5A**) (Zhong et al., 2005). In addition, the anomers of Glc*p*A in methylated and non-methylated forms are separable, thus enabling the calculation of (Me)Glc*p*A substitution in GX (Peña et al., 2007). The chemical environment for the AcGX is highly complex, thus signals in the ^{1}H NMR spectrum are broader and overlapped (**Figure 5B**) (Evtuguin et al., 2003; Yuan et al., 2013). To overcome the problem arising from overlapping signals, two-dimensional heteronuclear single quantum coherence (HSQC) NMR spectroscopy was utilized to further divide the cross peaks into anomeric and acetyl-Xyl*p* regions (Teleman et al., 2000). The HSQC spectrum simplifies the quantitation of acetylated Xyl*p* that is present in various forms in AcGX (Gonçalves et al., 2008; Naran et al., 2009; Teleman et al., 2000).

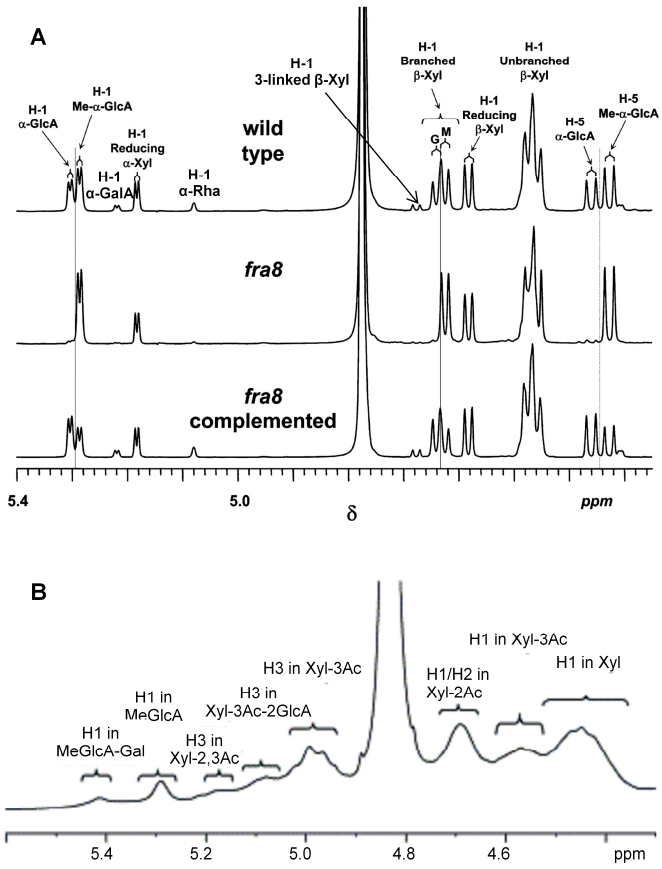

Figure 5. ^{1}H NMR spectra of (A) deacetylated glucuronoxylan (GX) isolated from Arabidopsis wild-type and mutant plants (*fra8* and *fra8* complemented; Zhong et al., 2005), and (B) *O*-acetylglucuronoxylans (AcGX) isolated from *eucalyptus globulus* (Evtuguin et al., 2003)

2.5.4. Oligosaccharide Mass Profiling (OLIMP) and MALDI-MS systems

The OLIMP method employing glycoside hydrolases solubilizes specific polysaccharides from the plant cell wall in the form of oligosaccharides, which are then analyzed by a sensitive detection system, such as matrix-assisted laser desorption ionization-mass spectrometry (MALDI-MS) (Lerouxel et al., 2002; Westphal et al., 2010). This is a specific

and sensitive method that can be utilized to fingerprint polysaccharide structural changes, using only low amounts of samples obtained via direct hydrolysis of plant tissue without prior chemical isolation. This method was first developed by Lerouxel et al. (2002), using a xyloglucan specific endoglucanase and MALDI–time-of-flight/MS (MALDI-TOF/MS) detection to elucidate the changes of xyloglucan structures in the Arabidopsis mutants. Besides using single hydrolytic enzymes, Westphal et al. 2010 have used an enzyme cocktail encompassing multiple polysaccharide (cellulose, pectin, xylan and xyloglucan) degrading enzymes to liberate several types of oligosaccharides, which were then detected using a MALDI-TOF/MS system to identify changes to the cell wall architecture in the biosynthetic mutants.

Besides MALDI-MS detection, the enzymatic hydrolyzates can be separated and quantified using a chromatographic system such as HPAEC-PAD (Ordaz-Ortiz et al., 2005; Rantanen et al., 2007), or electrophoretic methods such as capillary electrophoresis (Paulus and Klockow, 1996) and Carbohydrate gel Electrophoresis (PACE) (Goubet et al., 2002). Sample throughput is limited in PACE, as the separation time requires a few hours and only a few samples can be loaded at one time. Recently, a DNA sequencer-assisted Saccharide analysis in High throughput (DASH) system was developed by performing the capillary electrophoretic separation using a DNA sequencer (Li et al., 2013). The DASH method enables higher sample throughput, and better detection sensitivity down to fmol oligosaccharide, as well as a higher capability of separating larger oligosaccharides up to DP30 compared to that of PACE. However, oligosaccharide standards are needed for peak assignments in the chromatogram or electropherogram. Thus, analysis of the cell wall deriving enzymatic hydrolyzates is limited by the availability of the standards. Nonetheless, with the increasing interest in biomass research, many of the oligosaccharide standards derived from cell wall polysaccharides are now commercially available, making the peak identification and quantitation easier.

MALDI-MS systems

MALDI-MS is a sensitive technique for the mass profiling and structural analysis of carbohydrates. Carbohydrates are detected as [M+Na]+ in positive ion mode using 2,5-dihydroxybenzoic acid (DHB) as the matrix (Harvey, 2009). DHB yields poorer sensitivity

when carbohydrates are ionized in negative ion mode. In comparison, 2,4,6-Trihydroxyacetophenone (THAP) provides better sensitivity in negative ion mode but proper drying condition is vital to get a uniform matrix-analytes crystallization on the MALDI target plate (Papac et al., 1996). The MALDI ion source operating in vacuum condition imparts higher internal energy to the ions, causing more metastable fragmentation relative to ambient ionization (Zaia 2004). Therefore, the cleavages of labile sialic acid from sialylated carbohydrates were commonly observed upon ionization in the vacuum MALDI, and consequently, derivatization of the sialylated carbohydrates (Powell and Harvey, 1996) was needed.

Atmospheric pressure-MALDI (AP-MALDI), incorporated with an orthogonal acceleration TOF (oaTOF), was developed by Laiko et al. (2000) to analyze mixtures of peptides. The analysis of oligosaccharides has also been performed by combining the AP-MALDI ion source with other mass analyzers, such as ion trap (IT) MS (Creaser et al., 2002) and fourier transform-ion cyclotron resonance MS (Zhang et al., 2005). These studies showed that due to collisions with the surrounding gas, the ionization of analytes in AP-MALDI was softer than in the vacuum MALDI, which reduced the internal energy of the analyte ions. Therefore, the AP-MALDI was able to reduce the metastable fragmentation of labile oligosaccharides and was suitable to analyze carbohydrates containing labile groups, such as sialic acid, sulphate and fucosyl residues (Creaser et al., 2002; Laiko et al., 2000; Zhang et al., 2005).

2.5.5. Multi-stages Mass Fragmentation (MS^n)

The multi-stages mass fragmentation (MS^n) using electrospray ionization (ESI-) or MALDI-MS is increasingly important for the structural studies of carbohydrates. Fragment ions generated by collision induced dissociation, most of which originate from glycosidic and cross ring cleavages, provide the information on the sequence of individual sugars, glycosidic linkages, and location of branching in a complex oligosaccharide (Harvey, 2003). However, it is not possible to determine the ring format and anomeric configuration of the individual sugar present in a carbohydrate using MS^n analysis. The MS^n analysis of underivatized oligosaccharides in positive ion mode predominantly produced B- and Y-ions (**Figure 6**) (Harvey et al., 1997). This was demonstrated by an analysis of the α-(Me)Glc*p*A-(1→2)-linked XOS (Reis et al., 2003) and acetylated XOS (Reis et al., 2005) using a ESI-IT or ESI-

quadrupole-TOF (ESI-Q-TOF). Often, the MS^n analysis in positive ion mode results in a mixture of possible isomers. In comparison, the structure of an underivatized oligosaccharide is preferably analyzed by negative ion MS^n. The predominant ions produced are C-ions (Garozzo et al., 1990; Maina et al., 2013; Vinueza et al., 2013), which enable cross-ring cleavages at the reducing end sugars and, consequently, produce product ions that are diagnostic of linkages between sugars.

Labeling at the reducing end of oligosaccharides precludes the ambiguous assignment of fragment ions derived from glycosidic or cross ring cleavages. This has been attempted by ^{18}O labeling of arabino-XOS that were further analyzed by negative ion ESI-IT/ ESI-Q-TOF (Quemener et al., 2006) for elucidating the spatial distribution of Ara*f* substituents. Other labeling techniques, such as reductive amination using fluorophore e.g. 2-aminobenzoic acid (2-AA), has been demonstrated in the analysis of arabino-XOS isomers using positive ion MALDI-TOF-MS/MS (Maslen et al., 2007). Apart from isotopic or fluorescent labeling, sodium borohydride reduction combined with per-*O*-methylation of the free hydroxyl groups is also helpful for assigning the location of branching and monosaccharide sequences in a complex oligosaccharide (Matamoros Fernández et al., 2003; Mazumder and York, 2010).

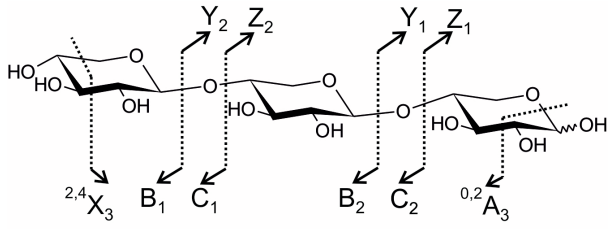

Figure 6. Nomenclature of the fragment ions derived from MS/MS of xylotriose. The naming system is according to Domon and Costello (1988).

3. AIMS OF THE STUDY

The overall aim of the thesis was to improve and develop the methods used for the compositional and structural studies of the substituents, i.e. (Me)Glc*p*A and acetyl present in the *O*-acetylglucuronoxylans (AcGX) in plant cell walls. Additionally, a microbial GH115 α-glucuronidase was expressed in the model dicot species *Arabidopsis thaliana* for the modification of (Me)Glc*p*A in AcGX. The structures and substitution patterns of AcGX in Arabidopsis wild type and the cell wall modified transgenic plants were studied using the improved and newly developed methods.

The main objectives were:

- To examine the accuracy of MeGlc*p*A quantitation using the commercial Glc*p*A as the calibration standard in acid methanolysis and GC analysis (paper **I**).

- To develop a xylan OLIMP method encompassed GH10 endoxylanase hydrolysis and AP-MALDI-ITMS measurement to fingerprint the AcGX structural differences in various hardwood species and Arabidopsis (paper **II**).

- To determine the spatial distribution of acetyl residue and a pentose substitution at the Glc*p*A side branch in AcGX of Arabidopsis by mass fragmentation analysis (papers **III** & **IV**).

- To determine the alteration of acetylation pattern in AcGX of the Arabidopsis biosynthetic mutants, *irx7*, *irx9, irx10*, *irx14* and *gux1gux2*, using xylan OLIMP and HSQC spectroscopic analysis (paper **IV**).

- To isolate the gene encoding GH115 α-glucuronidase produced by the white rot fungus, *Scizophyllum commune*, and express the corresponding enzyme in Arabidopsis for studying transgene effects in plant development, (Me)Glc*p*A modification, and other cell wall chemistry (papers **V** & **VI**).

4. MATERIALS AND METHODS

This section highlights and summarizes the major materials and methods that have been utilized in paper I-VI.

4.1. Materials

4.1.1. Carbohydrates and enzymes

The carbohydrates and enzymes used for the studies in paper I-VI were either purchased or obtained as a kind gift from the sources listed in **Table 5**.

Table 5. Monosaccharide, oligosaccharides, polysaccharides and enzymes

	Source	**Paper**
Xylobiose (X_2), xylotriose (X_3), xylotetraose (X_4)	Megazyme (Bray, Ireland)	III, V, VI
Purified MeGlcA standard MeGlcA-Xyl_3 (UXX) MeGlcA-Xyl_3 (XUX) MeGlcA-Xyl_4 (XUXX)	Dr. Sanna Koutaniemi University of Helsinki	II, III, VI
Eucalyptus xylooligosaccharides (XOS)	Prof. Juan Carlos Parajó University of Vigo, Spain	II, IV
Birchwood glucuronoxylans (GX)	Sigma (St. Louis, MO)	I, V
Stem or woody tissues of *populus tremula* (aspen), *betula pendula* (birch), *eucalyptus globulus* (eucalyptus), *picea abies* (spruce) and wheat straw	Prof. Stefan Willför Åbo Akademi University	I, II
Pure GH10 endo-1,4-β-xylanase of *Aspergillus aculeatus*	Novozymes A/S (Bagsvaerd, Denmark)	II, IV, V
Ultraflo L enzyme	Novozymes A/S (Bagsvaerd, Denmark)	I

4.1.2. Seeds of Arabidopsis wild-type and mutant plants

Seeds of the *Arabidopsis thaliana* wild-type (WT) (Col-0 ecotype), and mutant plants were obtained or purchased from the sources listed in **Table 6**.

Table 6. Seeds of Arabidopsis wild-type and mutant plants.

Genotype	Source	Paper
WT (Col-0 ecotype)	Nottingham Arabidopsis Stock Centre	I, II, III, IV, VI
irx7 (also known as *fra8*), *irx9-1*, *irx10*, and *irx14*	Provided by the authors (Zhong et al., 2005; Wu et al., 2009; Wu et al., 2010)	III, IV
gux1gux2	Professor Björn Sundberg Swedish University of Agricultural Sciences	IV, VI
*Sc*AGU115 homozygotic lines	Professor Ewa Mellerowicz Swedish University of Agricultural Sciences	VI

4.1.3. Sample preparation

The alcohol insoluble residues and *O*-acetylglucuronoxylans studied in papers 1-VI were prepared from plant materials listed in **Table 7**.

Table 7. Sample preparation for the studies in papers I-VI

	Source	Paper
Alcohol insoluble residues (AIR)	Stem tissues	I, II, III, IV, VI
Isolation of *O*-acetylglucuronoxylans (AcGX)	Stem tissues	IV, VI

4.2. Determination of MeGlcA content in plant cell walls (I & VI)

4.2.1. Purification and quantitation of MeGlcA with ^{1}H NMR spectroscopy

Birch GX was hydrolyzed with high dosages of xylan degrading enzymes present in Ultraflo L (dosed at 3000 U xylanase and 10 U α-glucuronidase /g xylan). The MeGlcA was purified from the hydrolyzate with the anion exchange chromatography and gel filtration (Koutaniemi et al., 2012). The concentration of the purified MeGlcA was determined with ^{1}H NMR spectroscopy against known amounts of mannobiose. Sum integrals of α- and β- anomeric protons for MeGlcA and mannobiose were obtained, and the amount of MeGlcA was calculated based on the relative ratio. The MeGlcA concentration in the purified preparation was 5.3 mg/ml.

4.2.2. Quantitation of non-cellulosic sugars using acid methanolysis and GC analysis

An amount of 10 mg stem/woody tissues of Arabidopsis, wood and wheat straw were degraded in 2M HCl/MeOH following the acid methanolysis method described by Sundberg et al., (1996). The method was later adapted to a smaller scale using 1 mg AIR for the analysis of Arabidopsis stem tissues in paper **VI**. The liberated methyl glycoside/methyl ester methyl glycosides were further trimethylsilylated (TMSi) and analyzed with Agilent 6890N gas chromatography (GC) equipped with a flame ionization detector (Agilent Technologies, Waldbronn, Germany). The capillary column used was a DB-1 (30 m, 0.25 mm i.d., 0.25 μm film thickness) from Agilent Technologies. Oven temperature profile was as follows: 150 ^{o}C (3 min)—1 ^{o}C/min—155 ^{o}C (1 min)—2 ^{o}C/min—200 ^{o}C—20 ^{o}C/min—325 ^{o}C.

Monosaccharide contents were calculated from external calibration curves that were plotted as total peak area ratios against known amounts of monosaccharide standards: arabinose (Ara), xylose (Xyl), rhamnose (Rha), galactose (Gal), mannose (Man), glucose (Glc), galacturonic acid (GalA), glucuronic acid (GlcA) and the purified MeGlcA. Sorbitol was used as an internal standard. The total peak area ratio for a sugar standard was obtained from the sum of peak areas of all TMSi derivatives to that of internal standards. Overlapped peaks were

excluded in the calibration standard. The monosaccharide composition was calculated from triplicate samples and expressed as % anhydro-monosaccharides of dry weight.

4.3. The development of xylan OLIMP method (II, III & IV)

This section summarizes the development of the xylan OLIgosaccharide Mass Profiling (OLIMP) method that includes GH10 endoxylanase hydrolysis, mass spectrometric detection, and data analysis. Summary of the workflow is depicted in **Figure 7**.

4.3.1. GH10 endoxylanase hydrolysis and MALDI-MS detections

An amount of 3 mg AIR derived from hardwood (aspen, birch, and eucalyptus) and Arabidopsis stem tissues were incubated in a 20 mM sodium acetate buffer (pH 5.0), with the GH10 endo-1,4-β-xylanase of *A. aculeatus* (20,000 nkat/g AIR), for 24 h or 48 h. The liberated XOS were desalted and separated into neutral and acidic fractions using Hypersep Hypercarb Porous Graphitized Carbon (PGC) columns (Thermo Scientific, MA), according to the established protocols (Packer et al., 1998), with modifications. The neutral and acidic XOS were eluted from the column by 40% (*v/v*) acetonitrile (ACN) and 50% (*v/v*) ACN in 0.05% (*v/v*) trifluoroacetic acid (TFA), respectively. The eluents were dried and re-constituted in 30 µl of Milli-Q water prior to MS analysis.

The 2,5-dihydroxybenzoic acid (DHB) solution (10 mg/1ml ACN/Milli-Q water (3:7, *v/v*)) was employed as a matrix for atmospheric pressure-matrix assisted laser desorption ionization (MALDI)-MS analysis. The neutral XOS were crystallized on a target plate by mixing 1 µl of the sample with 1 µl of the DHB solution. The acidic XOS were pre-mixed with DHB and ammonium sulfate ($(NH_4)_2SO_4$) (7 mg/ml) solutions according to procedures described by Enebro et al. (2006). An aliquot of 5 µl acidic XOS was added into 20 µl DHB and 0.5 µl $(NH_4)_2SO_4$, mixed, and 1 µl of the mixed solution was crystallized on a target plate.

The atmospheric pressure (AP)-MALDI-ion trap (IT) MS was the combination of an AP-MALDI ion source (Mass Tech Inc., MD) and Agilent 6330 ITMS (Agilent Technologies).

The AP-MALDI ion source was operated as described by Salo *et al.*, (2005) with modifications. The extended capillary was operated with a potential of 3200 V to direct ions formed at the ion trap; the drying gas was set to a flow rate of 5 L/min and temperature of 300 °C. The ion trap settings were as follows: accumulation time, 100 ms; averages, 10; rolling averaging, on; and skimmer voltage, 40 V. The capillary exit and trap drive were set at [200V, 50] and [300V, 80] for analyzing neutral and acidic XOS, respectively. The detection mass range was from *m/z* 300 to 2000 and the ultra scan mode was chosen. For MS/MS measurements, the fragmentation amplitude varied according to the decrease in the precursor ion peak intensities to about 10% to 30% of the main product ion. The ITMS mass spectrometer was calibrated by the commercial ESI tuning mix (Agilent Technologies).

The MALDI-time of flight (TOF)/MS Ultraflex system (Bruker Daltonics, Bremen, Germany) was equipped with a 337 nm laser and the mass spectra were acquired in a positive ion mode. The operating parameters were as follows: acceleration voltage, 25 kV; delay extraction time, 40 ns; and the ions were detected in a reflector mode. The TOF mass spectrometer was calibrated by commercial peptide standards (Bruker Daltonics, Bremen, Germany).

4.3.2. Calculation of % peak intensity and PCA analysis

The peak intensities of the identified mass peaks (the mass list can be found at **Suppl. Table S1-S4 in paper II**) were extracted from the MS raw data and calculated for the % peak intensity. In the case of the eucalyptus samples, the peak intensity corresponding to the MeGlcA-XOS carrying a hexose residue was summed together with the MeGlcA-XOS (without a hexose linked residue) in similar XOS chain length. The % peak intensity was calculated by dividing the intensity of a single peak with the total sum of the peak intensities in neutral/acidic XOS profile and then converted to a % value. Further on, % intensities for all the (Me)GlcA-XOS were analyzed in Principal Components Analysis (PCA) with SIMCA-P+ 12.0.1 (Umetric; Umeå, Sweden) to reveal differences between the samples.

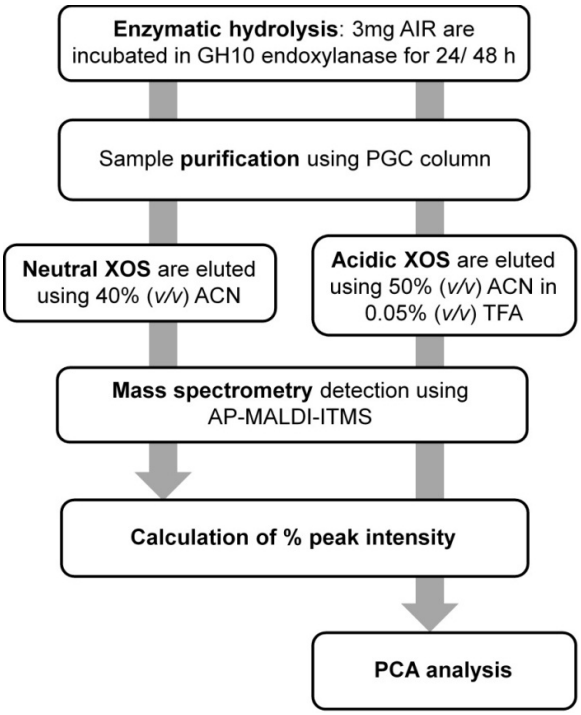

Figure 7. Workflow for the xylan OLIgosaccharide Mass Profiling (OLIMP) method.

4.4. Xylan structural analysis (I, III, IV, VI)

4.4.1. Proton and HSQC NMR spectroscopy analysis

Before the nuclear magnetic resonance (NMR) measurements, AcGX and deacetylated GX were exchanged three times with deuterium oxide (D_2O) (99.8% D, Merck) and finally dissolved in 0.6 ml of D_2O. NMR spectra were recorded at 22 °C on a 600 MHz Bruker Avance III NMR spectrometer equipped with a Q-CPN cryoprobe. The 1D ^1H spectra were acquired with 4s presaturation of the residual water signal using Bruker's noesygppr1d pulse sequence. 64k data points were collected, and the free ionization decay was multiplied by a 0.5 Hz line broadening function before the Fourier transformation. The 2D total correlation spectroscopy (TOCSY) spectra were acquired using standard Bruker pulse sequences with a mixing time (DIPSI2) of 80 ms.

The quantitative heteronuclear single quantum coherence (qHSQC) spectra were acquired using echo/antiecho-TPPI selection, and matched sweep adiabatic pulses were used for all 180° ^{13}C pulses to compensate for the differences in the 1JCH coupling constants (Zwahlen et al., 1997). For the 2D spectra, typically a matrix of 2048 × 256 data points was collected and zero filled once in F1. A $\pi/2$ shifted squared sine bell weighting function was applied in both dimensions before the Fourier transformation. The chemical shifts were referenced to acetone (δH = 2.225 ppm and δC = 31.55).

4.4.2. Multi-stages mass spectrometry analysis with negative ion ESI-ITMS

An electrospray (ESI) ion source equipped with an ITMS (Agilent Technologies) was used. Before the ESI-ITMS analysis, 3-5µl of XOS were added into 400 µl of MeOH:water (1:1, v/v). The sample mixtures were introduced in the ESI unit at a flow rate of 5 µl/min and ionized in the negative ion mode with the following operation parameters: HV Capillary, 3500 V; nebulizer pressure, 15 psi; dry gas flow rate, 5 l/min; temperature, 300 °C. For the ion optic: skimmer voltage, -40 V; capillary exit, -131 V; octopole RF amplitude, 200 Vpp; trap drive, 50; oct 1 DC, -12 V and oct 2 DC -2 V. Mass scanning was set at ultra-scan mode, and the detection mass range was set from *m/z* 300 to 2000.

4.5. Isolation of gene encoding GH115 α-glucuronidase from *Schizophyllum commune* (V)

4.5.1. Cultivation of *S. commune* and total RNA isolation

The *Schizophyllum commune* strain H4-8 (VT# H4-8, FGSC# 9210) was grown for 5-7 days at 30 ^{o}C on polycarbonate membranes (47mm, pore size 0.1µm, GE Osmonic, MN) placed on top of a minimal media (MM) plate containing 25 mM glucose. The colonies were then transferred to new MM plates containing different carbon sources (25 mM Glc, 25 mM Xyl, 25 mM GlcA, 1% oat spelt GAX, 1% birchwood GX, 1% α-cellulose, 1% α-cellulose + 1% birchwood GX, and 3% birchwood powder). The mycelia were harvested one day after transfer and were frozen in liquid nitrogen. The frozen samples were kept at -80 ^{o}C prior to

RNA isolation. Total RNA was extracted from the mycelia using TRIzol reagent (Thermo Fisher Scientific, MA) following the manufacturer protocols.

4.5.2. Isolation of *Sc*AGU115 encoding gene sequence

The *S. commune* GH115 α-glucuronidase protein and nucleotide sequences were identified using a BlastP homology search against the *S. commune* genome database (Ohm et al. 2010) using the published N-terminal sequence (Tenkanen and Siika-aho, 2000). The *Sc*AGU115 cDNA lacking the 3' end sequence was isolated from the total RNA using primers (**Table 8**) designed according to the putative nucleotide sequence. The upstream 3′ end sequence was determined by 3′ RACE PCR and 3' nested PCR (**Table 8**) using Q_T primer (5′-ccagtgagcagagtgacgaggactcgagctcaagctttttttttttttttt-3′; Zhang & Frohman 2000) for reverse transcription. The PCR products were cloned into pGEMT easy vector (Promega, WI) and sent for sequencing (Haartman Institute, Finland).

Table 8. Primer pairs used for the isolation of full length cDNA sequence encoding GH115 α-glucuronidase from *S. commune*

	Primer name	**Nucleotide sequence**
1	cDNA lacking the 3' end sequence	
	agu1_cDNA_dw	5′-atgttcagtcgcgcggccct-3′
	agu1_cDNA_up	5′-ccagtgagcagagtgacgag-3′
2	3' RACE PCR	
	agu1_3′RACE_dw	5′-gtgatggtgtggtgtccttc-3′
	Upstream Q_o	5′-ccagtgagcagagtgacg-3′
3	3' Nested PCR	
	agu1_3′RACE_nestedDW	5′-gtggaccgtaattcccgatt-3′
	Upstream Q_1	5′-gaggactcgagctcaagc-3′

4.6. Expression of *Sc*AGU115 α-glucuronidase in Arabidopsis (VI)

4.6.1. Gene expression analysis

For the screening of Arabidopsis homozygotic plants expressing *Sc*AGU115 α-glucuronidase, fragment genes encoding *Sc*AGU115 and Actin2 were amplified using gene specific primers listed in **Table 9**. The expected size of the PCR product is 315 bp and 201 bp, respectively.

Table 9. Gene specific primers designed for the amplification of *ScAGU115* and *Actin2*

	Primer name	**Nucleotide sequence**
1	*ScAGU115*	
	SP5(F)	5'-tggaatgcacagggtatga-3'
	R1(R):	5'-caagcaccaacgtgcacggactcaggtgg-3'
2	*Actin2*	
	ACT1(F)	5'-ggtaacattgtgctcagtggtgg-3'
	ACT3(R)	5'-ctcggccttggagatccacatc-3'

4.6.2. Protein Analysis

α-Glucuronidase activity assay

Protein extract buffer A (0.2M sodium succinate, 10 mM $CaCl_2$ and 1% (*w/v*) PVPP, pH 5.5) and buffer B (0.2 M sodium succinate, 10 mM $CaCl_2$ and 1 M NaCl, pH 5.5) were used to isolate the soluble and wall bound protein from the stem tissues of Arabidopsis WT and *Sc*AGU115 expressing plants, respectively (Franková and Fry, 2011). Concentrations of the protein isolates were determined according to the Bradford method (Sambrook et al., 2000), and the concentration of soluble and wall bound proteins were adjusted to 0.6 and 0.2 mg/ml, respectively, using Milli-Q water before the enzymatic assay. Equal amount of 16 µg of protein was used in the α-glucuronidase activity assay using the commercial product from Megazyme (K-AGLUA). The substrate used was a mixture of aldouronic acid.

Western analysis

Aliquots of soluble protein samples, equivalent to 12 µg proteins, were separated on sodium dodecyl sulfate-polyacrylamide gel electrophoresis (SDS-PAGE), alongside 60 ng of the native *S. commune* α-glucuronidase (Tenkanen and Siika-aho, 2000). Western analysis was performed as described by Sambrook and Russel, 2000 (Sambrook et al., 2000). The proteins were blotted on a polyvinylidene difluoride membrane and labeled with the primary antibody (1:2 000) raised in rabbit against the *S. commune* α-glucuronidase (Chong et al., 2011a). The secondary antibody (1:10 000) was horseradish peroxidase conjugated anti-rabbit IgG (GE Healthcare, NJ).

TLC analysis of XUXX hydrolyzates

The α-glucuronidase activity in the protein samples were analyzed against the MeGlcA-Xyl_4, XUXX (Fauré et al., 2009). Aliquots of samples equivalent to 12 µg proteins were incubated with 30 µg XUXX in extraction buffer A at 37 ^{o}C overnight. The hydrolyzates were examined by thin layer chromatography following the procedures described in Franková and Fry, (2011). The wall bound proteins were desalted with Microcon centrifugal filters (30,000 molecular weight cut-off; EMD Millipore, MA) according to the manufacturer recommended procedures, to ease the mobility of the hydrolyzates when separating on the silica plate.

4.6.3. Cell wall chemotypic analysis

The analysis of lignin content and wall digestibility in the stem tissues of Arabidopsis *Sc*AGU115 expressing and WT plants were carried out by the collaborators listed in **Table 10**.

Table 10. Analysis of cell wall chemistry in Arabidopsis *Sc*AGU115 expressing and WT plants

Analysis	Method	Performed by	Reference
Lignin content	pyrolysis-GC/MS	Dr. Lorenz Gerber	Gerber et al., 2012
Saccharification of biomass	reducing sugars analysis	Dr. Leonardo D. Gómez	Gomez et al., 2010

4.6.4. Immunolocalization of xylan and (Me)GlcA distribution in basal stem sections

Basal 1 cm stems were cut and immersed in a fixative solution (4% paraformaldehyde and 0.05% glutaldehyde in 25 mM phosphate buffer, pH 7.2), and later dehydrated in a gradient ethanol (30, 50, 70, 80, 90, 95 and 99.5 %) series for embedment in LR White resin according to manufacturer's instructions (TAAB, Reading, UK). Transverse 0.5 µm section were labeled with UX1 (1:3) (Koutaniemi et al., 2012) and AX1 (1:20) (Guillon et al., 2004b) primary antibody that recognized the (Me)GlcA and xylan epitodes, respectively.

5. RESULTS

5.1. Determination of MeGlcA content in plant cell walls using the purified MeGlcA and commercial GlcA (I)

Uronic acids present in the plant cell walls are usually quantified using a colorimetric assay (Filisetti-Cozzi and Carpita, 1991). However, this method also measures pectin deriving GalA, in addition to (Me)GlcA. Quantitation with a chromatographic method requires an authentic calibration standard for estimating monosaccharide content in plant cell walls. However, MeGlcA standard is not commercially available, thus GlcA is employed as a calibration standard for the estimation of MeGlcA content. In paper **I**, the accuracy of GC analysis using GlcA standard for determining the MeGlcA content in plant cell walls was evaluated.

To compare the accuracy of MeGlcA quantitation by GC employing the commercial GlcA as standard, the lignocellulosic samples (stem or woody tissues of wheat straw, Arabidopsis, aspen, birch and spruce), as well as the sugar standards: GlcA and the purified MeGlcA, were degraded in 2M hydrochloric acid/methanol, trimethylsilylated, prior to GC analysis. Sugars generally form four glycosides after acid methanolysis, constituting α and β anomers of both pyranosides and furanosides. However, the MeGlcA and GlcA yielded two and six peaks, respectively (**Figure 8**). The reasons are ascribed to the methoxy group at C-4 position of MeGlcA preventing the formation of furanosides, while the GlcA lactonizes in an acidic condition, thus yielded two extra peaks corresponding to glucurono-6,3-lactone.

Four calibration curves were plotted from the GlcA standard by summing up the total peak area ratios derived from either all six (GlcA6p; **Figure 8**), four (GlcA4p; excluded peaks corresponding to lactones), two main (GlcA2p; retention time (RT): 20.4 and 28 min) or only the main (GlcA1p; RT: 28 min) GlcA peak(s). The MeGlcA contents calculated based on the four GlcA calibration curves were compared to that of the value obtained from the purified MeGlcA standard.

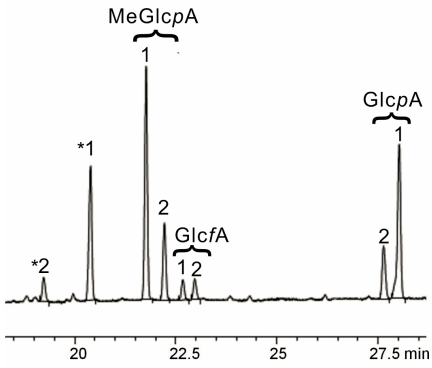

Peaks	Retention time (RT)/ min
*1	20.4
*2	19.2
MeGlc*p*A1	21.8
MeGlc*p*A2	22.2
Glc*f*A1	22.7
Glc*f*A2	23.0
Glc*p*A1	28.0
Glc*p*A2	27.6

Figure 8. GC chromatogram showing TMSi derivatives of GlcA and MeGlcA separated on a DB-1 column. The MeGlcA yielded two pyranosides (MeGlc*p*A), whereas GlcA yielded six peaks corresponding to the two pyranosyl (Glc*p*A), furanosyl (Glc*f*A) forms of GlcA, and two glucurono-6,3-lactones (*); after acid methanolysis. The retention times are shown alongside the chromatogram. (adapted from **Fig. 2A in paper I**)

The calculated amounts of MeGlcA differed between calibration curves, based on the purified MeGlcA and commercial GlcA standards. With the purified MeGlcA standard, the average MeGlcA contents were 1.3% of dry weight for Arabidopsis, 2.2% for aspen, 2.2% for birch, 2.2% for spruce, and 1.2% for wheat straw (**Figure 9**). When the MeGlcA contents were calculated using GlcA standards by summing up the total peak area of all six peaks (GlcA6p; **Figure 9**) in the calibration curve, the average MeGlcA yields were reduced by approximately 30% across all samples. Another way for calculating the amount of MeGlcA in samples is to omit the peaks corresponding to the lactones. In this case, the average MeGlcA yields were close to the ones calculated from the purified MeGlcA standard with only 2–8% overestimation (GlcA4p; **Figure 9**). On the other hand, if the two main peaks corresponding to the main lactone peak (RT: 20.4 min; **Figure 8**) and the main Glc*p*A peak (RT: 28 min; **Figure 8**) were selected to calculate MeGlcA content, since these two peaks were most visible on GC chromatogram, the average MeGlcA yields were approximately 10% (GlcA2p; **Figure 9**) less than those calculated from purified MeGlcA standard. If only the main GlcA peak (RT: 28 min; **Figure 8**) was chosen to create the calibration curve, the calculated MeGlcA yields were overestimated by 50–70% (GlcA1p; **Figure 9**).

Indeed, the MeGlcA content is underestimated by nearly 30% when all forms of GlcA derivatives are included in the calculation. The MeGlcA is best estimated by including only the two main GlcA peaks (RT 20.4 and 28 min; **Figure 8**) or the summation of all Glc*p*A and Glc*f*A in the calibration curve since the error is only ±10% compared to the values determined by the purified MeGlcA standard.

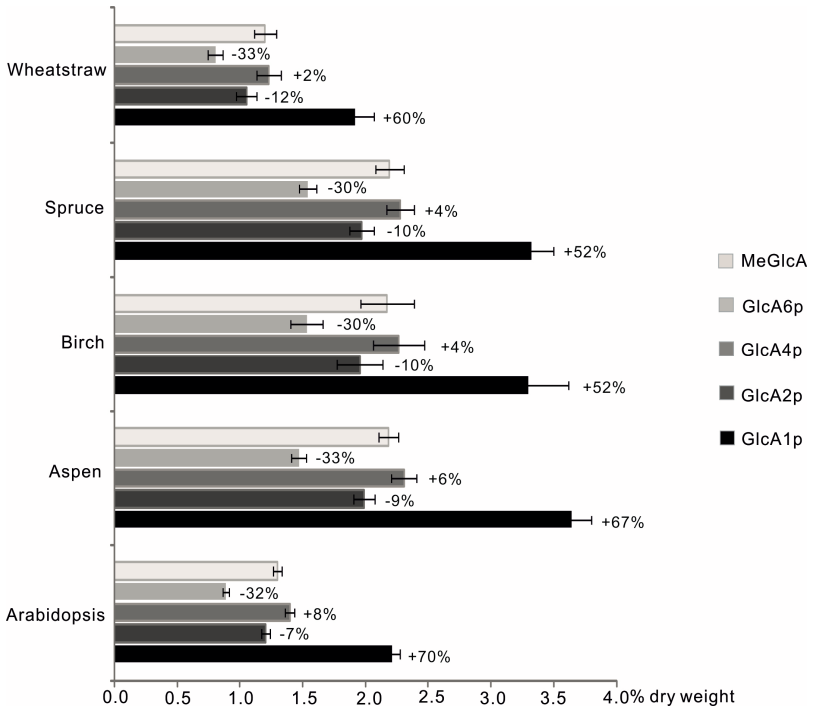

Figure 9. The MeGlcA content (% dry weight) present in stem or woody tissues of Arabidopsis, aspen, birch, spruce and wheatstraw. The MeGlcA content was determined using calibration standards created from purified MeGlcA and commercial GlcA standards by summing up total area ratios of all six GlcA peaks (GlcA6p), the α and β anomers of furanosyls and pyranosyls derivatives (GlcA4p), the two main peaks at RT 20.4 and 28 min (GlcA2p), and main peak at RT 28 min (GlcA1p) in the calibration curves. Error bar represents standard deviation of three technical replicates. (created from **Table 1 in paper I**)

5.2. Xylan OLIgosaccharide Mass Profiling (OLIMP) for studying substitution pattern in AcGX (II)

Xylan isolation is usually carried out in an alkaline solution that concomitantly destroys any esterified components in the cell walls including the *O*-acetyl residues. Paper **II** describes the development of the xylan OLIgosaccharide Mass Profiling (OLIMP) method combining endoxylanase hydrolysis and mass spectrometry detection. The endoxylanase hydrolysis was carried out at a milder condition, e.g. near neutral pH. Thus, more structural information about AcGX such as acetylation are obtainable, compared to the conventional alkaline isolation. The atmospheric pressure-matrix assisted laser desorption ionization-ion trap mass spectrometry (AP-MALDI-ITMS) was employed for the mass profiling of endoxylanase liberated xylo-oligosaccharides (XOS). This system has the advantage of analyzing the mass and structures of macromolecules in one system, but it has not been reported for the analysis of plant derived oligosaccharides.

5.2.1. Feasibility of AP-MALDI-ITMS in the analysis of acetylated XOS

The AP-MALDI-ITMS was evaluated by analyzing a mixture of acetylated XOS isolated from the hydrothermally treated eucalyptus wood. The sample was separated into *O*-acetyl-XOS (neutral XOS) and MeGlcA α-(1→2)-linked *O*-acetyl-XOS (acidic XOS) prior to MS measurement to ease the interpretation of mass spectra and to circumvent the problem of competition for ionization between both ion species. Mass spectra for MALDI-time of flight (TOF)/MS were also obtained for comparison.

The neutral XOS with degree of polymerization (DP)2 to DP9 carrying 1 to 5 acetyl residues, were detected by both AP-MALDI-ITMS (**Figure 10A**) and MALDI-TOF/MS (**Fig. 1B in paper II**). Main peaks (labeled *) observed from the AP-MALDI-ITMS mass spectrum were Xyl_2Ac_1, Xyl_3Ac_1, Xyl_3Ac_2 and Xyl_4Ac_2, which were similarly observed from the MALDI-TOF mass spectrum. In addition, there were peaks representing XOS with a higher degree of acetylation (labeled #), Xyl_3Ac_3, Xyl_4Ac_4 and Xyl_5Ac_5 detected by the AP-MALDI-ITMS only.

The acidic XOS detected by AP-MALDI-ITMS ranged from DP3 to DP10 and carried 1 to 6 acetyl groups (**Figure 10B**). In addition, a series of hexose linked acidic XOS was also observed. The hexose (H) was likely an α-(1→2)-linked Gal or Glc residue attached at the 2-

O position of the MeGlcA unit (Shatalov et al., 1999). Main peaks (labeled *): MeGlcA-Xyl_6Ac_3, MeGlcA-Xyl_7Ac_3, MeGlcA-Xyl_7Ac_4 and MeGlcA-Xyl_8Ac_4 were similarly observed in AP-MALDI-ITMS and MALDI-TOF/MS (**Fig. 2B in paper II**). Minor peaks representing larger XOS: H-MeGlcA-$Xyl_{10}Ac_6$, MeGlcA-$Xyl_{11}Ac_{4\text{-}5}$, and H-MeGlcA-$Xyl_{11}Ac_{4\text{-}6}$ were detected only with the MALDI-TOF/MS.

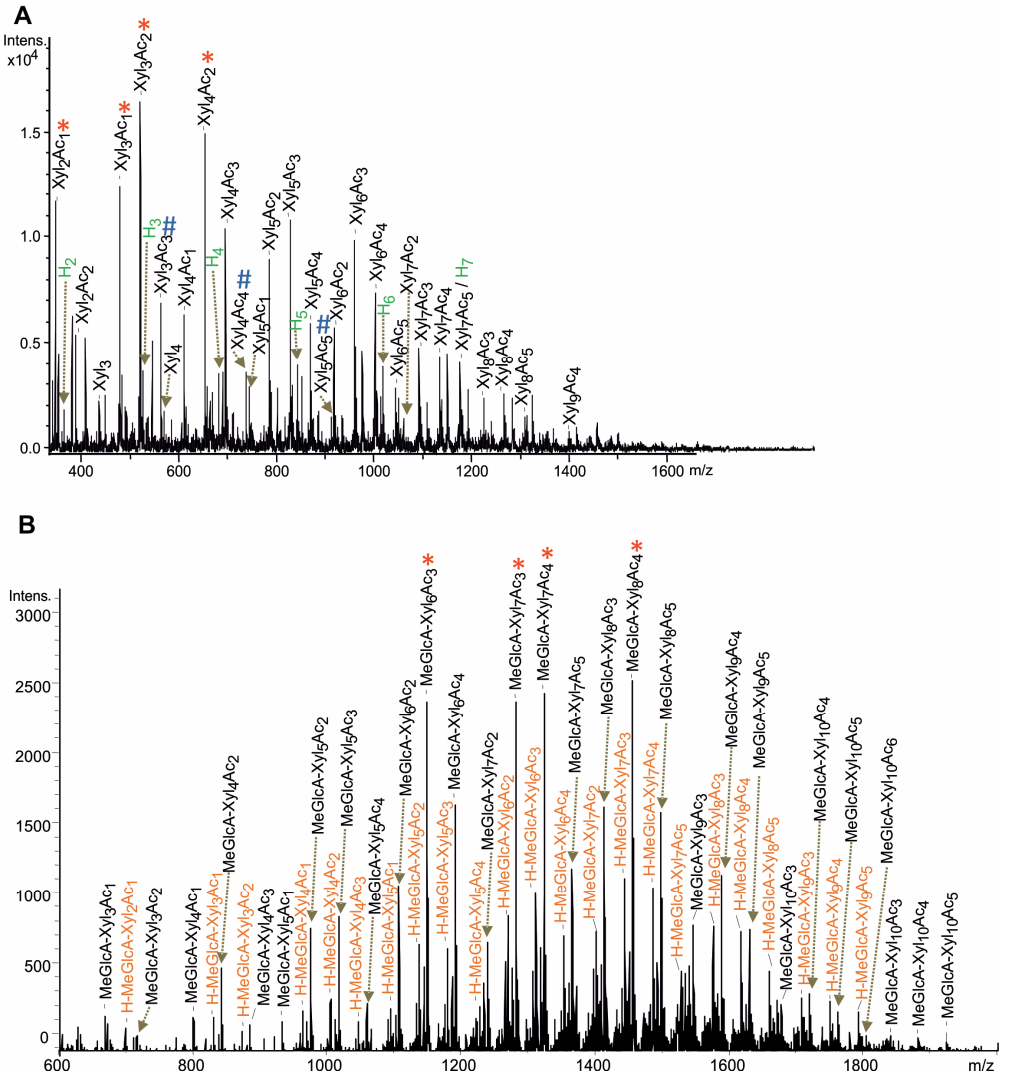

Figure 10. Positive ion AP-MALDI-ITMS mass spectra showing (A) neutral and (B) acidic XOS purified from hydrothermally treated eucalyptus wood. Peaks were sodium adducts. *,

main peaks; #, not detected by MALDI-TOF/MS; Xyl, (1→4)-linked β-D-Xylose; Ac, *O*-acetyl; MeGlcA, (1→2)-linked 4-*O*-methylglucuronic acid; H, hexose; numeric symbol, number of Xyl or Ac residues (**Fig 1A and 2A in paper II**)

5.2.2. Xylan OLIMP of AcGX in hardwoods

As the AP-MALDI-ITMS was suited for studying both neutral and acidic *O*-acetyl-XOS, the system was then employed to develop a method for xylan OLIMP. Acetylated XOS were liberated directly from plant tissues by GH10 endoxylanase, which were then subjected to PGC column purification and AP-MALDI-ITMS detection.

The OLIMP method was first employed for the structural fingerprinting of AcGX in the woody tissues of hardwood species: aspen. In comparison to the eucalyptus XOS obtained via hydrothermal treatment, the AP-MALDI-ITMS mass spectra for neutral (**Figure 11A**) and acidic XOS (**Figure 11B**) had simpler mass peaks after the endoxylanase hydrolysis. The neutral XOS that ranged from Xyl_2 to Xyl_5 were carrying 1 to 5 acetyl residues. Xylobiose (Xyl_2) with one and two acetyl groups were the two most abundant peaks. A minor peak representing non-acetylated Xyl_2 was also observed.

The acidic MeGlcA-XOS liberated from aspen contained 3 to 7 Xyl residues, with a single MeGlcA residue and a varying number of acetyl groups. The three main peaks observed were MeGlcA-Xyl_4Ac_2, MeGlcA-Xyl_5Ac_4, and MeGlcA-Xyl_6Ac_5. Taken together, the acetylation is limiting the action of endoxylanase as the hydrolysis of deacetylated GX by GH10 enzyme results in MeGlcA-Xyl_3 as the major acidic XOS (Biely et al., 1997).

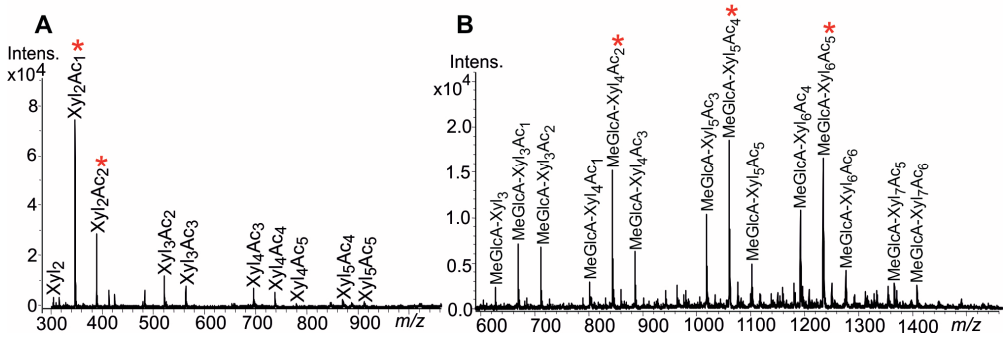

Figure 11. *O*-acetyl-XOS, (A) neutral and (B) acidic XOS liberated by GH10 endoxylanase from woody tissues of aspen. Mass spectra were acquired by positive ion AP-MALDI-ITMS and peaks were sodium adducts. Xyl, (1→4)-linked β-D-Xylose; MeGlcA, (1→2)-linked 4-*O*-methylglucuronic acid; Ac, *O*-acetyl; numeric symbol, number of Xyl or Ac residues; *, main peaks (**Fig. 3 in paper II**)

5.2.3. Comparison of AcGX substitutions in hardwoods

It was shown that the substituents in AcGX were limiting the enzymatic actions of GH10 endoxylanase, and thus the xylan OLIMP method was likely suitable for studying the substitution patterns in AcGX. To further investigate whether the OLIMP method can distinguish differences in AcGX substitution patterns between samples, woody tissues of hardwood species: aspen, birch and eucalyptus were analyzed. Mass lists were extracted for calculating the % peak intensity. The results obtained from acidic XOS were more interesting and revealed differences among the species. The observed chain lengths of acidic XOS in the aspen were from DP3 to DP7, whereas for birch and eucalyptus hydrolyzates, the oligosaccharides were somewhat shorter, only up to DP6 (**Figure 12**). In addition, the most abundant peak (labeled *) observed in birch and eucalyptus was only MeGlcA-Xyl_4Ac_2, whereas the aspen hydrolyzate was showing MeGlcA-Xyl_4Ac_2 and MeGlcA-Xyl_5Ac_4 as the major peaks. The peaks representing highly acetylated acidic XOS, such as MeGlcA-Xyl_5Ac_6, MeGlcA-Xyl_6Ac_6 and MeGlcA-$Xyl_7Ac_{5\text{-}6}$, were only observed in the aspen. Based on the xylan OLIMP analysis, the substitution patterns in the AcGX of aspen differed from birch and eucalyptus.

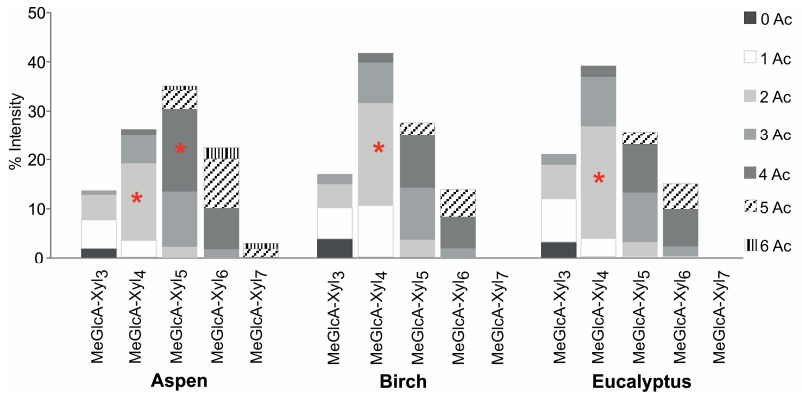

Figure 12. Comparison of acidic XOS liberated by GH10 endoxylanase from the hardwoods, aspen, birch, and eucalyptus. The mass peaks are calculated as % intensities. Xyl, (1→4)-linked β-D-Xylose; MeGlcA, (1→2)-linked 4-*O*-methylglucuronic acid; Ac, *O*-acetyl; numeric symbol, number of Xyl or Ac residues; *, main peaks. (adapted from **Fig. 4 in paper II**)

The overall MeGlcA-XOS fragments derived from birch and eucalyptus after GH10 endoxylanase hydrolysis were shorter than those derived from aspen, indicating that the degree of substitution, which restricts the action of endoxylanase, was lower in birch and eucalyptus than in aspen. This observation was supported by lower acetylation found in birch and eucalyptus (**Table 11**). The average MeGlcA substitution of Xyl residues in aspen, birch and eucalyptus were 9, 6, and 14 per 100 Xyl residues, respectively; whereas, the average degree of acetylation per 100 Xyl residue was 84, 72 and 74, respectively. The MeGlcA substitution level in eucalyptus seems to be the highest; however, this result was not implied by the higher hindrance effect on the enzymatic action, as longer XOS fragments were seen in aspen hydrolyzate. The acetyl substitution in hardwood AcGX was much more restrictive to the enzyme hydrolysis, and thus the distribution of the chain lengths of XOS obtained mainly reflect the differences in the acetylation.

Table 11. The amount of xylose (Xyl), 4-*O*-methylglucuronic acid (MeGlcA), and acetyl residues (Ac) present in the woody tissues of aspen, birch, and eucalyptus (adapted from **Table 1 in paper II**)

Woody sample	Monosaccharides and acetyl content (µmol / 100 mg wood powder)			Average molar ratio (per 100 Xyl residues)	
	Xyl	**MeGlcA**	**Ac**	**MeGlcA**	**Ac**
Aspen	130 ± 13	12 ± 2	109 ± 10	9	84
Birch	180 ± 13	11 ± 1	129 ± 14	6	72
Eucalyptus	112 ± 3	17 ± 1	83 ± 7	14	74

±, standard deviation of three technical replicates

5.3. Structural analysis of AcGX in Arabidopsis by MS^n (II, III & IV)

Arabidopsis is the model dicot species employed for xylan biosynthetic studies (**Table 3**), thus a thorough AcGX structural analysis is needed for a better understanding of the structure-function relationship of AcGX in plant cell walls. With the analysis of AcGX in hardwood, the xylan OLIMP showed its potential for studying acetylation patterns in AcGX. Moreover, the method is able to analyze low amounts of samples due to the high sensitivity of the MS detection. Thus, the xylan OLIMP can be useful for studying acetylation in the AcGX of Arabidopsis, especially the mutant plants that contain low amount of xylans.

5.3.1. Xylan OLIMP analysis of Arabidopsis WT (II)

The xylan OLIMP was first used for the structural analysis of AcGX in Arabidopsis wild type (WT) plants. Similar to the neutral XOS obtained from aspen, the two most abundant peaks observed were Xyl_2Ac_1 and Xyl_2Ac_2 (labeled *) (**Figure 13A**). Two series of acidic XOS representing GlcA-XOS and MeGlcA-XOS ranging from DP3 to DP6, and substituted by single (Me)GlcA and multiple acetyl groups, were obtained from the Arabidopsis WT (**Figure 13B**). Main peaks were GlcA-Xyl_4Ac_2 and MeGlcA-Xyl_4Ac_2 (labeled *). Mass peaks

for the MeGlcA-XOS were higher than the adjacent GlcA-XOS as two thirds of the GlcA in the xylan of Arabidopsis were methylated (Peña et al., 2007). However, two GlcA-XOS: GlcA-Xyl_4Ac_1 and GlcA-Xyl_5Ac_2 (labeled ♦), showed abnormally high intensities compared to the adjacent MeGlcA-XOS.

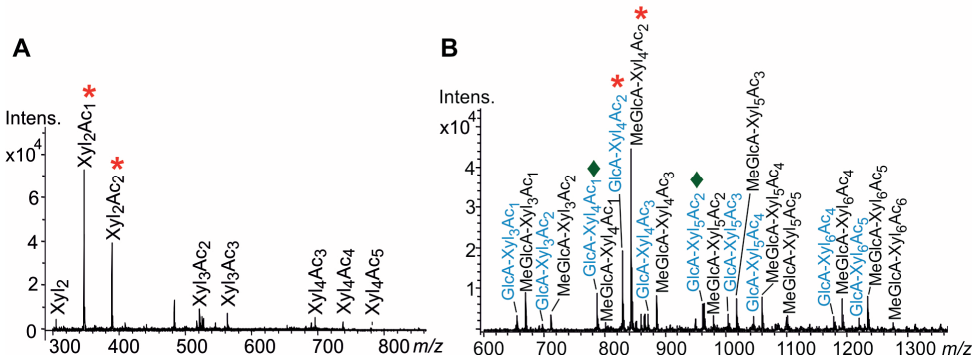

Figure 13. Positive ion AP-MALDI-ITMS mass spectra of (A) neutral and (B) acidic XOS liberated by *A. aculeatus* GH10 endoxylanase from the stem tissues of Arabidopsis WT. *, main peaks; ♦, the abnormal peaks. (**Fig. 2A and 3A in paper IV**)

5.3.2. Distribution of acetyl residues on XOS fragments liberated by GH10 endoxylanase (IV)

With the advantage of AP-MALDI-ITMS analyzing the mass and structure of oligosaccharides in one system, several major peaks in the hydrolyzate of Arabidopsis WT were selected for MS/MS fragmentation analysis, to thereby elucidate the distribution of acetyl residues. The elucidation of the XOS structure is aided by the known enzymatic specificities of GH10 endoxylanases that can act close to the (Me)GlcA substituents and leave them primarily on the non-reducing end Xyl (Xyl_t), while the reducing end Xyl unit (Xyl_{red}) is non-substituted (Biely et al., 1997; Kolenová et al., 2006).

The MS^2 spectrum of Xyl_2Ac_1 (*m/z* 347, **Figure 14A**) obtained by the positive ion AP-MALDI-ITMS showed that the product ion *m/z* 287 formed by loss of 60 Da was the major fragmentation pathway. Loss of 60 Da could be ascribed to $^{0,2}A$ (Domon and Costello, 1988)

cross-ring cleavages at the Xyl_{red} due to the β(1→4) linked backbone, or cleaving of the labile *O*-acetyl residue. The formation of a Y_1 ion at *m/z* 173 and a B_1 ion at *m/z* 197 was ascribed to the loss of XylAc residue resulting from glycosidic cleavages. The fragments imply two possible isomers, in which the acetyl residue is located either on the Xyl_{red} or Xyl_t residue (**Figure 14A**). However, the GH10 endoxylanase requires a non-substituted Xyl_{red} before the cleaved linkage to catalyze the hydrolytic action; thus, the expected position for mono-acetylation is on the nonreducing end of Xyl_2. Similar acetyl distribution was observed in Xyl_2Ac_2 based on the MS^2 analysis, where the both acetyls were located on the Xyl_t residue (**Figure 14B**).

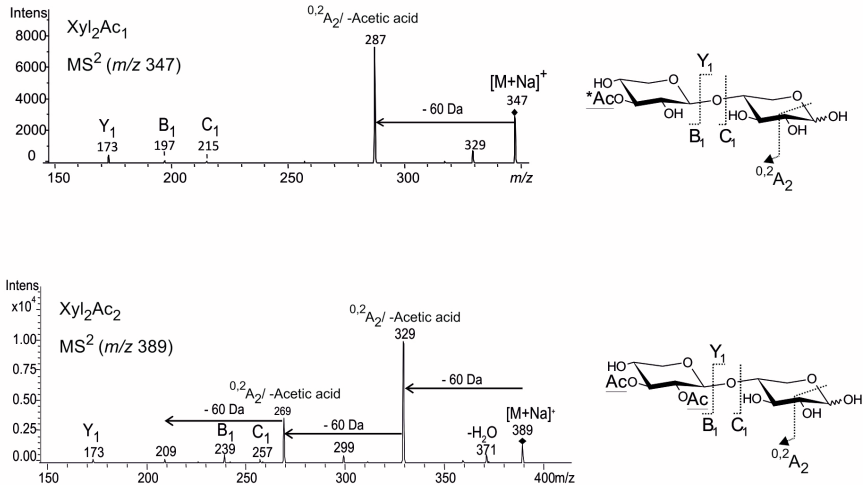

Figure 14. MS^2 analysis of two main peaks, (A) Xyl_2Ac_1 (*m/z* 347) and (B) Xyl_2Ac_2 (*m/z* 389) in the neutral XOS released from Arabidopsis WT by GH10 endoxylanase hydrolysis. Their possible structures are suggested alongside the mass spectra. The analysis was carried out with positive ion AP-MALDI-ITMS, and the ion peaks were sodium adducts. Xyl, (1→4)-linked β-D-Xylose; Ac, *O*-acetyl; numeric symbol, number of Xyl or Ac residues; *Ac, Ac residing either on 2-*O* or 3-*O* position of Xyl. (**Fig. 4 in paper IV**)

For the MS^2 analysis of the main acidic XOS, MeGlcA-Xyl_4Ac_2 (*m/z* 843; **Figure 15**), the major fragmentation pathway observed was loss of MeGlcA/GlcA (-190 Da/-176 Da) residue (Reis et al., 2004). Two feasible structures were deduced from the fragment ions in the MS^2 spectrum. The major structure was formed by the placement of the acetyl residue on the second Xyl residue from the reducing end of Xyl_4 due to loss of a non-substituted Xyl_{red}, and subsequent loss of a XylAc (-174 Da). The third glycosidic cleavage was the loss of a non-substituted Xyl residue (-132 Da) leading to formation of a B_2 ion, *m/z* 387. The *m/z* 387 was characteristic of MeGlcA-XylAc, indicating the Xyl_t residue was doubly substituted by MeGlcA and acetyl residues. There was also a minor compound containing a non-substituted Xyl_t residue since a $^{\#}Y_3$ ion, *m/z* 711, formed by the loss of 132 Da was detected. The MeGlcA and acetyl residues were then placed at the second Xyl residue from the non-reducing end of Xyl_4 due to the detection of a Y_2 ion (*m/z* 347), while the second acetyl residue resided on the third Xyl residue from the nonreducing end of Xyl_4.

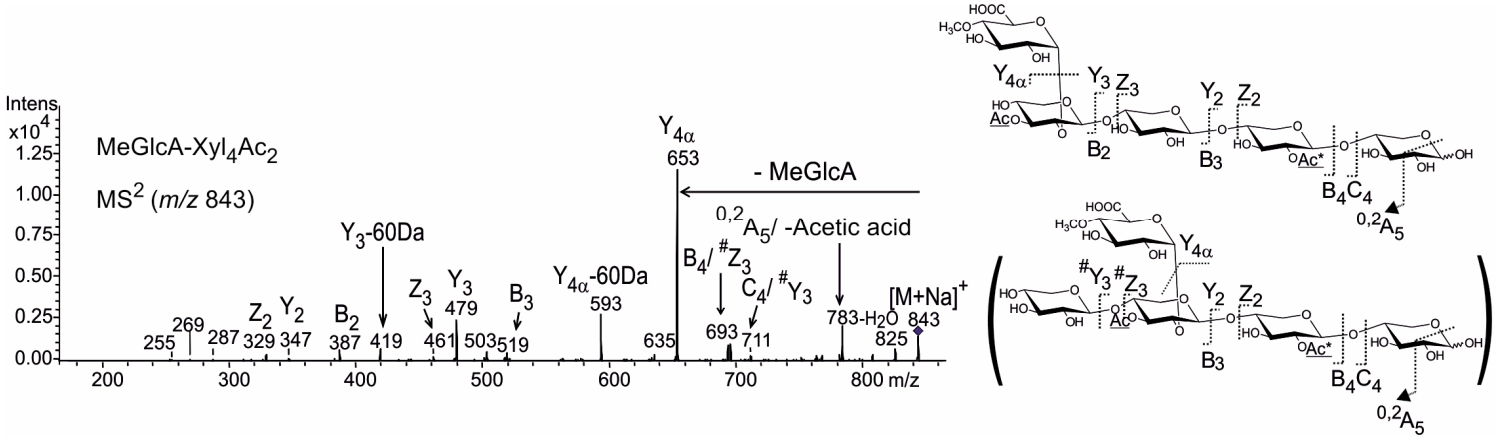

Figure 15. MS^2 analysis of MeGlcA-Xyl_4Ac_2 (*m/z* 843) released from Arabidopsis WT by GH10 endoxylanase hydrolysis. The possible isomers are suggested alongside the mass spectrum. The isomeric structure in parenthesis is present as a minor compound. The MS^2 analysis was carried out with positive ion AP-MALDI-ITMS, and the ion peaks were sodium adducts. Xyl, (1→4)-linked β-D-Xylose; MeGlcA, (1→2)-linked 4-*O*-methylglucuronic acid; Ac, *O*-acetyl; numeric symbol, number of Xyl or Ac residues; *Ac, Ac residing either on 2-*O* or 3-*O* position of Xyl residue. (**Fig 6A in paper IV**)

5.3.3. The GlcA in AcGX of Arabidopsis carries a pentose substituent (III)

In the OLIMP analysis of Arabidopsis WT, two peaks corresponding to GlcA-Xyl_4Ac_1 (*m/z* 787) and GlcA-Xyl_5Ac_2 (*m/z* 961), showed significantly higher peak intensities than their 4-*O*-methylated counterparts in the positive ion AP-MALDI-ITMS mass spectrum (**Figure 13B**). This peculiarity urged a structural elucidation of these peaks using MS^n.

A typical MS^2 of acidic XOS resulted in loss of (Me)GlcA as the major fragmentation pathway (**Figure 15**), and a similar result was obtained in the MS^2 of MeGlcA-Xyl_4Ac_1 (*m/z* 801) (**Figure 16A**). However, the MS^2 spectra of GlcA-Xyl_4Ac_1 (*m/z* 787; **Figure 16B**) and GlcA-Xyl_5Ac_2 (*m/z* 961) (data not shown) were instead showing a loss of 60 Da as the major peak, suggesting that these GlcA-substituted XOS (*m/z* 787 and *m/z* 961) were structurally different from the adjacent MeGlcA-Xyl_4Ac_1 (*m/z* 801) and MeGlcA-Xyl_5Ac_2 (*m/z* 975), respectively. A similar -60 Da fragmentation was observed in the earlier MS^n analysis of (2-*O*-α-Gal-4-*O*-α-MeGlcA)-$Xyl_{2\text{-}3}Ac_1$, the typical acidic XOS from eucalyptus AcGX (Reis et al., 2005). Therefore, the oligosaccharide with *m/z* 787 could be formed by the GlcA-Xyl_3Ac_1 carrying a pentose substituent at the GlcA residue.

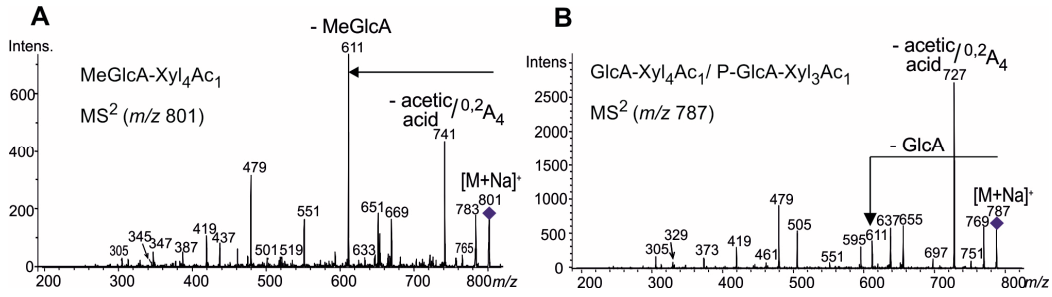

Figure 16. The MS^2 analysis of (A) MeGlcA-Xyl_4Ac_1 (*m/z* 801), and (B) GlcA-Xyl_4Ac_1 (*m/z* 787) selected from the acidic XOS (**Figure 13B**) liberating by endoxylanase from Arabidopsis WT. The mass spectra were acquired by positive ion AP-MALDI-ITMS, and peaks were sodium adducts. Xyl, (1→4)-linked β-D-Xylose; (Me)GlcA, (1→2)-linked (4-*O*-methyl)glucuronic acid; Ac, *O*-acetyl; numeric symbol, number of Xyl or Ac residues. (**Fig. 1C and 1D in paper III**)

OLIMP analysis was also performed on the *irx9-1* (defected xylan backbone) and *irx7* (missing RS) mutants defective in the glycosyltransferases from families GT43 and GT47, respectively, which are involved in the secondary wall GX biosynthesis (**Table 3**). Interestingly, AP-MALDI-ITMS analysis revealed significant amounts of the GlcA-Xyl_4Ac_1 (*m/z* 787) and GlcA-Xyl_5Ac_2 (*m/z* 961) in the hydrolyzates of *irx9-1* (**Fig. 2 in paper III**) and *irx7* (data not shown). Furthermore, the MS^2 spectrum of *m/z* 787 in the hydrolyzate of *irx7* was dominated by a loss of 60 Da and almost completely lacked the peak corresponding to the loss of GlcA (**Suppl. Fig. 1 in paper III**).

To further examine the putative substitution of GlcA residues, an AIR sample from *irx9-1* was deacetylated with NaOH, hydrolyzed with the GH10 endoxylanase, and the acidic XOS released were detected as deprotonated ions in the negative ion ESI-ITMS. Compared with the acidic XOS liberated from AcGX, GH10 endoxylanase hydrolysis of the deacetylated GX released shorter oligosaccharides, with MeGlcA-Xyl_3 (*m/z* 603) as the main product (**Figure 17A**). The peak at *m/z* 721 that can represent GlcA-Xyl_4 or GlcA-Xyl_3 carrying additional pentose substituents at the GlcA residue (P-GlcA-Xyl_3) was selected for MS^n analysis to further determine the branched structure. The MS^2 spectrum showed two consecutive losses of 60 Da and 78 Da, which are typical types of cross ring cleavages of non-substituted Xyl residue from the reducing end, suggesting the GlcA is located at least on the third Xyl residue from the reducing end of the XOS.

The peak corresponding to the C_4 ion at *m/z* 589 was further selected for MS^3 analysis (**Figure 17C**). The B_3 ion (*m/z* 439) had a higher intensity than the C_3 ion (*m/z* 457), which was in contrast to that of the relative ratio between C_4 and B_4 ions (**Figure 17B**). The strong tendency to form a B_3 ion indicated that the third Xyl residue from the reducing end was different than the two preceding Xyl residues. The peak at *m/z* 367 corresponded to cross ring cleavage $^{0,2}X_2$ (loss of 90 Da) (**Figure 17C**). As charge is preferably retained at the GlcA residue, which has the most acidic proton, this fragmentation indicated the presence of a Xyl residue carrying a P-GlcA disaccharide side branch at *O*-2. The structure is further confirmed by analyzing the H-MeGlcA-Xyl_3 liberated by GH10 enoxylanase from the hydrothermally treated XOS of eucalyptus (**Fig. 4 in paper III**), and similar fragmentation behavior to that of *m/z* 721 in the *irx 9-1* hydrolyzate further confirmed the presence of an additional pentose substituent at the GlcA residue of GlcA-Xyl_3.

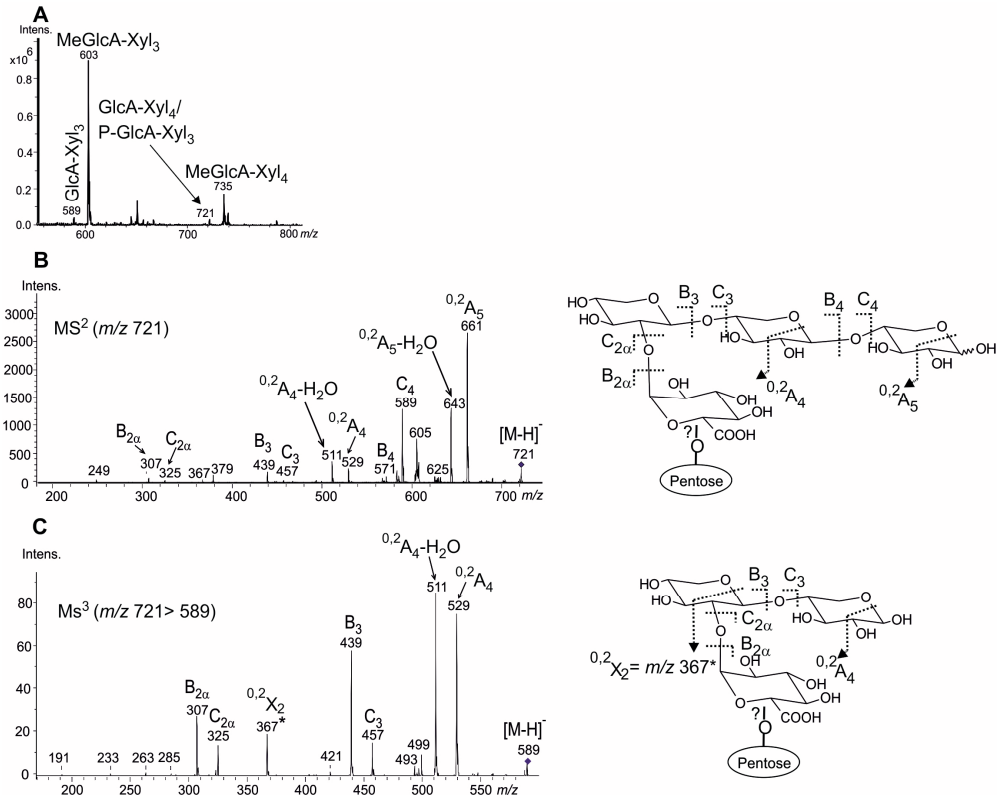

Figure 17. The MS^n analysis of ion peak at *m/z* 721 liberated by GH10 endoxylanase from the deacetylated AIR of *irx9-1*. (A) Mass spectrum of the hydrolyzate was acquired by ESI-ITMS in negative ion mode, and the peaks were deprotonated ions. The ion peak at *m/z* 721 implying two possible isomers was selected for (B) MS^2, and (C) MS^3 analysis. The possible structures are suggested alongside the MS^n spectra. P, pentose residue; * diagnostic fragment ion indicates P-GlcA disaccharide side branch linked to the nonreducing end xylotriose; Xyl, (1→4)-linked β-D-Xylose; (Me)GlcA, (1→2)-linked (4-*O*-methyl)glucuronic acid; numeric symbol, number of Xyl residues (**Fig. 3 in paper III**).

5.4. Acetylation of AcGX in Arabidopsis WT and xylan biosynthetic mutants (IV)

The xylan OLIMP was utilized to further investigate the acetylation of AcGX in the Arabidopsis xylan biosynthetic mutants, *irx7*, *irx9-1*, *irx10, irx14*, and *gux1gux2* (**Table 3**). *O*-acetylation of AcGX in these mutant plants has not been analyzed previously, as the xylans isolated for structural studies were deacetylated due to the alkaline isolation. Before studying with xylan OLIMP, the distribution of acetyl residues in AcGX of Arabidopsis WT was determined quantitatively using the heteronuclear single quantum coherence (HSQC) nuclear magnetic resonance (NMR) spectroscopy.

5.4.1. qHSQC NMR spectroscopic study of the DMSO-extracted AcGX from Arabidopsis WT

The AcGX were solubilized in DMSO from a large batch of AIR pooled from 30 Arabidopsis WT plants, and the recovered yield was ca. 20%. The anomeric region at ^{1}H 5.45-4.30 ppm and ^{13}C 105-98 ppm (**Figure 18A**), and the *O*-acetyl-Xyl*p* region at ^{1}H 5.45-4.30 ppm and ^{13}C 82-70 ppm (**Figure 18B**), were identified in the qHSQC spectrum. Five types of substitutions on the Xyl*p* units: i) 2-*O*-acetyl- (X2), ii) 3-*O*-acetyl- (X3), iii) 2,3-*O*-acetyl- (X23), iv) (Me)Glc*p*A (1→2) linked 3-*O*-acetyl- (X3G2), and v) (Me)Glc*p*A (1→2) linked (XG2) Xyl*p* units were identified. The chemical shifts were assigned based on the previously published data (Teleman et al., 2000; Evtuguin et al., 2003). The cross peaks for the MeGlc*p*A- and Glc*p*A-substituted Xyl*p* units were unresolved in the qHSQC spectrum.

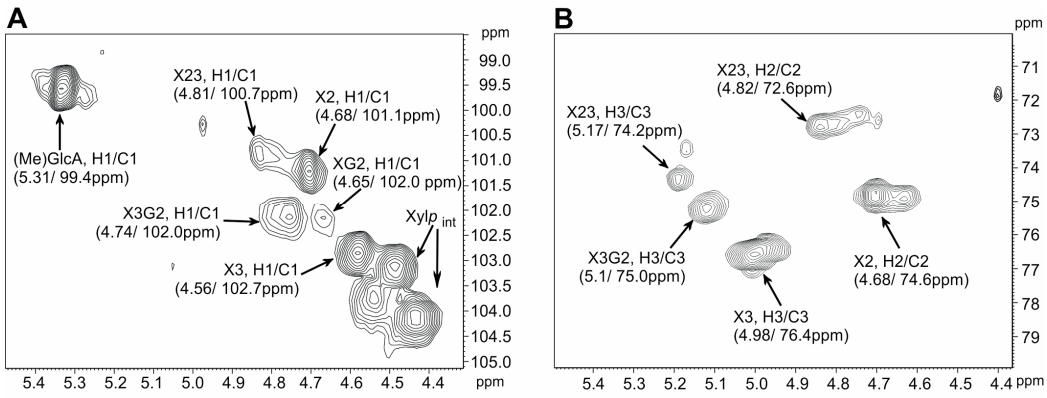

Figure 18. 2D qHSQC spectrum of DMSO-extracted *O*-acetylglucuronoxylan from Arabidopsis WT. Cross peaks for (A) anomeric Xyl*p* units and (B) *O*-acetyl-Xyl*p* units were assigned according to Evtuguin et al. (2003) and Teleman et al. (2000). (**Fig. 1 in paper IV**)

To determine the relative content of the *O*-acetyl-Xyl*p* units in the AcGX, the signals in the anomeric region were summed up to 100%, and the signals in the *O*-acetyl-Xyl*p* region were integrated separately to calculate the relative content for each form of *O*-acetyl-Xyl*p* unit (**Table 12**). Major components found in the AcGX of Arabidopsis WT were single acetyl substitutions (*O*-2 or *O*-3) that accounted for 44% of the Xyl*p* units, while only 6% of the Xyl*p* units were doubly acetylated on their *O*-2 and *O*-3 positions (X23). The % of 3-*O* acetylated Xyl*p* substituted by (1→2) linked (Me)Glc*p*A (X3G2) was 10%, and the non-acetylated Xyl*p* (1→2)-linked with (Me)Glc*p*A (XG2) was 3%. The degree of acetylation (DA) calculated from the total sum of the *O*-acetyl-Xyl*p* units in Arabidopsis WT was 60% (**Table 12**).

5.4.2. Xylan acetylation patterns in the biosynthetic mutants

The AcGX of the biosynthetic mutants (**Table 3**), *irx7* (missing reducing end tetrasaccharide sequence, RS); *irx9-1*, *irx10*, *irx14* (defected xylan backbone, DP); and *gux1gux2* ((Me)GlcA deficient), were then subjected to qHSQC NMR spectroscopic study to compare the acetylation pattern (**Table 12**). Interestingly, the degree of acetylation (DA) in the AcGX of *irx7* and *irx9-1* was 31% and 32%, respectively; which was only half of the level found in the

WT plants (60%). In *irx14*, the DA was 42%. The DA was not affected in *irx10*. The lowering DA observed in *irx7*, *irx9-1*, and *irx14* was mainly due to a decrease in the mono-acetylation at 2-*O* (X2) or 3-*O* (X3) position of Xyl*p*. Nonetheless, the relative content of the X23 and X3G2 was not affected in *irx7*, *irx9-1* and *irx14* compared to WT. The DA in the (Me)Glc*p*A-deficient mutant, *gux1gux2*, was similar to the WT. Due to the missing (Me)Glc*p*A moieties in the AcGX of *gux1gux2*, the level of X3G2 was greatly reduced to only 3%, and, in turn, the level of mono-acetylation (X2 + X3) was significantly elevated to 55%. Taken together, *O*-acetylations, mainly mono-acetylations, were affected in *irx7*, *irx9-1*, *irx14* and *gux1gux2*, despite the diverse functions of the enzymes being knockout in these mutants.

Table 12. Substituted and non-substituted internal Xyl*p* present in *O*-acetylglucuronoxylan of Arabidopsis WT and xylan biosynthetic mutants determined based on the integration of cross peaks in the qHSQC NMR spectra. (**Table 1 in paper IV**)

Genotype	CAZy family	Activity	Xyl*p* units (%)						DA%
			X2	X3	X23	X3G2	XG2	X	
WT			15	29	6	10	3	37	60
irx7	47	RS	5	8	4	14	n.d.	69	31
irx9-1	43	DP	4	8	5	15	n.d.	68	32
irx10	47	DP	16	27	8	11	n.d.	38	62
irx14	43	DP	9	15	5	13	n.d.	58	42
gux1gux2	8	GlcAT	22	33	5	3	n.d.	37	63

X2, [2-*O*-Ac]-β-D-Xyl*p*; X3, [3-*O*-Ac]-β-D-Xyl*p*; X23, [2,3-*O*-Ac]-β-D-Xyl*p*; X3G2, [α-D-(Me)Glc*p*A(1→2)][3-*O*-Ac]-β-D-Xyl*p*; XG2, [α-D-(Me)Glc*p*A(1→2)]-β-D-Xyl*p*; DA, degree of acetylation; RS, reducing end tetrasaccharide sequence; DP, degree of polymerization; GlcAT, glucuronyltransferase; n.d., not detected

5.4.3. Xylan OLIMP analysis of the biosynthetic mutants

In the xylan OLIMP analysis, the neutral XOS profile obtained from the biosynthetic mutants differed in many ways from that of WT (**Figure 19**). The ratio of the intensity of Xyl_2Ac_1 to Xyl_2Ac_2 was reduced in *irx7, irx9-1, irx10* and *irx14*. The change was more pronounced in

irx7 and *irx9-1* than in *irx10* and *irx14*. Lower relative intensity of Xyl_2Ac_1 observed in the *irx* mutants reflecting the reduced mono-acetylation of Xyl*p* residues was in agreement with the NMR data. The neutral XOS profile in *gux1gux2* was changed in an opposite way compared to the other mutants, indicating a higher ratio of Xyl_2Ac_1 to Xyl_2Ac_2. This was also corresponding to the NMR data showing an increase of the relative content of X2+X3 to X23 (**Table 12**).

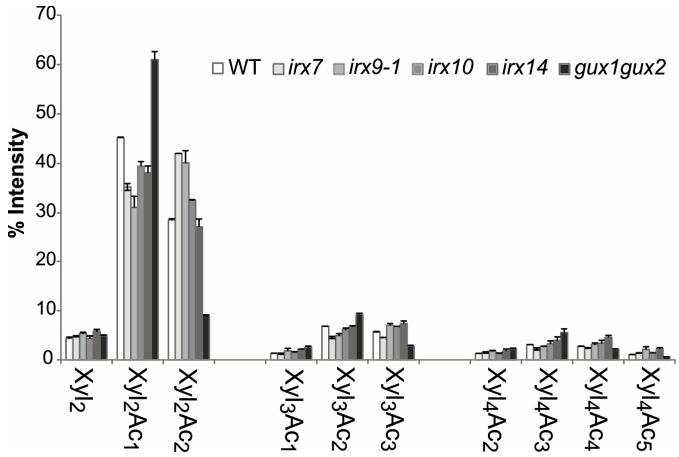

Figure 19. Neutral XOS liberated from AIR of Arabidopsis WT and the biosynthetic mutants (*irx7*, *irx9-1*, *irx10*, *irx14* and *gux1gux2*) by GH10 endoxylanase hydrolysis. % intensity was calculated based on the raw data extracted from the AP-MALDI-ITMS mass spectra. Error bar represents standard deviation of two technical replicates obtained from a pool of 30 or 60 plants. Xyl, (1→4)-linked β-D-Xylose; Ac, *O*-acetyl; numeric symbol, number of Xyl residues. (**Fig. 2B in paper IV**)

Principal component analysis (PCA) was applied to the acidic XOS in order to identify the main variables that separate the different genotypes. The result for *gux1gux2* was excluded from the PCA, as only a small amount of (Me)GlcA was present. The PCA scores scatter plot (**Figure 20A**) showed a distinct separation of WT from the mutants by the first component (47% variance), whereas WT, *irx10* and *irx14* were separated from *irx7* and *irx9-1* by the second component (31% variance). The loading plot for the first component (**Figure 20B**) showed that the MeGlcA-XOS were more abundant in all the mutants than in WT. As

expected, the GlcA moieties were nearly all methylated in these mutants (Peña et al., 2007; Brown et al. 2007; Brown et al. 2009; Wu et al. 2009; Wu et al. 2010). The loading plot of the second component discriminated *irx7* and *irx9-1* from WT and other mutants based on the XOS chain length. The relative intensity of the shortest acidic XOS up to MeGlcA-Xyl_4Ac_1 was higher in the endoxylanase hydrolyzates of *irx7* and *irx9-1* compared to WT, *irx10* and *irx14*. This is consistent with lower DA in the *irx7* and *irx9-1* mutants.

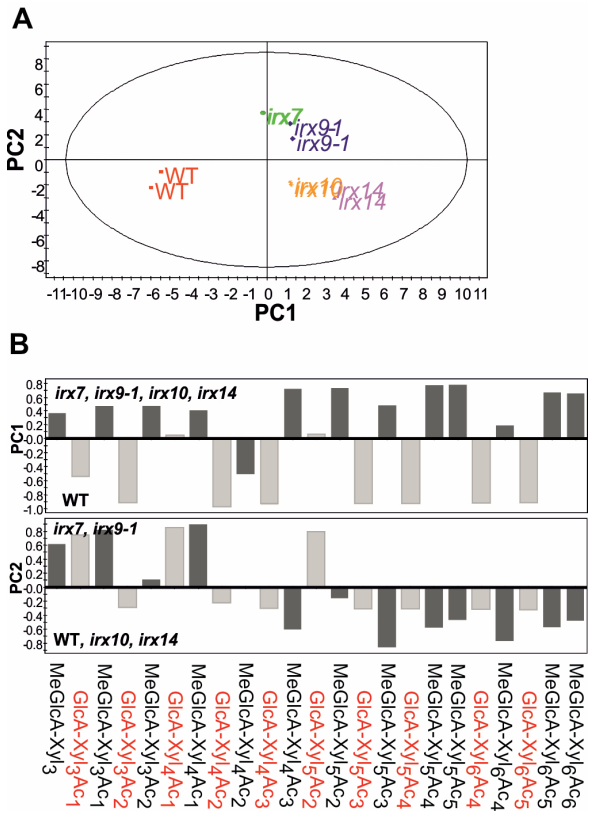

Figure 20. Acidic XOS liberated from AIR of Arabidopsis WT and the biosynthetic mutants (*irx7*, *irx9-1*, *irx10*, *irx14* and *gux1gux2*) by GH10 endoxylanase hydrolysis. (A) Principal component analysis (PCA) scores scatter plot showing the separation WT, *irx7*, *irx9-1*, *irx10* and *irx14*. (B) Loading plots for principal components (PC). PC1 (47% variance) shows mass peaks separating WT (negative) from all mutants (positive). PC2 (31% variance) shows mass peaks separating WT, *irx10* and *irx14* (negative) from *irx7* and *irx9-1* (positive). Two technical replicates were prepared from each genotype. (adapted from **Fig. 3B and 3C in paper IV**)

5.5. Post synthetic modification of (Me)GlcA in Arabidopsis with an GH115 α-glucuronidase (V & VI)

5.5.1. The gene encoding GH115 α-glucuronidase from *Schizophyllum commune* (V)

The α-glucuronidase of white rot basidiomycete, *Schizophyllum commune,* was shown acting on xylan polymers (Tenkanen and Siika-aho, 2000). Thus, it is a suitable candidate for expressing in plant to target the (1→2) linkage between the (Me)GlcA and xylan backbone. The encoding gene sequence was obtained by BlastP search against the *S. commune* genome database (Ohm et al. 2010) with the published N-terminal sequence (Tenkanen and Siika-aho, 2000). The α-glucuronidase of *S. commune* belongs to the family GH115, and the phylogenetic analysis of family GH115 showed that the fungal proteins constituted a group that was separated from bacterial proteins (**Fig. 3 in paper V**). The fungal clade consisted of three distinct branches. The first one consisted exclusively of basidiomycete sequences, including the GH115 α-glucuronidase of *S. commune*. The second branch consisted exclusively of ascomycete sequences and included the characterized protein from *Pichia stipitis* (Ryabova et al., 2009). The third branch contained no biochemically characterized sequences, and consisted mostly of sequences from ascomycetes, but it also contained a second GH115 protein from *S. commune*. The GH115 members of Aspergilli were divided over branch 2 and 3 of the fungal clade. *Aspergillus oryzae* has 4 members divided over branch 2 and 3, whereas *Aspergillus terreus* has two members in branch 2. In addition, *Aspergillus clavatus*, *Aspergillus fumigatus*, and *Neosartorya fischeri* have one member in branch 2. The well-studied species *Aspergillus niger* contained no GH115 members at all. Additionally, the other important industrial fungus, *T. reesei* (*Hypocrea jecorina*) has a member in branch 3.

5.5.2. Production of an active GH115 α-glucuronidase in Arabidopsis (VI)

The full length cDNA (GenBank accession ADV52250.1) was optimized for codon usage in plants, and a synthetic gene lacking low frequency codons (<30%) was cloned in Arabidopsis. The *ScAGU115* cDNA was cloned under the cauliflower mosaic virus 35S promoter, and the native signal peptide was replaced by the signal peptide from the aspen cellulase *Ptt*CEL9B3 for targeting the enzymes to apoplast. Transformation of Arabidopsis with 35S:CEL9B3SP:*Sc*AGU115 resulted in 15 independent homozygotic lines. The cloning and

selection of *Sc*AGU115 mutant lines were done by the co-authors in Swedish University of Agricultural Sciences.

Only three of the expressing plants showed α-glucuronidase activity above the WT level (**Suppl. Fig. 1 in paper VI**). The three lines (lines 4, 5, and 10) that showed α-glucuronidase activity, and the one line (line 6) that did not show a detectable level α-glucuronidase activity were selected for further analysis and re-grown. Gene expression analysis, performed on the re-grown lines, showed that the levels of the *ScAGU115* transcripts were higher in lines 4, 5, and 10, and lower in line 6 (**Figure 21A**). Sodium dodecyl sulfate-polyacrylamide gel electrophoresis (SDS-PAGE) analysis of soluble proteins revealed the presence of two novel protein bands in lines 4, 5, and 10, which were not detected in the WT and in line 6 (**Figure 21B**). Western blot analysis using the anti-*Sc*AGU115 antibody confirmed that the novel bands contained *Sc*AGU115, since signals were detected in lines 4, 5, and 10 (**Figure 21C**). Plant growth was not affected in these high expressing plants (**Fig. 5 in paper VI**).

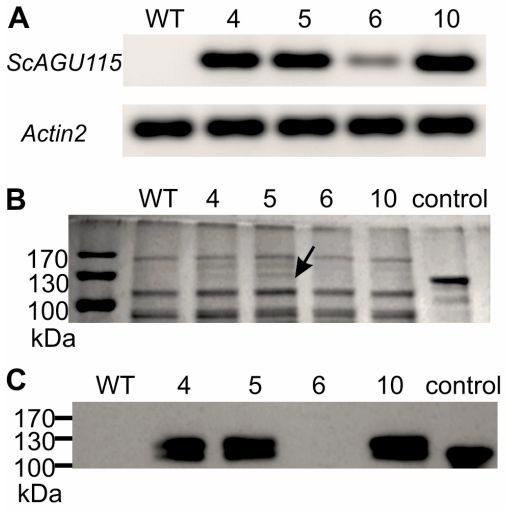

Figure 21. *Sc*AGU115 gene expression and protein analysis in Arabidopsis transgenic and WT plants. (A) RT-PCR analysis of *ScAGU115* expression. (B) The soluble protein was separated on SDS-PAGE and visualized with Coomassie staining. The arrow indicates the novel protein bands that are visible in lines 4, 5, and 10. (C) Western analysis of the soluble proteins with anti-*Sc*AGU115 primary antibody. Control, *Sc*AGU115 native enzyme. (**Fig. 3 in paper VI**)

The α-glucuronidase activity in the protein extracts was assayed with a commercial test kit, which measures GH67 and GH115 types of activities. Specific α-glucuronidase activity in the soluble and wall bound proteins extracted from lines 4, 5 and 10 was about five to six fold higher than the background WT level (**Figure 22A**). The α-glucuronidase activity in line 6 was similar to the background WT level. To test more specifically for the AGU115 type of activity, the soluble proteins from Arabidopsis were further analyzed for their activity toward the internally substituted aldopentaouronic acid, XUXX. Thin layer chromagraphy (TLC) analysis clearly showed that the XUXX substrate was degraded to xylotetraose and MeGlcA by lines 4, 5 and 10 (**Figure 22B**), while no apparent degradation of XUXX was observed in the WT extract or water blank (**Figure 22B**). Only a faint band corresponding to xylotetraose was detected in line 6. The enzymatic activity of the wall-bound proteins showed similar degradation profiles (**Figure 22C**). Taken together, lines 4, 5 and 10 were deemed to be the high *Sc*AGU115 expressing plants, and the expressed enzymes were active toward the internally substituted MeGlcA. Thus, it was of interest to further analyze the transgene effect on the cell wall chemistry and digestibility.

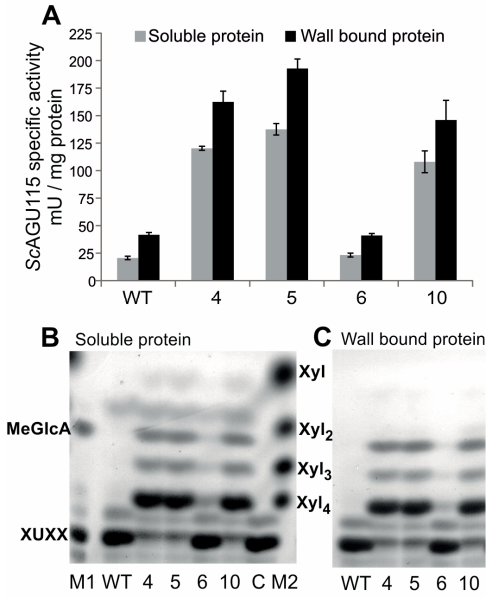

Figure 22. Analysis of *Sc*AGU115 enzyme activity in Arabidopsis transgenic and WT plants. (A) The soluble and wall-bound proteins were analyzed for α-glucuronidase activity using a commercial assay. The error bar represents the standard deviation of three biological

replicates. (B) and (C) TLC analysis of XUXX incubated with soluble (B) or wall-bound (C) protein. XUXX, a xylotetraose carrying MeGlcA at penultimate xylose from the nonreducing end; C, water blank; M1, marker for XUXX and MeGlcA; M2, marker for xylose (Xyl), xylobiose (Xyl_2), xylotriose (Xyl_3), and xylotetraose (Xyl_4). (**Fig. 4 in paper VI**)

5.5.3. Cell wall chemistry and integrity of the *Sc*AGU115 expressing plants

The alcohol insoluble residues (AIR) of the inflorescence stem tissues were examined for chemotypic changes caused by the expression of *Sc*AGU115 in the apoplast. The analyses were performed only on lines 4 and 5 that produced the highest levels of the recombinant enzyme. The analysis of non-cellulosic sugars showed that there were no changes in the (Me)GlcA or other sugar components in lines 4 and 5 compared to the WT (**Table 13**). In addition, neither the lignin content (**Suppl. Table 1 in paper VI**) or cell wall digestibility (**Suppl. Fig. 3 in paper VI**) were affected in these expressing plants. As a comparison, the (Me)GlcA deficient mutant, *gux1gux2* was also studied (Mortimer et al., 2010; **Table 3**). As expected, a significant decrease in total (Me)GlcA content was detected in *gux1gux2* (**Table 13**). Notably, the amount of Xyl and Man was increased by 59% and by 30%, respectively, in *gux1gux2* compared to the WT, whereas no changes in Xyl or Man levels were detected in the *Sc*AGU115 transgenic lines (**Table 13**). Thus, the *in planta* MeGlcA modification via knockout of the glucuronyltransferase activity is more effective than expression of the *Sc*AGU115 α-glucuronidase *in muro*.

Table 13. Non-cellulosic sugar content (% of de-starched AIR) in the inflorescence stem tissues of Arabidopsis transgenic (lines 4, 5) and WT plants. The (Me)GlcA-deficient mutant, *gux1gux2* (Mortimer et al., 2010), was also analyzed with the corresponding wild-type (WT#) plants.

Genotype	Ara	Rha	Xyl	Man	Gal	Glc	GalA	MeGlcA	GlcA
WT	1.3±[a]0.0	1.7±0.1	14.1±0.9	1.3±0.0	1.6±0.0	2.6±0.1	6.6±0.1	1.2±0.1	0.7±0.1
line 4	1.4±0.1	1.7±0.1	13.2±0.6	1.2±0.1	1.6±0.1	2.5±0.1	6.6±0.3	1.1±0.1	0.7±0.1
line 5	1.2±0.2	1.6±0.1	13.1±0.8	1.2±0.1	1.5±0.1	2.5±0.2	6.5±0.4	1.1±0.0	0.7±0.1
WT#	1.2±[b]0.1	1.2±0.1	14.8±1.1	1.3±0.1	1.6±0.1	2.5±0.3	4.3±0.3	1.1±0.1	1.0±0.1
gux1gux2	1.3±0.4	1.4±0.3	23.5±0.9*	1.7±0.1*	1.8±0.4	2.4±0.4	4.7±0.9	0.6±0.0*	0.4±0.0*

a, ± represents the standard deviation of five biological replicates; b, ± represents the standard deviation of three technical replicates from a pool of 30 plants; * indicates significance different from WT# (t test, p value < 0.05). (**Table 1 in paper VI**)

The basal stem sections were labeled with anti-UX1 (Koutaniemi et al., 2012) to visualize the distribution of the (Me)GlcA residues. A weak signal was evident in the water-treated WT (**Figure 23A**), especially in the interfascicular fibers, but it was missing in the water-treated samples of line 4 (**Figure 23B**) and line 5 (**Figure 23C**). In the alkaline-treated stem sections, where esterified acetyl residues were removed, the signal was strongly visible in all samples, and the signal strength was the same for the transgenic and WT plants. No signal was detected in either the water- or alkaline-treated *gux1gux2* sections (**Figure 23D**), despite there being some amount of (Me)GlcA detected in sugar analysis (**Table 13**). The water- and alkaline-treated sections were labeled with the xylan-specific AX1 antibody (Guillon et al., 2004a), indicating that xylan was present and accessible to the antibodies in all samples. Acetylation is known to restrict the binding of UX1 to (Me)GlcA residues (Koutaniemi et al., 2012). Therefore, the small difference observed on the water treated section of line 4 and 5 compared to WT suggests that only a very small fraction of the (Me)GlcA moieties, which are not in close contact with the acetyl substituents, are cleaved in the ScAGU115 expressing plants.

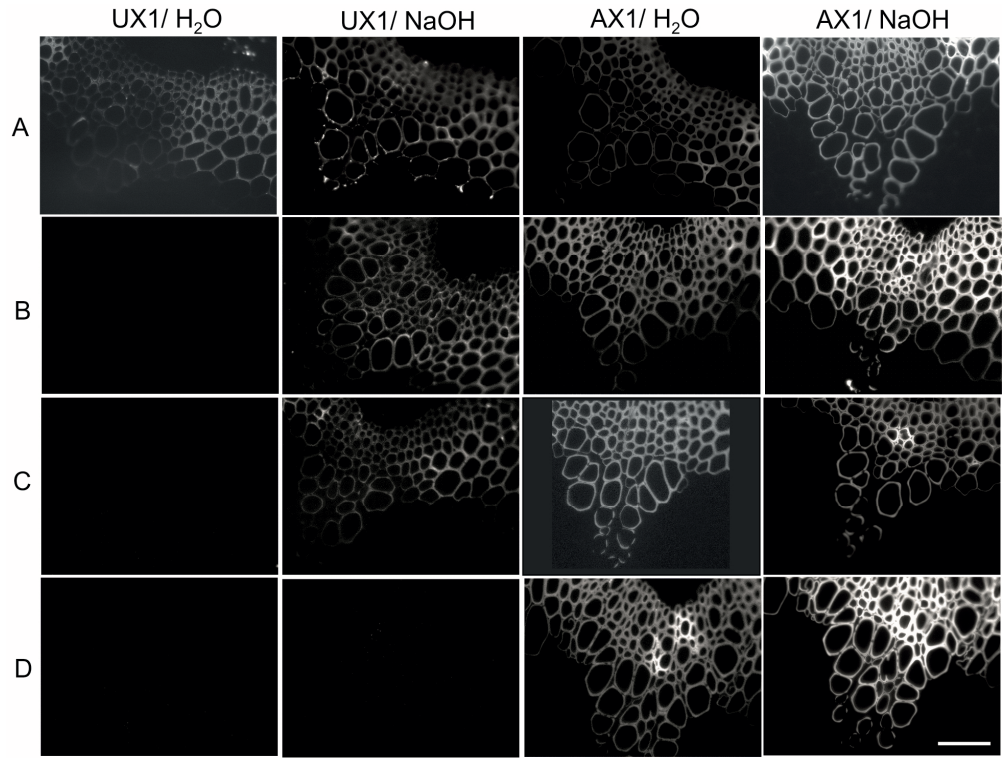

Figure 23. Immunolabeling of the basal stem sections with (Me)GlcA specific (UX1) and xylan specific (AX1) antibodies. The 0.5 µm sections of WT (A), transgenic plants line 4 (B) and line 5 (C), and the (Me)GlcA-deficient mutant, *gux1gux2* (D). The sections were pretreated either in water or 0.05 M NaOH overnight before the labeling. Bar = 50 µm. (**Fig. 7 in paper VI**)

6. DISCUSSION

6.1. Choosing the right GlcA derivatives to determine the MeGlcA content in plant cell walls by acid methanolysis and GC analysis

When using an appropriate GlcA derivative in the calibration curve, the MeGlcA content determined by the commercially available GlcA standard closely estimates values obtained from the authentic MeGlcA standard. Specifically, a calibration curve that includes only the four peaks corresponding to the pyranosyl and furanosyl forms of GlcA (GlcA4p) or the two main GlcA peaks (GlcA2p) can be used for the estimation of MeGlcA content. The error generated by using the GlcA4p or GlcA2p calibration curves only deviated ±10% from the values calculated with the authentic MeGlcA standard.

Interestingly, the reports that have hitherto determined the MeGlcA content by acid methanolysis and GC analysis, did not reveal which of the GlcA glycosides were included in the calibration curve. Since the logical way would be to include all of the GlcA peaks, it is likely that MeGlcA content was underestimated in these cases by nearly 30% (**Figure 9**). On the other hand, the main GlcA peak(s) might be chosen from the chromagram for determining the MeGlcA content if a highly complex chromatogram is obtained. If the calibration curve was created from the main Glc*p*A peak (GlcA1p), the MeGlcA content could be overestimated by more than 50%. Otherwise, the MeGlcA content could be closely estimated if the two main GlcA derivatives were included in the calibration curve (GlcA2p).

The choice of glycosides to be included in the calibration curve depends on the complexity of the chromatogram obtained from the hydrolyzate, since some of glycosides are overlapping, and these peaks should be avoided in the calculations. For example, the Glc*f*A peak was unresolved from its adjacent galacturonic acid glycoside in the GC chromatogram (**Fig. 2 in paper I**). The GlcA2p is likely the best calibration of choice for estimating the MeGlcA content when using GlcA as the standard. However, the use of fresh reagents and the same type of column and separation conditions might be essential for the reproducibility of the result. Therefore, a thorough inter-laboratory cross validation is needed to verify the proposed method of calculation for determining the MeGlcA content.

6.2. Xylan OLIMP – a tool for the fingerprinting of acetylation pattern in AcGX

The AP-MALDI-ITMS was well suited to analyze the acetylated XOS using DHB as the matrix. The mass spectra of acidic XOS were simplified by the addition of $(NH_4)_2SO_4$ into the matrix-analyte mixture, and thus, the double sodiated peaks were eliminated due to the high affinity of the sulphate anion on the alkali cation (Enebro et al., 2006). Moreover, the quality of mass spectra was further improved with the separation of acetylated XOS into neutral and acidic fractions to prevent the problem arising from ion suppression due to different chemical properties in both types of XOS. Of all the reports that have thus far analyzed the endoxylanase hydrolyzate liberated from the GX or AcGX of the cell wall modified mutants, the XOS were not separated prior to the MALDI-MS analysis (Brown et al., 2007; Wu et al., 2010; Yuan et al., 2013; Busse-Wicher et al., 2014). This might complicate the relative quantitation of mass peaks, especially if the endoxylanase hydrolysis was performed on the AcGX liberating vast array of acetylated XOS. The obtained mass spectra were crowded with peaks as a result (Yuan et al., 2013; Busse-Wicher et al., 2014), and this might complicate the peak assignments and interfere with the relative quantitation of the XOS peaks due to ion suppression.

The AP-MALDI was found suitable for the analysis of biomolecules harboring the labile substituents such as sialic acid, acetyl, sulfate, and phosphate (Moyer et al., 2003). In this study, when analyzing the acetylated XOS of eucalyptus, the AP-MALDI-ITMS was found to be more suitable for detecting the neutral XOS with higher degree of acetylation than MALDI-TOF/MS. Ionization of the analytes is softer at atmospheric conditions, and therefore the acetyl is more stable at the XOS moiety. Although the sensitivity of the AP-MALDI-ITMS measurement is poorer in analyzing longer oligosaccharides compared to MALDI-TOF/MS, this system can effectively analyze the XOS derived from plant cell walls by GH10 endoxylanase hydrolysis. The GH10 endoxylanase of *A. aculeatus* was acting close to the substituents (Rantanen et al., 2007), producing the XOS that fall within the scanning mass range of the AP-MALDI-ITMS.

The xylan OLIMP can be a tool for the relative comparison of acetylation pattern in AcGX. Though the degree of hydrolysis by direct application of a single endoxylanase on tissue samples might be limited by other cell wall components, such as cellulose or lignin, characterization of XOS from the enzyme-accessible part in the plant cell wall enabled comparative analyses of GX acetylation. This was demonstrated by comparing the acidic XOS liberated from three hardwood species, whereby the acidic XOS liberated from the

AcGX of aspen differed from that of birch and eucalyptus, and was shown to be more highly acetylated in AcGX of aspen compared to birch and eucalyptus.

For the quantitative application of MALDI-MS, inclusion of an internal standard might be crucial to compensate for the irregularities arising from spot crystallization, and MALDI-MS measurement (Sleno and Volmer, 2006). The choice of internal standard should have a molecular weight and properties similar to the analytes (Seipert et al., 2008), but the acetylated oligosaccharides are unfortunately not commercially available. Other choices of internal standard, such as the hexose oligosaccharides, may not be suitable since these compounds are sometimes observed in the mass spectra due to the presence of endogenous sugars, such as sucrose, in plant tissues. Additionally, the internal standard that carries an acidic proton is needed for normalizing the mass peaks of acidic XOS. Therefore, the selections of the suitable internal standards and their optimization for normalizing the MALDI-MS data will be subjected to future work.

6.3. The study of acetylation pattern in AcGX of Arabidopsis using xylan OLIMP and qHSQC NMR spectroscopy

The xylan OLIMP has shown its suitability for analyzing the powderized stem tissues of Arabidopsis WT and mutant plants. The required AIR for endoxylanase hydrolysis was only 1 to 3 mg, even for the mutant plants with severely decreased xylan content. Thus, this method is a selective and sensitive tool for detecting the changes of acetylation pattern in AcGX of the mutant plants. Moreover, the MALDI target plate that enables multiple sample spotting has offered an advantage for analyzing samples in a high throughput manner. However, the sample throughput is limited by the sample preparation using PGC column purification. Direct enzymatic hydrolysis on a MALDI plate has been attempted to circumvent the sample preparation (Obel et al., 2009; Gunl et al., 2010), but this method may just be workable on soft tissues such as seedling or leave tissues. Ambient MS sampling such as desorption electrospray ionization (DESI) can be an interesting tool for direct extraction of the analytes from sample surfaces or dried droplets by directing the analyte to the electrospray capillary inlet using a flow of solvent/aqueous mixture, thus minimizing the need for solid phase extraction (SPE) (Harris et al., 2011). However, this new sampling technique is more often used for the analysis of small molecules, such as metabolites, extractives, etc., and thus its applicability in the analysis of biomolecules larger than *m/z* 1000 is yet to be proven. Of the

two potential methods for minimizing the need for SPE purification, neither of them is able to separate the hydrolyzate into neutral and acidic XOS.

Before comparing the acetylation pattern in AcGX of Arabidopsis mutant plants using xylan OLIMP, the AcGX was first extracted from a large batch of stem tissues, and was then subjected to qHSQC NMR analysis. The purpose was to verify the comparative result obtained from xylan OLIMP, and also to quantitatively determine the distribution of acetyl residues in the AcGX of Arabidopsis WT and mutant plants. The measured DA of 60% in AcGX of Arabidopsis WT was similar to those reported for other dicot species (Teleman et al. 2000; Evtuguin et al. 2003; Naran et al. 2009; Yuan et al. 2013), whereas the distribution of the acetyl groups closely resembled the results published recently by Yuan et al. (2013) that analyzed the DMSO extracted AcGX with ^{1}H NMR spectroscopy. Nearly half (44%) of the Xyl*p* units were mono-acetylated, i.e., 2-*O* (X2) or 3-*O* (X3) -acetyl-Xyl*p* units, while 2,3-*O*-acetyl-Xyl*p* units (X23) were a minority. The content of (Me)GlcA substituted Xyl*p* units was 13% (X3G2 + XG2), of which three quarters were also acetylated on *O*-3 position (Table 1). Unfortunately, (Me)GlcA (1→2) linked Xyl*p* units were not reported by Yuan et al. (2013), probably because the signal could not be identified in the ^{1}H NMR spectrum.

A good correlation between xylan OLIMP analysis and the qHSQC NMR studies was obtained since both methods have revealed similar differences between the xylan biosynthetic mutants and WT plants. Thus, the xylan OLIMP enables a fast and sensitive measurement of acetylation pattern in AcGX; however, it only allows a relative quantitation when comparing the samples. The NMR analysis permits the quantitation of acetyl distribution in AcGX, but the measurement requires large amounts of isolated xylans, which may not be sufficiently available from the mutant plants with dwarf phenotype or severely reduced xylan content. In addition, the laborious procedures in DMSO extraction may not be practical for handling large quantity of samples. Recently, the acetylation of xylans in Arabidopsis has also been studied with HSQC NMR analysis by direct solubilization of AIR in DMSO-d6 containing 1-ethyl-3-methylimidazolium acetate (Cheng et al., 2013), which allowed studying various cell wall components in one measurement. With this method, the requirement for DMSO extraction can be circumvented. However, the high complexity of cross-peak signals derived from various cell wall components did not allow the characterization of complete acetylation pattern in xylans. For example, signals for the 2,3-*O*-acetyl-Xyl*p* (X23), (Me)GlcA (1→2) linked 3-*O*-acetyl-Xyl*p* (X3G2) and Xyl*p* (XG2) could not be identified in the work by Gille et al. (2011) or Xiong et al. (2013), which also studied acetylation of AcGX in the Arabidopsis mutant plants.

6.4. New structural features in AcGX of Arabidopsis

6.4.1. The alternating acetyl substitution pattern in AcGX

With the advantage of ITMS performing MS^n analysis, the AP-MALDI-ITMS is capable of analyzing mass and structure of oligosaccharide in one system. Therefore, in the analysis of the Arabidopsis WT hydrolyzate sample, several main peaks observed from the mass scanning of neutral and acidic XOS were further selected for MS^2 analysis.

The MS^2 analysis of Xyl_2Ac_1 and Xyl_2Ac_2 (**Figure 14**); and (Me)GlcA-Xyl_4Ac_2 (*m/z* 829/843) (**Figure 15**) suggested that these main XOS fragments carried the acetyl residues in every alternate Xyl unit. Additionally, there was also a lower abundance of larger XOS fragments, which were highly acetylated but not analyzed by the MS^n analysis. They were the neutral XOS (Xyl_3Ac_{1-3} and Xyl_4Ac_{2-5}), and acidic XOS (MeGlcA-Xyl_5Ac_{2-5} and MeGlcA-Xyl_6Ac_{4-6}) that might harbor two adjacent acetylated Xyl units. The MS^n analysis is highly complicated to perform on the larger XOS carrying multiple units of acetyl residues, since these substituents are labile and not sustainable after the precursor ion is fragmented.

Nonetheless, the alternating acetyl substitution in every other Xyl*p* unit may form the major part in xylans. This is supported by the recent work of Busse-Wicher et al. (2014) that has suggested a similar hypothesis. In addition, the systematic addition of a side group on xylan backbone has been recently demonstrated by two distinctive (Me)GlcA substitution domains synthesized by two different GT8 enzymes, GUX1 and GUX2 in Arabidopsis (Bromley et al., 2013). Busse-Wicher et al. (2014) suggested that the alternate patterning of acetylation was likely present in the major domain of xylans having the evenly substituted (Me)GlcA. When observing the absorption of AcGX on cellulose in the molecular dynamic analysis, these GlcA and acetyl residues were extending outwardly from a cellulose surface through a helical rotation (Busse-Wicher et al., 2014; Reis and Vian, 2004). Thus, this arrangement is expected to aid a closer contact between the xylan-cellulose composite and lignin due to the hydrophobicity of the acetyl substituents (Pawar et al., 2013).

6.4.2. A novel pentose substitution in the GlcA side branch of AcGX

With the MS^2 analysis using positive ion AP-MALDI-ITMS, two abnormal GlcA-XOS, GlcA-Xyl_4Ac_1/P-GlcA-Xyl_3Ac_1 and GlcA-Xyl_5Ac_2 were identified, which showed different fragmentation routes compared to the other (Me)GlcA-XOS. The presence of a pentose

substitution in the GlcA substituent was proven with the MS^n analysis using negative ion ESI-ITMS. Interestingly, this novel pentose substitution was seemingly enriched in the stem tissue of the xylan biosynthesis mutant *irx9-1* and *irx7*, in which the thickness of the secondary wall was greatly reduced (Brown et al., 2007). This indicates that the unique Pentose-GlcA side branch may instead originate from the primary wall.

Branching on the GlcA residues may indicate the crosslinking of AcGX with other polysaccharides, as was recently described for arabinoxylan linked to rhamnogalacturonan I and arabinogalactan (Tan et al., 2013). Additionally, it is also possible that the crosslinking is formed between two AcGX chains catalyzed by the action of transglycosylating enzymes. Such enzymes are known for xyloglucan (xyloglucan endotransglucosylase) (Fry et al., 1992; Nishitani and Tominaga, 1992), mannan (Schröder et al., 2006), and xylan (Derba-Maceluch et al., 2014; Franková and Fry, 2011; Johnston et al., 2013). For eucalyptus, Evtuguin et al. (2003) indicated that Gal and the proposed Glc substituents found in MeGlcA residues of xylan may arise from covalent linkages between GX and (rhamnoarabino)galactans and glucans, respectively.

The disaccharide side branch formed by β-Xyl*p*-(1→2)-α-Ara*f* is found in some of the Poaceae members (Hoije et al., 2006). The role of the Xyl-Ara branching in the cell wall is unclear, but the knockout of the rice GT61 XAX1, responsible for transferring UDP-Xyl onto (1→3) linked arabinosyl in GAX, has resulted in a decreased ferulic and *p*-coumaric acid content, and an increased saccharification efficiency of the cell wall (Chiniquy et al., 2012). This indicates that the Xyl-Ara branching is related to the feruloylation of the xylans.

However, the nature of the pentose residue (Xyl or Ara) and its linkage to Glc*p*A was not determined in this study. Due to the low abundance of this component in the AcGX present in stem tissues, it is not possible to perform a thorough structural analysis using NMR spectroscopy. Further work is needed to analyze the plant tissues that are enriched in the primary wall xylans, as this pentose-branched structural compound could be substantially available in the xylan present in primary walls.

6.5. Acetylation of xylans was affected by impaired biosynthesis process

Acetylation of xylans in the *irx* mutants has not been previously analyzed. It is important to gain the complete structural information of AcGX in order to detect the direct or indirect changes of cell wall chemistry due to knockout of the xylan biosynthetic gene. Mono-acetylation was reduced significantly in *irx7*, *irx9-1* and *irx14*, in which the effect was the same regardless of the type of xylan biosynthetic process being eliminated in the mutants, i.e., backbone or the reducing end sequence synthesis. The impairment of *O*-2 or *O*-3 acetylation due to knockout of the two important biosynthetic functions indicates that a reduction in xylan biosynthesis decreases mono-acetylation in AcGX. This suggests a regulatory mechanism that coordinates the expression of the xylan biosynthetic machinery in the cells undergoing secondary cell wall formation.

The *irx7* and *irx9* have lost 60% to 70% of AcGX, whereas *irx14* was affected less with 50% decreased AcGX content (Brown et al., 2007; Wu et al., 2010). The *irx10* mutant was the least affected mutant, losing just 20% of AcGX (Wu et al., 2009). Cellulose content was also reduced in *irx7*, *irx9* and *irx14*, as was thickness of the secondary walls (Brown et al., 2007). Recently, Petersen et al. (2012) reported that the lignin content was also reduced in *irx7* and *irx9*. Regulation of cellulose and lignin biosynthesis in these mutants might be part of the same coordinated secondary wall biosynthetic program, which affects AcGX acetylation in the *irx* mutants studied in this work. This could be part of the cell wall integrity (CWI) maintenance that changes the course of plant growth and wall composition in response to biotic/abiotic stress (Hamann, 2012; Doblin et al., 2014). Besides, as the three main cell wall components: cellulose, xylans and lignins are reduced in the secondary cell wall of the *irx* mutants, it is of interest to investigate further which of the constituents are increased in the biomass. Apart from the regulated secondary wall biosynthesis, the acetylation of xylans may also be post-synthetically modified by esterases present in the cell wall. Thus the characterization of two putative CE6 acetyl xylan esterases in Arabidopsis (http://www.cazy.org/CE6_eukaryota.html) will be an interesting subject to study.

The reduced lignin content in *irx7* and *irx9* might result from the changes in the properties of the cellulose-xylan composite. As was discussed earlier, the alternating substitution of acetyl is expected to enhance the hydrophobic interactions between cellulose-xylan and lignin. Thus, the reduced acetyl content in the AcGX would create a hydrophilic environment that is less favorable for lignification. Additionally, the reason could be ascribed to the severely reduced xylan content in these mutant plants, and thus less AcGX epitodes were available for forming the lignin carbohydrate linkages (Hao et al., 2014).

6.6. The (Me)GlcA modification and the effect on cell wall chemistry

6.6.1. Endogenous MeGlcA modification increases xylan content and mono-acetylation in xylans

The double disruption of GUX1 and GUX2 enzymes led to a drastic decrease in the (Me)GlcA content (**Table 13**; Mortimer et al. 2010). Unexpectedly, the amounts of xylan and mannan were elevated as indicated by the increased Xyl and Man content (**Table 13**). The increase in Xyl levels in *gux1gux2* was similarly observed by Lee et al. (2012). This may suggest a competing utilization of UDP-GlcA in the double mutant as the substrate for UDP-GlcA decarboxylase for production of UDP-Xyl (Harper and Bar-Peled, 2002). It is also possible that plants sense the lower mechanical stability of the cell walls, which was detected in the double mutant *gux1gux2* (Mortimer et al., 2010), leading to an activation of CWI maintenance.

The acetylation pattern in xylan was affected in *gux1gux2*. The NMR and OLIMP analysis showed that the mono-acetylation, primarily 2-*O* acetylation, was elevated by 25% compared to the WT plant (**Table 12**). This suggests opportunistic acetylation of the "free" OH-2 when the GUX1 and GUX2 enzymes are not operational and GlcA is not added, and that mono-acetylation occurs after GlcA addition. The process appears to be similar to 4-*O* methylation of GlcA, which is thought to occur after the GX assembly (Brown et al. 2007a; Peña et al. 2007; Wu et al. 2009).

Xylan extraction was improved in *gux1gux2* (Mortimer et al., 2010), which is likely due to the lack of covalent bonding with lignin when the MeGlcA substituents are missing. Despite the improvement in xylan extraction, the efficiency of saccharification in *gux1gux2,* or even the triple mutant *gux1gux2gux3,* was unchanged compared to the WT plant (Lee et al., 2012a). Acetylation of xylans is known to retard the accessibility of endoxylanases, and consequently, adversely affect the liberation of fermentable sugars (Zhang et al., 2011). Therefore, when mono-acetylation in the xylans of *gux1gux2* is elevated in *gux1gux2*, no improvement in saccharification is expected, unless a sufficient amount of esterases is supplemented in the lignocelluloytic enzyme preparation.

6.6.2. Post-synthetic (Me)GlcA modification by the GH115 α-glucuronidase is limited in plant

The codon-optimized *Sc*AGU115 α-glucuronidase produced in Arabidopsis was active against internally substituted (Me)GlcA. However, no decrease in the (Me)GlcA content or improved digestibility of the stem tissues was observed in the *Sc*AGU115 expressing plants. This suggests that the action of AGU115 is limited *in planta*.

The unchanged level of total (Me)GlcA in the *Sc*AGU115 expressing plants could be due to the high degree of acetylation in xylans, since 50% of the Xyl residues are either mono- or di-acetylated in Arabidopsis (**Table 12**). Furthermore, most of the (Me)GlcA-substituted Xyl residues carry acetylation at the 3-*O* position (**Table 12**). The hindering effect of acetyl substitution on *Sc*AGU115 action has been shown *in vitro* since only 10% of the theoretical MeGlcA was released from birch AcGX compared to the 49% yield from deacetylated GX (Tenkanen and Siika-aho, 2000). Thus, xylan acetylation could be a key parameter restricting the action of GH115 enzymes, especially since most of the Xyl residues that carry the (Me)GlcA are also 3-*O* acetylated. This might hinder the *Sc*AGU115 binding at the +1 subsite. Besides, the alternating acetyl substitution pattern is likely dominating a major part of xylans. Therefore, in addition to the important +1 subsite, the neighboring Xyl residues at the reducing end side (+R2, +R3) (nomenclature according to Mckee et al., (2012)), and the nonreducing end side (+NR2), of the xylan chain may be crucial for productive enzyme-substrate binding. The proposed shielding of (Me)GlcA substituents by acetylation is consistent with the immunolocalization results for the UX1 antibody (**Figure 23**), which shows a small but clear difference on water treated sections of transgenic and WT plants, suggesting that ScAGU115 acts on (Me)GlcA that are not in close contact with the acetyl substituents. Unfortunately, the small difference was not detectable by sugar analysis or the qHSQC NMR analysis on the DMSO extracted AcGX (**Suppl. Fig. 2 in paper VI**). Further work is needed to test the activity of this family of α-glucuronidases using model substrates with well-defined acetylation patterns.

Another possible reason why the (Me)GlcA substituents were not modified by *Sc*AGU115 *in planta* is that the accessibility of AcGX *in muro* is essentially different from conditions *in vitro*. The MeGlcA residues were likely surrounded by lignin, which create more hydrophobic conditions compared to the *in vitro* conditions. The *Sc*AGU115 enzyme has been found to exist as a dimer (Tenkanen and Siika-aho, 2000). Since the dimer exceeds 200 kDa, the compactness of the secondary wall may not permit the enzyme to work as effectively as *in vitro* where isolated xylans are present.

7. CONCLUSION

In this work, the substituents in the AcGX of Arabidopsis WT and the cell wall modified plants were studied. Acetylation in the AcGX of Arabidopsis WT was studied using xylan OLIMP and qHSQC analysis, and the change in the AcGX of xylan biosynthetic mutants was examined. Besides, the accuracy of MeGlcA quantitation using the commercially available GlcA in GC analysis was evaluated. Post synthetic modification of MeGlcA in AcGX of Arabidopsis via expressing the white rot basidiomycete *Schizophyllum commune* GH115 α-glucuronidase was attempted, and the effect was compared to that of *gux1gux2*.

This work demonstrated that the MeGlcA content can be closely estimated by selecting the right choices of GlcA derivatives in the chromatogram. The acid methanolysis and GC analysis is the preferred method for the compositional analysis of AcGX since the acid methanolysis is effective to liberate the (Me)GlcA substituents. It is important to find a way for the close estimation of MeGlcA content, as this sugar standard is not commercially available, and the GlcA standard is used instead. Accordingly, the method developed herein will benefit the analysis of cell wall modified mutant plants for estimating the MeGlcA content more accurately as the substituent will affect the extractability of xylans from plant cell walls (Mortimer et al., 2010).

The xylan OLIMP employing endoxylanase hydrolysis and AP-MALDI-ITMS detection is a selective and sensitive tool for comparing the substitution pattern in AcGX. The structural fingerprinting of AcGX in various hardwood species using xylan OLIMP suggests that the analysis can differentiate the samples that differed in acetylation pattern. For the future applicability of the method, it can be used for the analysis of large quantities of plants tissues derived from cell wall modifications or natural variations, and help reduce the number of samples for further detailed analyses. Since the endoxylanase hydrolysis of AcGX generates a complex set of acetylated XOS, PCA analysis is recommended for the MS data analysis to detect the differences among samples.

The AP-MALDI-ITMS has the advantage to analyze the mass and structure of oligosaccharides in one system, thus the main or interesting peaks can be conveniently selected from the mass scanning spectra of the endoxylanase hydrolyzates for the subsequent MS^2 analysis. Analysis of the acetylated XOS liberated from Arabidopsis WT plant suggests that the acetyl residue substitutes every alternate Xyl*p* residue. Though the presence of acetyl substituents on at least two adjacent Xyl*p* in the AcGX can not be excluded, the alternating substitution of acetyl residues is likely the major acetylation pattern in AcGX. This

systematic addition of acetyl residues in AcGX is proposed for the first time, and it will benefit to the study of xylan degradation, and the interactions of AcGX with other cell wall components.

The discovery of the novel pentose-GlcA side branch in the AcGX of Arabidopsis was unexpected. Further branching is rarely found in the AcGX of dicot species, thus this pentose-GlcA side branch may be present in the specialized tissues of Arabidopsis stem. As the structural studies are normally performed on the xylan isolated from whole tissues, the minor structural component can be easily masked by the average structure of xylan. Thus, this work shows again the sensitivity of mass spectrometry for identifying minor structural component in a complex carbohydrate. However, the starting material used in this work is a ground tissue from whole stem, thus the presence of the pentose-GlcA side branch is not spatially localized. Additionally, the nature of the pentose (arabinose or xylose) and its linkage to GlcA are also not identified. Therefore, the xylans that are enriched in this disaccharide side branch need to be localized within stem tissue for a thorough structural study. MALDI imaging on the stem section will be an interesting tool for localizing the xylan with different substitution patterns.

Using the developed xylan OLIMP and qHSQC NMR analysis methods, a decreased level of mono-acetylation in the AcGX of *irx7, irx9-1* and *irx14* mutant plants was detected. Since xylans are commonly isolated using an alkaline solution, the acetylation of AcGX in the *irx* mutants was not previously analyzed. Therefore, this work suggests that a thorough structural analysis of AcGX is needed in order to detect the structural changes of AcGX in the mutant plants. Acetylation of AcGX is affected by the mutation of an endogenous gene; however, it is not known whether the effect is a regulated mechanism during secondary cell wall biosynthesis or post-synthetically modified by the putative esterases. Therefore, further work is needed to address this question. It is important to get an in-depth understanding on the biosynthesis and remodeling of acetylation as nearly 60% of the Xyl*p* units in AcGX of dicot species are acetylated, and these substituents dictate the interactions of AcGX with other wall components within the plant cell walls, as well as the liberation of fermentable sugars from plant biomass.

The (Me)GlcA content was significantly reduced in the *gux1gux2* mutants due to the deletion of the endogenous glucuronyltransferase activities. However, the post-synthetic modification of (Me)GlcA via the heterologous expression of the *Sc*AGU115 α-glucuronidase was ineffective to remove the MeGlcA moieties in AcGX. If the enzymatic action of *Sc*AGU115 α-glucuronidase is hindered by xylan acetylation in plant cell walls, a viable approach could be co-expression with an acetyl xylan esterase (AXE) to obtain synergism between these side-

group removing enzymes. No improvement in saccharification was observed in *gux1gux2gux3* hydrolyzed without pretreatment (Lee et al., 2012a), which shows that a strong decrease in (Me)GlcA substitution by mutating endogenous glucuronyltransferases might not be optimal for biomass improvement for saccharification as the acetyl substituents are still present in the AcGX. Therefore, the co-expression of AGU115 and AXE in plants could be a strategic approach for designing a cell wall amenable to better xylan extractability and saccharification.

8. REFERENCES

Anders N, Wilkinson MD, Lovegrove A, Freeman J, Tryfona T, Pellny TK, Weimar T, Mortimer JC, Stott K, Baker JM, Defoin-Platel M, Shewry PR, Dupree P, Mitchell RAC. 2012. Glycosyl transferases in family 61 mediate arabinofuranosyl transfer onto xylan in grasses. P Natl Acad Sci 109:989-993.

Andersson S, Samuelson O, Ishihara M, Shimizu K. 1983. Structure of the reducing end-groups in spruce xylan. Carbohydr Res 111:283-288.

Appeldoorn MM, de Waard P, Kabel MA, Gruppen H, Schols HA. 2013. Enzyme resistant feruloylated xylooligomer analogues from thermochemically treated corn fiber contain large side chains, ethyl glycosides and novel sites of acetylation. Carbohydr Res 381:33-42.

Aspeborg H, Schrader J, Coutinho PM, Stam M, Kallas Å, Djerbi S, Nilsson P, Denman S, Amini B, Sterky F, Master E, Sandberg G, Mellerowicz E, Sundberg B, Henrissat B, Teeri TT. 2005. Carbohydrate-Active Enzymes involved in the secondary cell wall biogenesis in hybrid aspen. Plant Physiol 137:983-997.

Bae H, Kim HJ, Kim YS. 2008. Production of a recombinant xylanase in plants and its potential for pulp biobleaching applications. Bioresour Technol 99:3513-3519.

Balakshin MY, Capanema EA, Chang H. 2007. MWL fraction with a high concentration of lignin-carbohydrate linkages: isolation and 2D NMR spectroscopic analysis. Holzforschung 61:1-7.

Barnett JR, Bonham VA. 2004. Cellulose microfibril angle in the cell wall of wood fibres. Biol Rev 79:461-472.

Bauer S. 2012. Mass spectrometry for characterizing plant cell wall polysaccharides. Front Plant Sci 3:45. doi: 10.3389/fpls.2012.00045

Biely P, Vrsanska M, Tenkanen M, Kluepfel D. 1997. Endo-β-1,4-xylanase families: differences in catalytic properties. J Biotechnol 57:151-166.

Biely P, Mastihubová M, Tenkanen M, Eyzaguirre J, Li X, Vršanská M. 2011. Action of xylan deacetylating enzymes on monoacetyl derivatives of 4-nitrophenyl glycosides of β-D-xylopyranose and α-L-arabinofuranose. J Biotechnol 151:137-142.

Biely P. 2012. Microbial carbohydrate esterases deacetylating plant polysaccharides. Biotechnol Adv 30:1575-1588.

Biely P, Cziszárová M, Agger JW, Li X, Puchart V, Vršanská M, Eijsink VGH, Westereng B. 2014. *Trichoderma reesei* CE16 acetyl esterase and its role in enzymatic degradation of acetylated hemicellulose. Biochim Biophys Acta 1840:516-525.

Borkhardt B, Harholt J, Ulvskov P, Ahring BK, Jørgensen B, Brinch-Pedersen H. 2010. Autohydrolysis of plant xylans by apoplastic expression of thermophilic bacterial endo-xylanases. Plant Biotechnol 8:363-374.

Bouchabke-Coussa O, Quashie M, Seoane-Redondo J, Fortabat M, Gery C, Yu A, Linderme D, Trouverie J, Granier F, Teoule E, Durand-Tardif M. 2008. ESKIMO1 is a key gene involved in water economy as well as cold acclimation and salt tolerance. BMC Plant Biol 8:125.

Bromley JR, Busse-Wicher M, Tryfona T, Mortimer JC, Zhang Z, Brown DM, Dupree P. 2013. GUX1 and GUX2 glucuronyltransferases decorate distinct domains of glucuronoxylan with different substitution patterns. Plant J 74:423-434.

Brown DM, Goubet F, Wong VW, Goodacre R, Stephens E, Dupree P, Turner SR. 2007. Comparison of five xylan synthesis mutants reveals new insight into the mechanisms of xylan synthesis. Plant J 52:1154-1168.

Brown DM, Zhang Z, Stephens E, Dupree P, Turner SR. 2009. Characterization of IRX10 and IRX10-like reveals an essential role in glucuronoxylan biosynthesis in Arabidopsis. Plant J 57:732-746.

Brown DM, Zeef LAH, Ellis J, Goodacre R, Turner SR. August 2005. Identification of novel genes in arabidopsis involved in secondary cell wall formation using expression profiling and reverse genetics. Plant Cell 17:2281-2295.

Buanafina Md, Langdon T, Dalton S, Morris P. 2012. Expression of a *Trichoderma reesei* β-1,4 endo-xylanase in tall fescue modifies cell wall structure and digestibility and elicits pathogen defence responses. Planta 236:1757-1774.

Buchert J, Siika-aho M, Bailey M, Puls J, Valkeajärvi A, Pere J, Viikari L. 1993. Quantitative determination of wood-derived soluble oligosaccharides by HPLC. Biotechnol. Tech. 7:785-790.

Busse-Wicher M, Gomes TCF, Tryfona T, Nikolovski N, Stott K, Grantham NJ, Bolam DN, Skaf MS, Dupree P. 2014. The pattern of xylan acetylation suggests xylan may interact with cellulose microfibrils as a twofold helical screw in the secondary plant cell wall of Arabidopsis thaliana. Plant J 79:492-506.

Caffall KH, Mohnen D. 2009. The structure, function, and biosynthesis of plant cell wall pectic polysaccharides. Carbohydr Res 344:1879-1900.

Carpita NC, Gibeaut DM. 1993. Structural models of primary cell walls in flowering plants: consistency of molecular structure with the physical properties of the walls during growth. Plant J 3:1-30.

Cheng K, Sorek H, Zimmermann H, Wemmer DE, Pauly M. 2013. Solution-state 2D NMR spectroscopy of plant cell walls enabled by a dimethylsulfoxide-d6/1-ethyl-3-methylimidazolium acetate solvent. Anal Chem 85:3213-3221.

Chin L, Ali ZM, Lazan H. 1999. Cell wall modifications, degrading enzymes and softening of carambola fruit during ripening. J Exp Bot 50:767-775.

Chiniquy D, Sharma V, Schultink A, Baidoo EE, Rautengarten C, Cheng K, Carroll A, Ulvskov P, Harholt J, Keasling JD, Pauly M, Scheller HV, Ronald PC. 2012. XAX1 from glycosyltransferase family 61 mediates xylosyltransfer to rice xylan. P Natl Acad Sci 109:17117-17122.

Chiniquy D, Varanasi P, Oh T, Harholt J, Katnelson J, Singh S, Auer M, Simmons B, Adams PD, Scheller HV, Ronald PC. 2013. Three novel rice genes closely related to the Arabidopsis IRX9, IRX9L, and IRX14 genes and their roles in xylan biosynthesis. Front Plant Sci 4:83. doi: 10.3389/fpls.2013.00083

Choi I, Kim H, Choi Y. 2000. Gene cloning and characterization of α-glucuronidase of *Bacillus stearothermophilus* No. 236. Biosci Biotechnol Biochem 64:2530-2537.

Choi J, Kim K, Jeon J, Lee Y. 2013. Fungal plant cell wall-degrading enzyme database: a platform for comparative and evolutionary genomics in fungi and Oomycetes. BMC Genomics 14:S7. doi:10.1186/1471-2164-14-S5-S7

Ciucanu I, Kerek F. 1984. A simple and rapid method for the permethylation of carbohydrates. Carbohydr Res 131:209-217.

Ciucanu I. 2006. Per-*O*-methylation reaction for structural analysis of carbohydrates by mass spectrometry. Anal Chim Acta 576:147-155.

Collins T, Gerday C, Feller G. 2005. Xylanases, xylanase families and extremophilic xylanases. FEMS Microbiol Rev 29:3-23.

Cosgrove DJ. 1999. Enzymes and other agents that enhance cell wall extensibility. Annu Rev Plant Physiol Plant Mol Biol 50:391-417.

Cosgrove DJ. 2005. Growth of the plant cell wall. Nat Rev Mol Cell Biol 6:850-861.

Coutinho PM, Deleury E, Davies GJ, Henrissat B. 2003. An evolving hierarchical family classification for glycosyltransferases. J Mol Biol 328:307-317.

Creaser CS, Reynolds JC, Harvey DJ. 2002. Structural analysis of oligosaccharides by atmospheric pressure matrix-assisted laser desorption/ionization quadrupole ion trap mass spectrometry. Rapid Commun Mass Spectrom. 16:176-184.

de O. Buanafina MM. 2009. Feruloylation in grasses: current and future perspectives. Mol Plant 2:861-872.

de Ruiter GA, Schols HA, Voragen AGJ, Rombouts FM. 1992. Carbohydrate analysis of water-soluble uronic acid-containing polysaccharides with high-performance anion-exchange chromatography using methanolysis combined with TFA hydrolysis is superior to four other methods. Anal Biochem 207:176-185.

de Vries R, Battaglia E, Coutinho P, Henrissat B, Visser J. 2011. (Hemi-)cellulose degrading enzymes and their encoding genes from *Aspergillus* and *Trichoderma*. In: Hofrichter M (ed) The Mycota: A comprehensive treatise on fungi as experimental systems for basic and applied research. Springer-Verlag Berlin Heidelberg, Germany. 10:341-355.

de Vries RP, Poulsen CH, Madrid S, Visser J. 1998. *aguA*, the gene encoding an extracellular α-glucuronidase from *Aspergillus tubingensis*, is specifically induced on xylose and not on glucuronic acid. J Bacteriol 180:243-249.

Deniaud E, Quemener B, Fleurence J, Lahaye M. 2003. Structural studies of the mix-linked β-(1→3)/β-(1→4)-D-xylans from the cell wall of *Palmaria palmata* (Rhodophyta). Int J Biol Macromol 33:9-18.

Derba-Maceluch M, Awano T, Takahashi J, Lucenius J, Ratke C, Kontro I, Busse-Wicher M, Kosik O, Tanaka R, Winzéll A, Kallas Å, Léniewska J, Berthold F, Immerzeel P, Teeri TT, Ezcurra I, Dupree P, Serimaa R, Mellerowicz EJ. 2014. Suppression of xylan endotransglycosylase *PtxtXyn10A* affects cellulose microfibril angle in secondary wall in aspen wood. New Phytol. doi: 10.1111/nph.13099

Doblin MS, Johnson KL, Humphries J, Newbigin EJ, Bacic A. 2014. Are designer plant cell walls a realistic aspiration or will the plasticity of the plant's metabolism win out? Curr Opin Biotechnol. 26:108-114.

Domon B, Costello CE. 1988. A systematic nomenclature for carbohydrate fragmentations in FAB-MS/MS spectra of glycoconjugates. Glycoconj J. 5:397-409.

Donaldson LA. 2001. Lignification and lignin topochemistry — an ultrastructural view. Phytochemistry 57:859-873.

Dons JJM, De Vries OMH, Wessels JGH. 1979. Characterization of the genome of the basidiomycete *Schizophyllum commune*. Biochim Biophys Acta Nucleic Acids Protein Synth. 563:100-112.

Duus JØ, Gotfredsen CH, Bock K. 2000. Carbohydrate structural determination by NMR spectroscopy: Modern methods and limitations. Chem Rev 100:4589-4614.

Ebringerová A, Heinze T. 2000. Xylan and xylan derivatives - biopolymers with valuable properties, 1. Naturally occurring xylans structures, isolation procedures and properties. Macromol Rapid Commun 21:542-556.

Edgar RC. 2004. MUSCLE: multiple sequence alignment with high accuracy and high throughput. Nucleic Acids Res. 32:1792-1797.

Enebro J, Karlsson S. 2006. Improved matrix-assisted laser desorption/ionization time-of-flight mass spectrometry of carboxymethyl cellulose. Rapid Commun Mass Spectrom. 20:3693-3698.

Evtuguin D, Tomás J, Silva AS, Neto C. 2003. Characterization of an acetylated heteroxylan from *Eucalyptus globulus* Labill. Carbohydr Res. 338:597-604.

Fauré R, Courtin CM, Delcour JA, Dumon C, Faulds CB, Fincher GB, Fort S, Fry SC, Halila S, Kabel MA, Pouvreau L, Quemener B, Rivet A, Saulnier L, Schols HA, Driquez H, O´Donohue MJ. 2009. A brief and informationally rich naming system for oligosaccharide motifs of heteroxylans found in plant cell walls. Aust J Chem. 62:533-537.

Fazary AE, Ju Y. 2007. Feruloyl esterases as biotechnological tools: current and future perspectives. Acta Bioch Bioph Sin 39:811-828.

Filisetti-Cozzi TMCC, Carpita NC. 1991. Measurement of uronic acids without interference from neutral sugars. Anal Biochem 197:157-162.

Franková L, Fry SC. 2011. Phylogenetic variation in glycosidases and glycanases acting on plant cell wall polysaccharides, and the detection of transglycosidase and trans-β-xylanase activities. Plant J 67:662-681.

Fromm J (2013) Xylem development in trees: from cambial divisions to mature wood cells. In: Fromm J (ed) Cellular aspect of wood science. Springer-Verlag, Berlin Heidelberg, Germany.

Fry SC, Smith RC, Renwick KF, Martin DJ, Hodge SK, Matthews KJ. 1992. Xyloglucan endotransglycosylase, a new wall-loosening enzyme activity from plants. Biochem J 282:821-828.

Garozzo D, Giuffrida M, Impallomeni G, Ballistreri A, Mon taudo G. 1990. Determination of linkage position and identification of the reducing end in linear oligosaccharides by negative ion fast atom bombardment mass spectrometry. Anal Chem 62:279-286.

Garrote G, Dominguez H, Parajo JC. 2001. Study on the deacetylation of hemicelluloses during the hydrothermal processing of Eucalyptus wood. Holz Roh- Werkst. 59:53-59.

Geisler-Lee J, Geisler M, Coutinho PM, Segerman B, Nishikubo N, Takahashi J, Aspeborg H, Djerbi S, Master E, Andersson-Gunnerås S, Sundberg B, Karpinski S, Teeri TT, Kleczkowski LA, Henrissat B, Mellerowicz EJ. 2006. Poplar carbohydrate-active enzymes. Gene identification and expression analyses. Plant Physiol 140:946-962.

Gerber L, Eliasson M, Trygg J, Moritz T, Sundberg B. 2012. Multivariate curve resolution provides a high-throughput data processing pipeline for pyrolysis-gas chromatography/mass spectrometry. J Anal Appl Pyrol 95:95-100.

Gille S, Pauly M. 2012. *O*-acetylation of plant cell wall polysaccharides. Front Plant Sci 3:12. doi: 10.3389/fpls.2012.00012

Gomez L, Whitehead C, Barakate A, Halpin C, McQueen-Mason S. 2010. Automated saccharification assay for determination of digestibility in plant materials. Biotechnol for Biofuels 3:23.

Gonçalves VMF, Evtuguin DV, Domingues MRM. 2008. Structural characterization of the acetylated heteroxylan from the natural hybrid *Paulownia elongata*/*Paulownia fortunei*. Carbohydr Res 343:256-266.

Goubet F, Jackson P, Deery MJ, Dupree P. 2002. Polysaccharide analysis using carbohydrate gel electrophoresis: a method to study plant cell wall polysaccharides and polysaccharide hydrolases. Anal Biochem 300:53-68.

Gröndahl M, Teleman A, Gatenholm P. 2003. Effect of acetylation on the material properties of glucuronoxylan from aspen wood. Carbohydr Polym 52:359-366.

Guillon F, Tranquet O, Quillien L, Utille J, Ordaz Ortiz JJ, Saulnier L. 2004a. Generation of polyclonal and monoclonal antibodies against arabinoxylans and their use for immunocytochemical location of arabinoxylans in cell walls of endosperm of wheat. J Cereal Sci 40:167-182.

Guillon F, Tranquet O, Quillien L, Utille J, Ordaz Ortiz JJ, Saulnier L. 2004b. Generation of polyclonal and monoclonal antibodies against arabinoxylans and their use for immunocytochemical location of arabinoxylans in cell walls of endosperm of wheat. J. Cereal Sci. 40:167-182.

Gunl M, Gille S, Pauly M. 2010. OLIgo Mass Profiling (OLIMP) of extracellular polysaccharides. J Vis Exp 40. e2046. doi:10.3791/2046

Hamann T. 2012. Plant cell wall integrity maintenance as an essential component of biotic stress response mechanisms. Front in Plant Sci 3:77. doi: 10.3389/fpls.2012.00077

Harholt J, Bach IC, Lind-Bouquin S, Nunan KJ, Madrid SM, Brinch-Pedersen H, Holm PB, Scheller HV. 2010. Generation of transgenic wheat (*Triticum aestivum* L.) accumulating heterologous endo-xylanase or ferulic acid esterase in the endosperm. Plant Biotechnol 8:351-362.

Hao Z, Mohnen D. 2014. A review of xylan and lignin biosynthesis: Foundation for studying Arabidopsis irregular xylem mutants with pleiotropic phenotypes. Crit Rev Biochem Mol Bio 49:212-241.

Hao Z, Avci U, Tan L, Zhu X, Glushka J, Pattathil S, Eberhard S, Scholes T, Rothstein GE, Lukowitz W, Orlando R, Hahn MG, Mohnen D. 2014. Loss of Arabidopsis GAUT12/IRX8 causes anther indehiscence and leads to reduced G lignin associated with altered matrix polysaccharide deposition. Front Plant Sc. 5:357. doi: 10.3389/fpls.2014.00357

Harper AD, Bar-Peled M. 2002. Biosynthesis of UDP-Xylose. Cloning and characterization of a novel arabidopsis gene family, UXS, encoding soluble and putative membrane-bound UDP-glucuronic acid decarboxylase isoforms. Plant Physiol 130:2188-2198.

Harris GA, Galhena AS, Fernández FM. 2011. Ambient sampling/ionization mass spectrometry: applications and current trends. Anal Chem 83:4508-4538.

Harvey DJ, Bateman RH, Green MR. 1997. High-energy collision-induced fragmentation of complex oligosaccharides ionized by matrix-assisted laser desorption/ionization mass spectrometry. J Mass Spectrom 32:167-187.

Harvey DJ. 2003. Matrix-assisted laser desorption/ionization mass spectrometry of carbohydrates and glycoconjugates. Int J Mass Spectrom 226:1-35.

Harvey DJ. 2009. Analysis of carbohydrates and glycoconjugates by matrix-assisted laser desorption/ionization mass spectrometry: an update for 2003-2004. Mass Spectrom. Rev. 28:273-361.

Henrissat B. 1991. A classification of glycosyl hydrolases based on amino acid sequence similarities. Biochem J 280:309-316.

Herbers K, Wilke I, Sonnewald U. 1995. A Thermostable xylanase from *Clostridium thermocellum* expressed at high levels in the apoplast of transgenic tobacco has no detrimental effects and is easily purified. Nat Biotech 13:63-66.

Hoije A, Sandstrom C, Roubroeks JP, Andersson R, Gohil S, Gatenholm P. 2006. Evidence of the presence of 2-O-[β]-D-xylopyranosyl-[α]-L-arabinofuranose side chains in barley husk arabinoxylan. Carbohyd Res 341:2959-2966.

Hyunjong B, Lee D, Hwang I. 2006. Dual targeting of xylanase to chloroplasts and peroxisomes as a means to increase protein accumulation in plant cells. J Exp Botany 57:161-169.

Hu J, Arantes V, Pribowo A, Saddler J. 2013. The synergistic action of accessory enzymes enhances the hydrolytic potential of a "cellulase mixture" but is highly substrate specific. Biotech for Biofuels 6:112. doi:10.1186/1754-6834-6-112

Ishii T. 1997. Structure and functions of feruloylated polysaccharides. Plant Sci 127:111-127.

Jacobs A, Dahlman O. 2001. Characterization of the molar masses of hemicelluloses from wood and pulps employing size exclusion chromatography and matrix-assisted laser desorption ionization time-of-flight mass spectrometry. Biomacromolecules 2:894-905.

Johansson MH, Samuelson O. 1977. Reducing end groups in birch xylan and their alkaline degradation. Wood Sci Technol 11:251-263.

Johnston S, Prakash R, Chen N, Kumagai M, Turano H, Cooney J, Atkinson R, Paull R, Cheetamun R, Bacic A, Brummell D, Schröder R. 2013. An enzyme activity capable of endotransglycosylation of heteroxylan polysaccharides is present in plant primary cell walls. Planta 237:173-187.

Kabel MA, de Waard P, Schols HA, Voragen AGJ. 2003. Location of *O*-acetyl substituents in xylo-oligosaccharides obtained from hydrothermally treated Eucalyptus wood. Carbohyd Res 338:69-77.

Kenrick P, Crane PR. 1997. The origin and early evolution of plants on land. Nature 389:33-39.

Keppler BD, Showalter AM. 2010. IRX14 and IRX14-LIKE, Two Glycosyl Transferases Involved in Glucuronoxylan Biosynthesis and Drought Tolerance in Arabidopsis. Mol Plant 3:834-841.

Kimura T, Mizutani T, Tanaka T, Koyama T, Sakka K, Ohmiya K. 2003. Molecular breeding of transgenic rice expressing a xylanase domain of the *xynA* gene from *Clostridium thermocellum*. Appl Microbiol Biotechnol 62:374-379.

Kolenova K, Ryabova O, Vrsanska M, Biely P. 2010. Inverting character of family GH115 α-glucuronidases. FEBS Lett 584:4063-4068.

Kolenová K, Vršanská M, Biely P. 2006/2/10. Mode of action of endo-β-1,4-xylanases of families 10 and 11 on acidic xylooligosaccharides. J Biotechnol 121:338-345.

Koutaniemi S, van Gool MP, Juvonen M, Jokela J, Hinz SW, Schols HA, Tenkanen M. 2013. Distinct roles of carbohydrate esterase family CE16 acetyl esterases and polymer-acting acetyl xylan esterases in xylan deacetylation. J Biotechnol 168:684-692.

Koutaniemi S, Guillon F, Tranquet O, Bouchet B, Tuomainen P, Virkki L, Petersen H, Willats W, Saulnier L, Tenkanen M. 2012. Substituent-specific antibody against glucuronoxylan reveals close association of glucuronic acid and acetyl substituents and distinct labeling patterns in tree species. Planta 236:739-751.

Laiko VV, Baldwin MA, Burlingame AL. 2000. Atmospheric pressure matrix-assisted laser desorption/ionization mass spectrometry. Anal Chem 72:652-657.

Lao N, Long D, Kiang S, Coupland G, Shoue D, Carpita N, Kavanagh T. 2003. Mutation of a family 8 glycosyltransferase gene alters cell wall carbohydrate composition and causes a humidity-sensitive semi-sterile dwarf phenotype in Arabidopsis. Plant Mol Biol 53:687-701.

Lee C, Zhong R, Richardson EA, Himmelsbach DS, McPhail BT, Ye Z. 2007. The PARVUS gene is expressed in cells undergoing secondary wall thickening and is essential for glucuronoxylan biosynthesis. Plant Cell Physiol 48:1659-1672.

Lee C, Teng Q, Huang W, Zhong R, Ye Z. 2009. The F8H Glycosyltransferase is a Functional Paralog of FRA8 Involved in Glucuronoxylan Biosynthesis in Arabidopsis. Plant Cell Physiol 50:812-827.

Lee C, Teng Q, Huang W, Zhong R, Ye Z. 2010. The Arabidopsis family GT43 glycosyltransferases form two functionally nonredundant groups essential for the elongation of glucuronoxylan backbone. Plant Physiol 153:526-541.

Lee C, Teng Q, Zhong R, Ye Z. 2011. The four Arabidopsis REDUCED WALL ACETYLATION genes are expressed in secondary wall-containing cells and required for the acetylation of xylan. Plant Cell Physiol. 52:1289-1301.

Lee C, Teng Q, Zhong R, Ye Z. 2012a. Arabidopsis GUX proteins are glucuronyltransferases responsible for the addition of glucuronic acid side chains onto xylan. Plant Cell Physiol 53:1204-1216.

Lee C, Kibblewhite R, Wagschal K, Li R, Robertson G, Orts W. 2012b. Isolation and characterization of a novel GH67 α-glucuronidase from a mixed culture. J Ind Microbiol Biotechnol 39:1245-1251.

Lerouxel O, Choo TS, Seveno M, Usadel B, Faye L, Lerouge P, Pauly M. 2002. Rapid structural phenotyping of plant cell wall mutants by enzymatic oligosaccharide fingerprinting. Plant Physiol 130:1754-1763.

Li X, Jackson P, Rubtsov D, Faria-Blanc N, Mortimer J, Turner S, Krogh K, Johansen K, Dupree P. 2013. Development and application of a high throughput carbohydrate profiling technique for analyzing plant cell wall polysaccharides and carbohydrate active enzymes. Biotechnol for Biofuels 6:94.

Maina NH, Juvonen M, Domingues RM, Virkki L, Jokela J, Tenkanen M. 2013. Structural analysis of linear mixed-linkage glucooligosaccharides by tandem mass spectrometry. Food Chem 136:1496-1507.

Manabe Y, Nafisi M, Verhertbruggen Y, Orfila C, Gille S, Rautengarten C, Cherk C, Marcus SE, Somerville S, Pauly M, Knox JP, Sakuragi Y, Scheller HV. 2011. Loss-of-function mutation of

REDUCED WALL ACETYLATION2 in Arabidopsis leads to reduced cell wall acetylation and increased resistance to Botrytis cinerea. Plant Physiol 155:1068-1078.

Manabe Y, Verhertbruggen Y, Gille S, Harholt J, Chong SL, Pawar PM, Mellerowicz E, Tenkanen M, Cheng K, Pauly M, Scheller H. 2013. RWA proteins play vital and distinct roles in cell wall *O*-acetylation in *Arabidopsis thaliana*. Plant Physiol 163:1107-1117.

Margolles-Clark E, Tenkanen M, Nakari-Setälä T, Penttilä M. 1996. Cloning of genes encoding α-L-arabinofuranosidase and β-xylosidase from *Trichoderma reesei* by expression in *Saccharomyces cerevisiae*. Appl Environ Microbiol 62:3840-3846.

Maslen SL, Goubet F, Adam A, Dupree P, Stephens E. 2007. Structure elucidation of arabinoxylan isomers by normal phase HPLC–MALDI-TOF/TOF-MS/MS. Carbohyd Res 342:724-735.

Matamoros Fernández LE, Obel N, Scheller HV, Roepstorff P. 2003. Characterization of plant oligosaccharides by matrix-assisted laser desorption/ionization and electrospray mass spectrometry. J Mass Spectrom 38:427-437.

Mazumder K, York WS. 2010. Structural analysis of arabinoxylans isolated from ball-milled switchgrass biomass. Carbohyd Res. 345:2183-2193.

McKee LS, Peña MJ, Rogowski A, Jackson A, Lewis RJ, York WS, Krogh KBRM, Viksø-Nielsen A, Skjøt M, Gilbert HJ, Marles-Wright J. 2012. Introducing endo-xylanase activity into an exo-acting arabinofuranosidase that targets side chains. P Natl Acad Sci 109:6537-6542.

McNeil M, Darvill AG, Fry SC, Albersheim P. 1984. Structure and function of the primary cell walls of plants. Annu Rev Biochem 53:625-663.

Mellerowicz EJ (2006) Xylem cell expansion – lessons from poplar. In: Hayashi T (ed) The science and lore of the plant cell wall: biosynthesis, structure and function. BrownWalker Press, Florida, USA

Mohnen D. 2008. Pectin structure and biosynthesis. Curr Opin Plant Biol 11:266-277.

Mortimer JC, Miles GP, Brown DM, Zhang Z, Segura MP, Weimar T, Yu X, Seffen KA, Stephens E, Turner SR, Dupree P. 2010. Absence of branches from xylan in Arabidopsis gux mutants reveals potential for simplification of lignocellulosic biomass. P Natl Acad Sci 107:17409-17414.

Moyer SC, Marzilli LA, Woods AS, Laiko VV, Doroshenko VM, Cotter RJ. 2003. Atmospheric pressure matrix-assisted laser desorption/ionization (AP MALDI) on a quadrupole ion trap mass spectrometer. Int J Mass Spectrom 226:133-150.

Naran R, Black S, Decker SR, Azadi P. 2009. Extraction and characterization of native heteroxylans from delignified corn stover and aspen. Cellulose (Dordrecht, Neth.) 16:661-675.

Niederpruem DJ, Hobbs H, Henry L. 1964. Nutritional studies of development in *Schizophyllium commune*. J Bacteriol 88:1721-1729.

Niklas KJ. 2004. The cell walls that bind the tree of life. Bioscience 54:831-841.

Nishitani K, Tominaga R. 1992. Endo-xyloglucan transferase, a novel class of glycosyltransferase that catalyzes transfer of a segment of xyloglucan molecule to another xyloglucan molecule. J Biol Chem 267:21058-21064.

Obel N, Porchia AC, Scheller HV. 2002. Dynamic changes in cell wall polysaccharides during wheat seedling development. Phytochemistry 60:603-610.

Obel N, Erben V, Schwarz T, Kühnel S, Fodor A, Pauly M. 2009. Microanalysis of plant cell wall polysaccharides. Mol Plant 5:922-932.

Ohm RA, de Jong JF, Lugones LG, Aerts A, Kothe E, Stajich JE, de Vries RP, Record E, Levasseur A, Baker SE, Bartholomew KA, Coutinho PM, Erdmann S, Fowler TJ, Gathman AC, Lombard V, Henrissat B, Knabe N, Kuees U, Lilly WW, Lindquist E, Lucas S, Magnuson JK, Piumi F, Raudaskoski M, Salamov A, Schmutz J, Schwarze FWMR, van Kuyk PA, Horton JS, Grigoriev IV, Woesten HAB. 2010. Genome sequence of the model mushroom *Schizophyllum commune*. Nat Biotechnol 28:957-963.

Öhgren K, Bura R, Saddler J, Zacchi G. 2007. Effect of hemicellulose and lignin removal on enzymatic hydrolysis of steam pretreated corn stover. Bioresour Technol 98:2503-2510.

Ordaz-Ortiz J, Devaux M, Saulnier L. 2005. Classification of wheat varieties based on structural features of arabinoxylans as revealed by endoxylanase treatment of flour and grain. J Agric Food Chem 53:8349-8356.

Packer NH, Lawson MA, Jardine DR, Redmond JW. 1998. A general approach to desalting oligosaccharides released from glycoproteins. Glycoconj J 15:737-747.

Papac DI, Wong A, Jones AJS. 1996. Analysis of acidic oligosaccharides and glycopeptides by matrix-assisted laser desorption/ionization time-of-flight mass spectrometry. Anal Chem 68:3215-3223.

Park YB, Cosgrove DJ. 2012. A revised architecture of primary cell walls based on biomechanical changes induced by substrate-specific endoglucanases. Plant Physiol 158:1933-1943.

Pastell H, Tuomainen P, Virkki L, Tenkanen M. 2008. Step-wise enzymatic preparation and structural characterization of singly and doubly substituted arabinoxylo-oligosaccharides with non-reducing end terminal branches. Carbohyd Res 343:3049-3057.

Pastell H, Virkki L, Harju E, Tuomainen P, Tenkanen M. 2009. Presence of 1→3-linked 2-*O*-β-D-xylopyranosyl-α-L-arabinofuranosyl side chains in cereal arabinoxylans. Carbohyd Res 344:2480-2488.

Patel M, Johnson J, Brettell RS, Jacobsen J, Xue G. 2000. Transgenic barley expressing a fungal xylanase gene in the endosperm of the developing grains. Mol Breed 6:113-124.

Pattathil S, Avci U, Baldwin D, Swennes AG, McGill JA, Popper Z, Bootten T, Albert A, Davis RH, Chennareddy C, Dong R, O'Shea B, Rossi R, Leoff C, Freshour G, Narra R, O'Neil M, York WS, Hahn MG. 2010. A comprehensive toolkit of plant cell wall glycan-directed monoclonal antibodies. Plant Physiol 153:514-525.

Paulus A, Klockow A. 1996. Detection of carbohydrates in capillary electrophoresis. J Chrom A 720:353-376.

Pawar PM, Koutaniemi S, Tenkanen M, Mellerowicz EJ. 2013. Acetylation of woody lignocellulose: significance and regulation. Front Plant Sci 4:118. doi: 10.3389/fpls.2013.00118

Peña MJ, Zhong R, Zhou G, Richardson EA, O'Neill MA, Darvill AG, York WS, Ye Z. 2007. Arabidopsis *irregular xylem8* and *irregular xylem9*: Implications for the complexity of glucuronoxylan biosynthesis. Plant Cell 19:549-563.

Persson S, Wei H, Milne J, Page GP, Somerville CR. 2005. Identification of genes required for cellulose synthesis by regression analysis of public microarray data sets. P Natl Acad Sci 102:8633-8638.

Petersen PD, Lau J, Ebert B, Yang F, Verhertbruggen Y, Kim JS, Varanasi P, Suttangkakul p, Auer M, Loque D, Scheller HV. 2012. Engineering of plants with improved properties as biofuels feedstocks by vessel-specific complementation of xylan biosynthesis mutants. Biotechnol for Biofuels 5:84.

Pettolino FA, Walsh C, Fincher GB, Bacic A. 2012. Determining the polysaccharide composition of plant cell walls. Nat. Protocols 7:1590-1607.

Pogorelko G, Fursova O, Lin M, Pyle E, Jass J, Zabotina O. 2011. Post-synthetic modification of plant cell walls by expression of microbial hydrolases in the apoplast. Plant Mol Biol 77:433-445.

Pogorelko G, Lionetti V, Fursova O, Sundaram RM, Qi M, Whitham SA, Bogdanove AJ, Bellincampi D, Zabotina OA. 2013. Arabidopsis and *Brachypodium distachyon* transgenic plants expressing *Aspergillus nidulans* acetylesterases have decreased degree of polysaccharide acetylation and increased resistance to pathogens. Plant Physiol 162:9-23.

Popper ZA, Tuohy MG. 2010. Beyond the green: understanding the evolutionary puzzle of plant and algal cell walls. Plant Physiol 153:373-383.

Powell AK, Harvey DJ. 1996. Stabilization of sialic acids in N-linked oligosaccharides and gangliosides for analysis by positive ion matrix-assisted laser desorption/ionization mass spectrometry. Rapid Commun Mass Spectrom 10:1027-1032.

Quemener B, Ordaz-Ortiz JJ, Saulnier L. 2006. Structural characterization of underivatized arabino-xylo-oligosaccharides by negative-ion electrospray mass spectrometry. Carbohyd Res 341:1834-1847.

Rantanen H, Virkki L, Tuomainen P, Kabel M, Schols H, Tenkanen M. 2007. Preparation of arabinoxylobiose from rye xylan using family 10 *Aspergillus aculeatus* endo-1,4-β-D-xylanase. Carbohyd. Polym 68:350-359.

Ratnayake S, Beahan CT, Callahan DL, Bacic A. 2014. The reducing end sequence of wheat endosperm cell wall arabinoxylans. Carbohyd Res 386:23-32.

Reis A, Domingues MRM, Domingues P, Ferrer-Correia AJ, Coimbra MA. 2003. Positive and negative electrospray ionisation tandem mass spectrometry as a tool for structural characterisation of acid released oligosaccharides from olive pulp glucuronoxylans. Carbohyd Res 338:1497-1505.

Reis A, Pinto P, Coimbra MA, Evtuguin DV, Neto CP, Ferrer Correia AJ, Domingues MRM. 2004. Structural differentiation of uronosyl substitution patterns in acidic heteroxylans by electrospray tandem mass spectrometry. J Am Soc Mass Spectrom 15:43-47.

Reis A, Pinto P, Evtuguin DV, Neto CP, Domingues P, Ferrer-Correia AJ, Domingues MRM. 2005. Electrospray tandem mass spectrometry of underivatised acetylated xylo-oligosaccharides. Rapid Commun Mass Spectrom 19:3589-3599.

Reis D, Vian B. 2004. Helicoidal pattern in secondary cell walls and possible role of xylans in their construction. Comptes Rendus Biologies 327:785-790.

Rennie EA, Hansen SF, Baidoo EEK, Hadi MZ, Keasling JD, Scheller HV. 2012. Three members of the arabidopsis glycosyltransferase family 8 are xylan glucuronosyltransferases. Plant Physiol 159:1408-1417.

Rogowski A, Baslé A, Farinas CS, Solovyova A, Mortimer JC, Dupree P, Gilbert HJ, Bolam DN. 2014. Evidence that GH115 α-glucuronidase activity, which is required to degrade plant biomass, is dependent on conformational flexibility. J Bio Chem 289:53-64.

Ryabova O, Vrsanska M, Kaneko S, van Zyl WH, Biely P. 2009. A novel family of hemicellulolytic α-glucuronidase. FEBS Lett 583:1457-1462.

Saha BC. 2000. α-L-Arabinofuranosidases: biochemistry, molecular biology and application in biotechnology. Biotechnol Adv 18:403-423.

Salo PK, Salomies H, Harju K, Ketola RA, Kotiaho T, Yli-Kauhaluoma J, Kostiainen R. 2005. Analysis of small molecules by ultra thin-layer chromatography-atmospheric pressure matrix-assisted laser desorption/ionization mass spectrometry. J Am Soc Mass Spectrom 16:906-915.

Sambrook JF, Russell DW. 2001. Molecular cloning: A laboratory manual. 3rd edition. Cold Spring Harbor Laboratory Press.

Sarkar P, Bosneaga E, Auer M. 2009. Plant cell walls throughout evolution: towards a molecular understanding of their design principles. J Exp Botany 60:3615-3635.

Scheller HV, Ulvskov P. 2010. Hemicelluloses. Annu Rev Plant Biol 61:263-289.

Schröder R, Wegrzyn T, Sharma N, Atkinson R. 2006. LeMAN4 endo-β-mannanase from ripe tomato fruit can act as a mannan transglycosylase or hydrolase. Planta 224:1091-1102.

Seipert RR, Barboza M, Niñonuevo MR, LoCascio RG, Mills DA, Freeman SL, German JB, Lebrilla CB. 2008. Analysis and quantitation of fructooligosaccharides using matrix-assisted laser desorption/ionization fourier transform ion cyclotron resonance mass spectrometry. Anal Chem 80:159-165.

Shatalov AA, Evtuguin DV, Pascoal Neto C. 1999. (2-*O*-α-D-Galactopyranosyl-4-*O*-methyl-α-D-glucurono)-D-xylan from *Eucalyptus globulus* Labill. Carbohyd Res 320:93-99.

Shatalov AA, Pereira H. 2009. Impact of hexenuronic acids on xylanase-aided bio-bleaching of chemical pulps. Bioresour Technol 100:3069-3075.

Siika-aho M, Tenkanen M, Buchert J, Puls J, Viikari L. 1994. An α-glucuronidase from *Trichoderma reesei* Rut C-30. Enzyme Microb Technol 16:813-819.

Sleno L, Volmer DA. 2006. Assessing the properties of internal standards for quantitative matrix-assisted laser desorption/ionization mass spectrometry of small molecules. Rapid Commun Mass Sp 20:1517-1524.

Smith LG. 2001. Plant cell division: building walls in the right places. Nat Rev Mol Cell Biol 2:33-39.

Somerville C, Bauer S, Brininstool G, Facette M, Hamann T, Milne J, Osborne E, Paredez A, Persson S, Raab T, Vorwerk S, Youngs H. 2004. Toward a systems approach to understanding plant cell walls. Science 306:2206-2211.

St. John FJ, Rice JD, Preston JF. 2006. Characterization of XynC from *Bacillus subtilis* subsp. *subtilis* Strain 168 and analysis of its role in depolymerization of glucuronoxylan. J. Bacteriol. 188:8617-8626.

Sundberg A, Sundberg K, Lillandt C, Holmbom B. 1996. Determination of hemicelluloses and pectins in wood and pulp fibers by acid methanolysis and gas chromatography. Nord Pulp Pap Res J 11:216-219.

Takahashi N, Koshijima T. 1988. Ester linkages between lignin and glucuronoxylan in a lignin-carbohydrate complex from beech (*Fagus crenata*) wood. Wood Sci Technol 22:231-241.

Tan L, Eberhard S, Pattathil S, Warder C, Glushka J, Yuan C, Hao Z, Zhu X, Avci U, Miller JS, Baldwin D, Pham C, Orlando R, Darvill A, Hahn MG, Kieliszewski MJ, Mohnen D. 2013. An Arabidopsis cell wall proteoglycan consists of pectin and arabinoxylan covalently linked to an arabinogalactan protein. Plant Cell 25:270-287.

Taylor II LE, Dai Z, Decker SR, Brunecky R, Adney WS, Ding S, Himmel ME. 2008. Heterologous expression of glycosyl hydrolases in planta: a new departure for biofuels. Trends Biotechnol 26:413-424.

Teleman A, Harjunpää V, Tenkanen M, Buchert J, Hausalo T, Drakenberg T, Vuorinen T. 1995. Characterisation of 4-deoxy-b-L-threo-hex-4-enopyranosyluronic acid attached to xylan in pine kraft pulp and pulping liquor by ^{1}H and ^{13}C NMR spectroscopy. Carbohyd Res 272:55-71.

Teleman A, Lundqvist J, Tjerneld F, Stålbrand H, Dahlman O. 2000. Characterization of acetylated 4-*O*-methylglucuronoxylan isolated from aspen employing ^{1}H and ^{13}C NMR spectroscopy. Carbohyd. Res 329:807-815.

Tenkanen M, Gellerstedt G, Vuorinen T, Teleman A, Perttula M, Li J, Buchert J. 1999. Determination of hexenuronic acid in softwood kraft pulps by three different methods. J Pulp Pap Sci 25:306-311.

Tenkanen M, Siika-aho M. 2000. An α-glucuronidase of *Schizophyllum commune* acting on polymeric xylan. J Biotechnol 78:149-161.

Tenkanen M, Luonteri E, Teleman A. 1996. Effect of side groups on the action of b-xylosidase from *Trichoderma reesei* against substituted xylo-oligosaccharides. FEBS Lett 399:303-306.

Tenkanen M, Hausalo T, Siika-Aho M, Buchert J, Viikari L. 1995. Use of enzymes in combination with anion exchange chromatography in the analysis of carbohydrate composition of kraft pulps. Int Symp Wood Pulping Chem 3:189-194.

Tenkanen M, Vršanská M, Siika-aho M, Wong DW, Puchart V, Penttilä M, Saloheimo M, Biely P. 2013. Xylanase XYN IV from *Trichoderma reesei* showing exo- and endo-xylanase activity. FEBS J 280:285-301.

Testova L, Chong S, Tenkanen M, Sixta H. 2011. Autohydrolysis of birch wood: 11th EWLP, Hamburg, Germany, August 16-19, 2010. Holzforschung 65:535-542.

Timell TE. 1967. Recent progress in the chemistry of wood hemicelluloses. Wood Sci Technol 1:45-70.

Tsai AY, Canam T, Gorzsás A, Mellerowicz EJ, Campbell MM, Master ER. 2012. Constitutive expression of a fungal glucuronoyl esterase in Arabidopsis reveals altered cell wall composition and structure. Plant Biotechnol 10:1077-1087.

Turner SR, Somerville CR. 1997. Collapsed xylem phenotype of Arabidopsis identifies mutants deficient in cellulose deposition in the secondary cell wall. Plant Cell 9:689-701.

Uhliariková I, Vršanská M, McCleary BV, Biely P. 2013. Positional specifity of acetylxylan esterases on natural polysaccharide: An NMR study. Biochim Biophys Acta 1830:3365-3372.

Urbanowicz BR, Peña MJ, Ratnaparkhe S, Avci U, Backe J, Steet HF, Foston M, Li H, O'Neill MA, Ragauskas AJ, Darvill AG, Wyman C, Gilbert HJ, York WS. 2012. 4-*O*-methylation of glucuronic acid in Arabidopsis glucuronoxylan is catalyzed by a domain of unknown function family 579 protein. P Natl Acad Sci 109:14253-14258.

Urbanowicz BR, Peña MJ, Moniz HA, Moremen KW, York WS. 2014. Two Arabidopsis proteins synthesize acetylated xylan in vitro. Plant J 80:197-206.

Vinueza NR, Gallardo VA, Klimek JF, Carpita NC, Kenttämaa HI. 2013. Analysis of xyloglucans by ambient chloride attachment ionization tandem mass spectrometry. Carbohyd Polym 98:1203-1213.

Virkki L, Maina HN, Johansson L, Tenkanen M. 2008. New enzyme-based method for analysis of water-soluble wheat arabinoxylans. Carbohyd Res 343:521-529.

Vogel J. 2008. Unique aspects of the grass cell wall. Curr Opin Plant Biol 11:301-307.

Vršanská M, Kolenová K, Puchart V, Biely P. 2007. Mode of action of glycoside hydrolase family 5 glucuronoxylan xylanohydrolase from *Erwinia chrysanthemi.* FEBS J 274:1666-1677.

Wende G, Fry SC. 1997. 2-O-β-d-xylopyranosyl-(5-O-feruloyl)-l-arabinose, a widespread component of grass cell walls. Phytochemistry 44:1019-1030.

Weng X, Huang Y, Hou C, Jiang D. 2013. Effects of an exogenous xylanase gene expression on the growth of transgenic rice and the expression level of endogenous xylanase inhibitor gene RIXI. J Sci Food Agric 93:173-179.

Westphal Y, Schols HA, Voragen AGJ, Gruppen H. 2010. MALDI-TOF MS and CE-LIF fingerprinting of plant cell wall polysaccharide digests as a screening tool for arabidopsis cell wall mutants. J Agric Food Chem 58:4644-4652.

Wu A, Rihouey C, Seveno M, Hoernblad E, Singh SK, Matsunaga T, Ishii T, Lerouge P, Marchant A. 2009. The Arabidopsis IRX10 and IRX10-LIKE glycosyltransferases are critical for glucuronoxylan biosynthesis during secondary cell wall formation. Plant J 57:718-731.

Wu A, Hörnblad E, Voxeur A, Gerber L, Rihouey C, Lerouge P, Marchant A. 2010. Analysis of the Arabidopsis IRX9/IRX9-L and IRX14/IRX14-L pairs of glycosyltransferase genes reveals critical contributions to biosynthesis of the hemicellulose glucuronoxylan. Plant Physiol 153:542-554.

Xiong G, Cheng K, Pauly M. 2013. Xylan *O*-acetylation impacts xylem development and enzymatic recalcitrance as indicated by the Arabidopsis mutant *tbl29*. Mol Plant 6:1373-1375.

Yang P, Wang Y, Bai Y, Meng K, Luo H, Yuan T, Fan Y, Yao B. 2007. Expression of xylanase with high specific activity from *Streptomyces olivaceoviridis* A1 in transgenic potato plants (*Solanum tuberosum* L.). Biotechnol Lett 29:659-667.

Yuan Y, Teng Q, Zhong R, Ye Z. 2013. The Arabidopsis DUF231 domain-containing protein ESK1 mediates 2-*O*- and 3-*O*-acetylation of xylosyl residues in xylan. Plant Cell Physiol 54:1186-1199.

Zaia J. 2004. Mass spectrometry of oligosaccharides. Mass Spectrom Rev 23:161-227.

Zhang J, LaMotte L, Dodds ED, Lebrilla CB. 2005. Atmospheric pressure MALDI fourier transform mass spectrometry of labile oligosaccharides. Anal Chem 77:4429-4438.

Zhang J, Siika-aho M, Tenkanen M, Viikari L. 2011. The role of acetyl xylan esterase in the solubilization of xylan and enzymatic hydrolysis of wheat straw and giant reed. Biotechnol for Biofuels 4:60.

Zhang Y and Frohman MA. 2000. Using rapid amplification of cDNA ends (RACE) to obtain full-length cDNAs. Nucleic Acid Protoc Handb 69:61-87.

Zhong R, Pena MJ, Zhou G, Nairn CJ, Wood-Jones A, Richardson EA, Morrison WH,III, Darvill AG, York WS, Ye Z. 2005. Arabidopsis *fragile fiber8*, which encodes a putative glucuronyltransferase, is essential for normal secondary wall synthesis. Plant Cell 17:3390-3408.

Zwahlen C, Legault P, Vincent S, Greenblatt J, Konrat R, Kay LE. 1997. Methods for measurement of intermolecular NOEs by Multinuclear NMR Spectroscopy: Application to a Bacteriophage λ N-Peptide/boxB RNA Complex. J Am Chem Soc 119:6711-6721.